CHARCTERIZATION OF NANO CRYSTALLINE $Fe_{100-x}Cr_x$ ALLOYS PRODUCED BY MECHANICAL ALLOYING
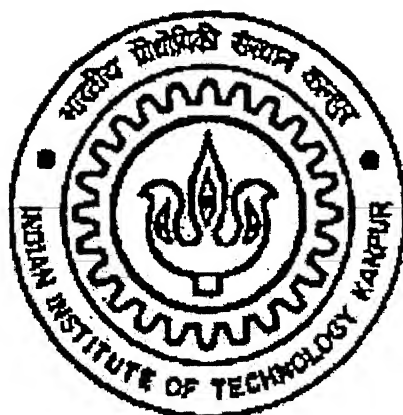
A Thesis Submitted
In Partial fulfillment of the requirements
for the degree of
MASTER OF TECHNOLOGY

BY

M.ANANDA RAO

ROLL NO: Y210617

to the

Department of Materials and Metallurgical Engineering
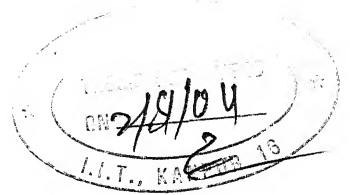
Indian Institute of Technology Kanpur,

India 208016

JULY-2004

TH
MME/2004/M
R18c

CERTIFICATE

This is to certify that the thesis entitled " **CHARACTERIZATION OF NANO CRYSTALLINE** $Fe_{100-x}Cr_x$ **ALLOY PRODUCED BY MECHANICAL ALLOYING**" by M.Ananda Rao (Y210617) has been carried out under my supervision and has not been submitted elsewhere for the award of a degree.

Prof. S.Bhargava
Dept. of Materials and Metallurgical Engg
Indian Institute of Technology
Kanpur, INDIA.

Dedicated to ……..

My Parents and Family members

ACKNOWLEDGEMENTS

ABSTRACT

In the present study, Fe –10 wt% Cr and Fe – 20 wt% Cr powders were milled in a Retsch planetary ball mill for different milling time ranging from 0-100 hrs in order to prepare nanocrystalline alloy powder. The progress of alloying in mechanically alloyed powders as well as refinement of grain size during the course of milling can be inferred from X-ray diffraction using Scherer method, it has been observed that the crystallite size decreases with milling time. The rate of decrease in crystalline size is very rapid between 0 - 40 hrs milling time. The crystallite size between milling time of 40 hrs and 100 hrs remains nearly stable. At 100 hrs of milling time, the crystalline size in both the alloys was found to be 6 - 7 nm which is of the same order of magnitude as determined by AFM studies. In view of both iron and Cr having the BCC crystal structure and both having very close parameters, X-ray diffraction studies are not very effective to monitor the progress of solid solution formation during mechanical alloying. In contrast, the progress of solid solution can be successfully studied using Mossbauer spectroscopy. As revealed by Mossbauer spectroscopy, it is found that regions of almost pure Fe still exist in the mechanically milled powder. After a milling of 40 hrs no regions of pure Fe are found in the milled powder. This implies that Fe-Cr solid solution forms in both the compositions between milling time of 20 – 40 hrs. Solid solution of an improved homogeneity is found to have occurred after a milling time of 65 hrs. As reveled by the scanning electron microscopy, powder morphology changes with increase in milling time. The particle morphology changes from equiaxed to elongated and then to flaky as the milling time increases. The extent of flakiness appears to be increasing with increasing Cr content in the mechanically milled alloys. As studied by AFM, the surface roughness of milled particles of Fe –10 wt% Cr decreases with increase in milling time. While the mean ridge height is found to be ~ 700 nm after a milling time of 5 hrs, the same decreases to ~ 180 nm after a milling time of 100 hrs. Interlamellar width in Fe –10 wt% Cr decreases with increase in milling time. While after a milling time of 20 hr the interlamellar width in Fe –10 wt% Cr is found to be 145 nm, it decreases to15 nm as the milling time was increases to 65 hrs. And grain

morphology of the milled Fe –10 wt% Cr alloy powder is changing from equiaxed to elongated as the milling time is increasing, and also from phase contrast study of the milled Fe –10 wt% Cr alloy, showing the alloying is uniform as the milling time is increasing. Microhardness is increasing with increase in milling time for the both the Fe –10 wt% Cr and Fe – 20 wt% Cr alloys. From 40hrs of milling time onwards hardness is increasing sharply and it is also found that scatter in the hardness value is more at the initial stages of milling, as the milling time was increasing scatter is found to be decreasing. Both the alloys of Fe-Cr are consolidated and sintered at 650°C for 45min and imaged under the optical microscope and observed the consolidation strategy with function of applied pressure.

TABLE OF CONTENTS

List of Figures

List of Tables

INTRODUCTION

The giant magneto-resistance (GMR) effect, which is exploited for use in memory devices, is observed not only in nanometer multilayers of e. g. Fe – Cu, Fe - Cr and Fe - Co, but also in heterogeneous Cu/Co or Cu/Fe alloy systems produced by mechanical alloying (MA). The phenomenon of GMR in mechanically alloyed systems is controlled by the mean radius and volume fraction of nano-sized single-domain ferromagnetic particles in the non-magnetic medium. Therefore, in order to maximize the GMR effect it is necessary to optimize the size and distribution of ferromagnetic domians on a nanometer scale.

Since 1970s a wide variety of equilibrium and non-equilibrium phases have been formed by mechanical alloying of elemental metallic powders. The mechanism of phase formation during the mechanical alloying process has been studied in great details and the progress in understanding its basic mechanism has been recently reviewed. In essence, the inter-dispersion of alloying elements occurs due to repeated cold welding and fracture of free powder particles arising from the impact energy of milling medium in a high energy attrition mill. The heavily dislocated structure formed due to the large scale deformation of individual or layered particles during their cold welding enhances the mutual solubility of elements and leads to their mixing at the atomic scale by progressively eliminating the concentration gradient between cold welded layered structure. Therefore, mechanical alloying is capable of producing powders in a nonequilibrium state by either accumulating mechanical energy or accelerating diffusion across the interface between unlike elements. The grain size of the alloyed material also simultaneously decreases as a function of milling time and eventually reaches a nano-scale. In some cases the continuous milling of the powder may also lead to the formation of the amorphous phase. The formation of mechanically alloyed end product, however, depends on many parameters such as milling conditions and the thermodynamic properties of the milled system.

The Fe-Cr alloy system displays unique possibilities for obtaining nanoscale structures by mechanical alloying approach. Both Fe and Cr crystallize in the body-centered cubic (bcc) structure and the difference in their lattice parameters is only 0.5%. The Fe-Cr equilibrium phase diagram, Figure 1, shows a broad miscibility gap for a wide range of concentrations below the temperature of about 830°C. At temperatures higher than 830°C, the Fe-Cr alloys are solid solutions. Thus during thermal treatment in the temperature range of 440–830°C, specially for the equiatomic compositions, an intermetallic phase σ can be formed. This phase is known to transform into bcc solid solution during ball milling. Fe-Cr alloys belonging to a wider compositional range can also be made to decompose into Fe-enriched and Cr-enriched solid solution either through nucleation and growth mechanism or through spinodal decomposition by heating between 400°C and 500°C. Nanoscale domains of ferromagnetic regions in nonmagnetic regions can thus be created in mechanically alloyed Fe-Cr systems. The diffusion in equilibrium Fe-Cr alloys is considered to be too low to allow the decomposition at temperatures < 400°C. The mechanical alloying, on the other hand is performed at room temperature. Due to (a) the likely increase in temperature due to the severe plastic deformation, (b) presence of many dislocations in the alloy synthesized and (c) nanoscale of the grain size the diffusion is expected to occur in Fe-Cr alloys synthesized by mechanical alloying even at lower temperatures. It is thus interesting to know whether a homogeneous $Fe_{1-x}Cr_x$ alloy can be produced by mechanical alloying although Cr and Fe atoms 'dislike' each other.

Starting from elemental powders, several workers have used the mechanical alloying approach for producing Fe-Cr alloys of different compositions [C Lemoine etal1999][T Koyano etal 1992][M.Murugesan etal 1999] synthesized, the milling conditions used and the characterization techniques used to examine the structure of alloy powders produced. A close examination of these results shows that the mechanical alloying is indeed capable of producing a nonoscale structure with grain size of ~ 10 nm. Such a conclusion is also generally corroborated by results obtained from the TEM analysis of the powders produced. Further, while the progress of alloying in mechanically alloyed powders as well as refinement of grain size during the course of milling can generally be inferred from X-ray diffraction using Scherer method, the heterogeneity in

as the fraction of Cr mixed with Fe can not be inferred through such a technique because the diffraction peaks of Cr and Fe overlap. In contrast, due to different magnetic properties of Fe and Cr and a strong composition dependence of magnetic properties in the $Fe_{100-x}Cr_x$ system, the use of Mossbauer Spectroscopy can be used to find the chemical inhomogeneity in the alloys synthesized and thus the progress of mechanical alloying. Mossbauer Spectroscopy has thus been used by several workers. In addition, Atomic Force Microscopy (AFM) is a imaging technique to resolve structural features at the atomic level, with this technique; extensive morphological studies on dependence of Grain shape on milling time, dependence of alloying on milling time, and dependence of lamellar spacing on milling time are to be analyzed for the Fe-Cr mechanically alloyed powder.

The work presented here is a part of a bigger research programme aimed at producing thin strips of $Fe_{100-x}Cr_x$ alloys by a powder processing route using mechanical alloying as the method of producing nanoscale structure. While techniques such as X-ray diffraction, Mossbauer spectroscopy, scanning electron microscopy were also used to characterize the structure of the Fe-Cr powders synthesized by mechanical alloying and have been discussed elsewhere, the present study deals with the results obtained by Atomic Force Microscopy in characterizing the structure of Fe-Cr alloys as function of milling time.

2.1 Nano Structured Materials

2.1.1 Introduction

In the recent years, the nano-technology has been identified as a new wave towards millennium innovations in the materials science and engineering. With the reduction of a characteristic length such as the grain size or the cluster or molecular size, the normal properties of materials were reported to be drastically changed.Nano-stuctured materials can be represented as "a broad class of materials, with microstructures modulated in zero to three dimensions on length scales less than 100nm" or in other words "materials with atoms arranged in nano sized clusters, which become the constituent grain or building blocks of materials". The emerging fields of nanoscale science, engineering and technology – the ability to work at the molecular level, atom by atom, to create large structures with fundamentally new properties and functions- are leading to unprecedented understanding and control over the basic building blocks and properties of natural man made things.

Scientists have opened a broad net of discoveries that does not leave any major research area untouched in physical, biological, and engineering and sciences. The importance and potential of nanotechnology is quite visible in the words of "Roco" as he predicts "As the 21st century unfolds, nano technology's impact on health, wealth and security of the world's of people is expected to be at least as significant as the combined influences in this century of antibiotics, integrated circuits, and other advanced materials"(Roco 2002). In 2001, virtually all the countries have initiated programs in this area or had national programs in advanced planning (Roco 2001). As shown in table ,, the world wide nanotechnology R&D investment reported by the government organizations including Japan , western Europe, and the USA has increased approximately five times in the last 5 years, between 1997 & 2002(Roco 2003).

In the coming years, it can be predicted that the convergence of nano-technology with information technology, modern biology, and social sciences will reinvigorate discoveries and innovations in almost all the areas of economy.

2.1.2 Definitions and Classification of Nanostructured Materials

The basic question, which arises during the discussion, is what nano structured materials are at all. In the way these materials should be defined? A number of researchers and Scientists have defined them in different ways. In this section, we will have overview of these materials including various definitions, their classification and a brief introduction of each of the class/type

Definitions

About nanocrystalline materials, the pioneering Gleiter says,

"Nanocrystalline solids are polycrystals, the crystal size of which is a few (typically 1 to 10) nanometers[Gleiter 1991].

According to R.W.Siegal,

"Nano phase materials are three dimensionally modulated, synthetic materials with average grain size, phase or other structural domain sizes below 100nm"[Siegel 1993].

At another place Gleiter defined NsM as,
"NsM are solids composed of structural element – mostly crystallites – with a characteristic size (in at least one direction) of a few nanometers"[Gleiter 1995].

The designation "nano powder" is usually used to describe powders with a particle diameter less than 1 micrometer (1000nm) [Eifert et al 2000].Some more definitions of NsM are as follows:

(i) According to Lu et al: "Nanostructured materials have characteristic length scale of a few (typically 1-10) nanometers" [Yulin and Liaw2001].

(ii) According to McHenry and Laughin: "the term nanocrystalline alloy is used to describe those alloys that have majority of grain diameters in the typical range from 1 to 50 nanometers"[Mc Henry et al 2000].

(iii) According to R.Birringer: "nanocrystalline materials are single-phase or multiphase polycrystals, the crystal size of which is of the order of a few (typically 1-10) nanometers, so that about 50 volumes % of the material consists of grain or interphase boundaries"[Birringer 1989].

(iv)   Gleiter again summarized NsM as,
         NsM are materials with microstucture, the characteristic length scale of which
         is on the order of a few (typically 1-10) nanometers" [Gleiter 2000].

On the basis of above information NsM can be defined as follows:
         "NsM are single phase or multiphase polycryastals having the crystal size of the
order of a few (typically 1-100) nanometers in at least one dimension".

Classification on the basis of Dimensionality

         Nano-structured materials can be classified on the basis of dimensionality (in
which length scale is in nanometers) as follows:
   (a) nano particles
   (b) Layered or lamellar structure
   (c) Filamentary structure
   (d) Bulk nano-structured materials

         Nano particles are atom clusters and can be considered zero dimensional (0-D) in
nature [Seigel 1994]. A layered or lamellar structure is a one dimensional (1-D) nano
structure in which the magnitudes of length and width are much greater than thickness
that is only a few nanometers in size. A two dimensional (2-D) nano-structure can be
termed as filamentary and in this the length is substantially larger than width or
diameters, which are of the nano dimensions [Suryanarayana 1995]. The most common
nano structure is basically equiaxed (all the 3-dimensions are in nm size) and are termed
nano structured crystallites or 3-D nano structures [Suryanarayana and Koch 1999].

The Nano Structured Materials may contain crystalline, quasicrystalline, or
amorphous phases and can be metals, ceramics, polymers or composites. If grains are
made up of crystals, the material is called nanocrystalline. On the other hand if they are
made up of quasicrystalline or amorphous (glassy) phases, they are termed nano-quasi-
crystals or nano-glasses [Suryanarayana 1995]. A detailed classification of NsM is shown
in Figure 2.1a & 2.1b and Table2.1
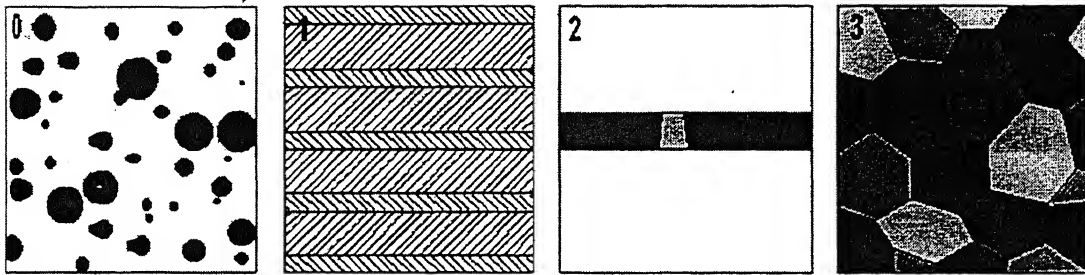
Figure 2.1a Schematic representation of four types of nano crystalline materials [Siegel 1994].
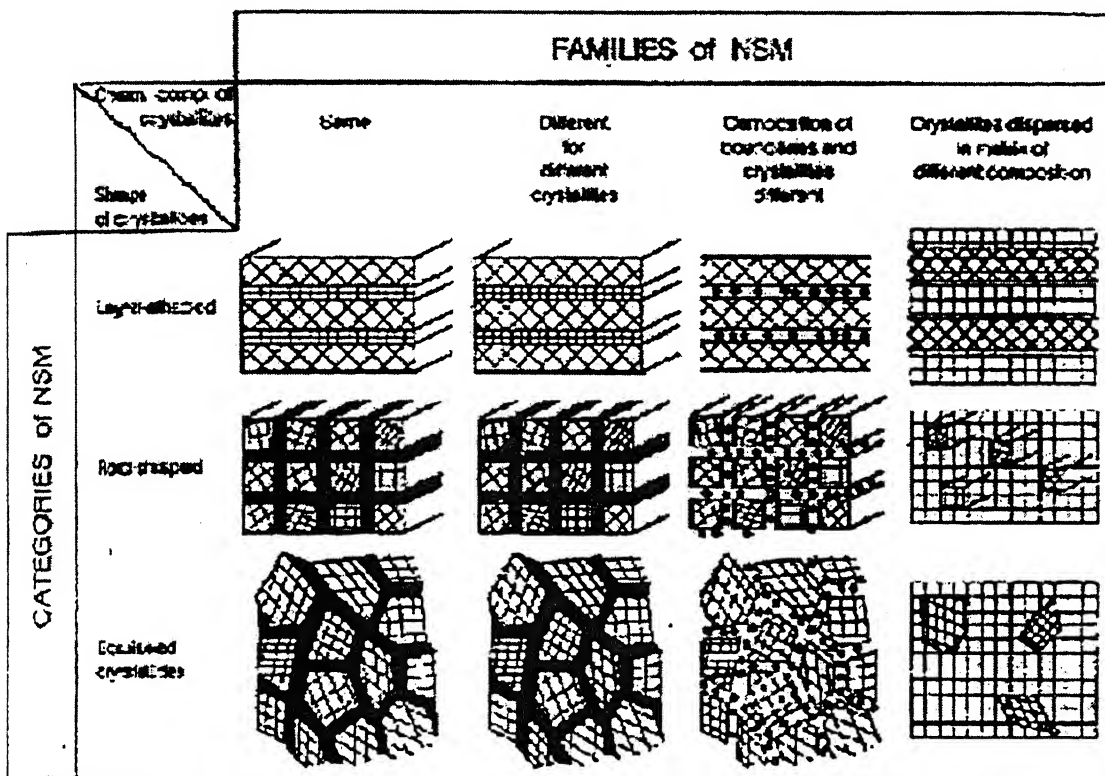
Figure2.1b Classification Scheme for NsM according to their chemical composition and the dimensionality (shape) of the crystallites (structural elements) forming the NsM[Gleiter2000].

2.1.3 Parameters Controlling the Properties of NsM

As the properties of solids depends on size, atomic structure and chemical composition, NsM exhibit new properties due to one or several of the following effects:

Size Effects

Size effects result if the characteristic size of the building blocks of the microstructure (e.g crystallite size, figure2.2) is reduced to the point where critical length scales of physical phenomena(e.g mean free paths of electrons or photons, a coherency length, a screening length, etc) become comparative with the characteristic size of the building blocks of the microstructure[Gleter 1998].

Table2.1 Classification of nano materials

Dimensionality	Designation	Typical Methods of Synthesis
Zero-Dimensional(0-D)	Clusters	Sol-Gel Method
One-Dimensional(1-D)	Layers(Lamellar)	Vapor Deposition Electro-Deposition
Two-Dimensional(2-D)	Filamentary	Chemical Vapor Deposition
Three-Dimensional(3-D)	Crystallites(equiaxed)	Gas Condensation Mechanical Alloying

Change of the Dimensionality of the System

If an NsM consists of thin needle-shaped or flat, two-dimensional crystallites (Figure 2.1a & 2.1b), only two or one dimension of the building blocks becomes comparable with the length scale of a physical phenomenon. In the later words, in these cases the NsM becomes a two or one-dimensional system with respect to this phenomenon [Gleiter2000].

Change of Atomic Structure

Change in the atomic structure results if a high density of incoherent interface(Figure 2.2) or other lattice defects such as dislocations, vacancies etc, are incorporated. The core of lattice defects represents a constrained state of solid matter differing structurally from (unconstrained) crystals and /or glasses. As a consequence, a solid containing a high density of defect cores differs structurally from a defect free solid with the same (average) chemical composition [Gleiter 2000].
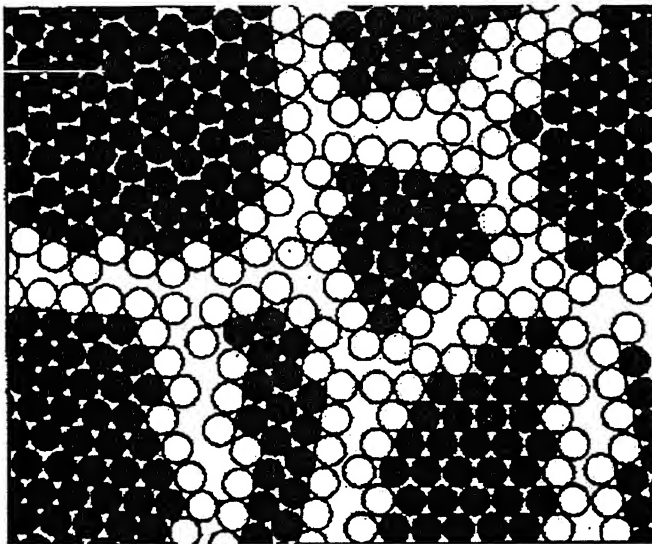
Figure2.2 Two Dimensional Model of nano structured material the atoms in the centers of the crystals are indicated in the black. The ones in the boundary core regions are represented in black [Gleiter 1998]

The boundaries in the Figure 2.2 represent an example of this effect. This misfit between adjacent crystallites changes the atomic structure (e.g the average atomic density, the nearest neighbor coordination, etc) in the boundary region relative to perfect crystal. At high defect densities the volume fractions of defect cores become comparable with the volume fraction of crystalline region. In fact, this is the case if crystal diameter becomes comparable with the thickness of interface, i.e for crystal sizes on the order of one or a few nanometers, as is the case in NsM.

Alloying of Components that are Immiscible in the Solid or the Molten State

Solute atoms (Figure 2.3) with lattice solubility in the crystallites frequently segregate to the boundary cores (e.g the free energy of the system in several alloys is reduced if large solute atoms segregate to the boundary core). Another type of nanostructured alloys results if crystallites of an NsM have different chemical compositions. Even if the constituents are immiscible in the crystalline and/ or molten state (e.g Fe & Ag), the formation of solid solution in the boundary regions of the NsM has been noticed (Figure2.4) [Herr et al 1990].
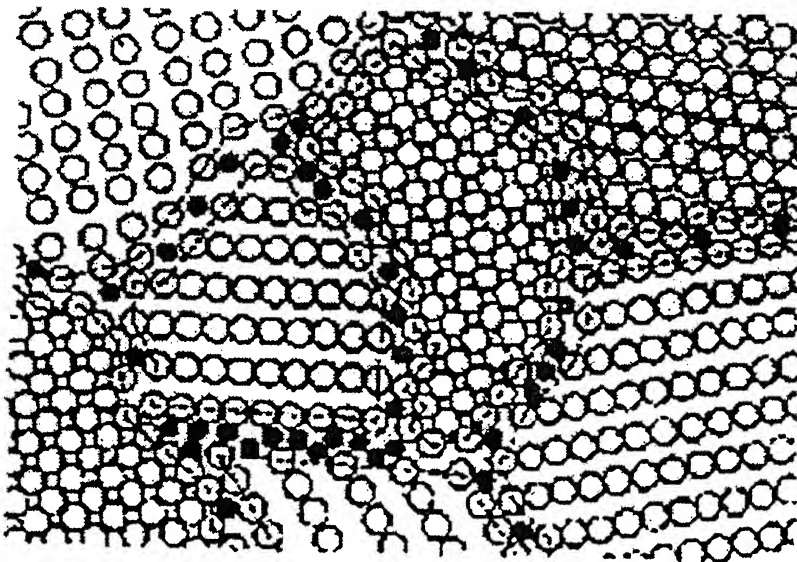
Figure2.3 Schematic model of nanostructured Cu-Bi and W-Ga alloys. The open circles represent Cu or W alloy, respectively, forming the nano sized crystals. The black circles are Bi or Ga atoms respectively, incorporated in the boundaries at the sites of enhanced local free volume. The atomic structure shown was deduced from EXAFS and X ray Diffraction measurements [Gleiter 1993].

2.1.4 Methods of Synthesis

In the recent times, numerous methods have been developed to prepare Nano-Structured materials. Any method capable of producing very fine grain –size polycrystalline materials can be adopted to produce Nano-crystalline materials. The grain size, morphology, and texture can be suitably modifying/controlling the process variables in these methods (Table 2.2).

If the phase transformation is involved, e.g liquid to solid, or vapor to solid, then

steps are needed to increase the nucleation rate and to decrease the growth rate during formation of the product phase. We will now describe the different methods of preparing NsM starting from vapor, liquid or solid phases.
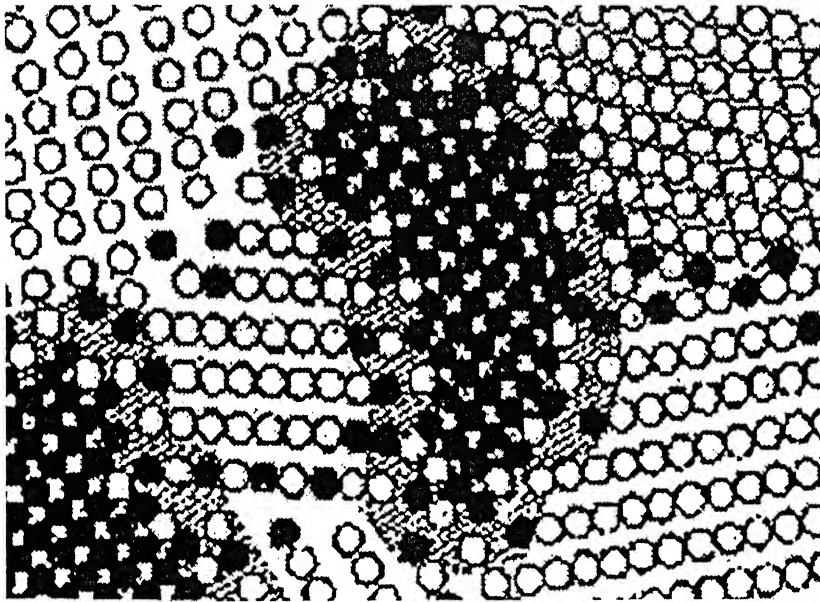
Figure2.4 Schematic model of nanocrystalline Ag-Fe alloys according to the data of Mossbauer spectroscopy. The alloys consist of a mixture of nanometer sized Ag and Fe crystals (represented by open and full circles, respectively). In the (strained) interfacial regions between Ag and Fe crystals, solid solutions of Fe atoms in Ag crystallites and Ag atoms in the Fe crystallites are formed although both compounds are immiscible in the liquid as well as solid state. Similar effects may occur in the grain boundaries between adjacent Fe and Ag crystals [Herr et al 1990].

Inert Gas Condensation

This method consists of evaporating a metal (by resistive heating, radio frequency heating , sputtering, electron beam, laser plasma heating, or iron sputtering) inside a chamber that is evacuated to a very high vaccum of about 10 torr and then backfilled with a low- pressure inert gas, typically a few hundred Pascal of He. The evaporated atoms collide with the gas atoms inside the chamber, lose their kinetic energy, and condense in the form of small, discrete crystals of loose powder.

Convection currents generated due to the heating of the inert gas by the evaporation source and then cooled by the liquid nitrogen – filled collection device (cold finger); carry the condensed fine powders to the collector device, from where they can be stripped off by moving an annular Teflon ring down the length of the tube in to a compaction device.

Table 2.2 Methods of synthesize nano structured materials

Starting Phase	Technique	Nature of Product
Vapor	Inert gas condensation	3-D
	Physical vapor deposition	1-D
	Plasma Processing	3-D
	Chemical vapor deposition	3-D,2-D
Liquid	Rapid solidification	3-D
	Electro deposition	1-D,3-D
	Chemical reaction	3-D
Solid	Mechanical alloying	3-D
	Devitrification	3-D
	Spark erosion	3-D
	Sliding wear	3-D

This method produces typically equiaxed (3-D) crystallites. The crystal size of the powder is few nanometers and size distribution is narrow. The crystal size is dependent upon the inert gas pressure, the evaporation rate, and the gas composition. Extremely fine particles can be produced by decreasing either the gas pressure in the chamber or the evaporation rate by using lighter gas, such as He, rather than heavier inert gas, such as Xe

This method of preparation is expensive in nature; hence it has not been used extensively for commercial purposes. The advantage of this method is cleanliness of the process and better control on the grain size of the final product by controlling the various parameters involved in the process. The size of the clusters, which upon consolidation become the grains of the nano crystalline material, can be easily controlled by variation

of type, pressure, and temperature of the inert condensing gas and very small clusters, which often exhibit particularly interesting mesoscopic physical and chemical behavior, can be obtained by specific design of the cluster source.

Rapid Solidification

It is possible to increase the nucleation rate and decrease the growth rate of the solid phase if cooling (or the under cooling) during rapid solidification of metallic melt is increased to high value. As a consequence, the grain size of the result product will be in the nanometer range. Nano composites have been produced by this method during rapid solidification of metallic melts or during diversification of metallic glasses produced by rapid solidification. Rapid solidification technique is usually applied at the place where the small grain size distribution range is required i.e uniform distribution of grain size is required. This method is proffered for bulk production of nano crystalline materials for industrial use due to easy processing route and cost effectiveness. Most of the commercial magnetic materials are prepared by this method.

Electro-Deposition

Multi layered metals can be obtained by electro-deposition route by using either two separate electrolytes or from one electrolyte by appropriate control of agitation and the electrical conditions(particularly voltage).these processes can be applied to the synthesis of pure metals, alloys and composites. These processes have high production rates, little size and shape limitations and require a low capital investment. Three dimensional nanostructured crystallites can be obtained using this method

Spray Conversion Processing

In this technique, aqueous solution precursors are used. The solution mixture is aerosolized and rapidly spray dried to give extremely fine mixture of complex compounds. To prevent grain growth, inhibitors are added during sintering as binders. WC-Co nanocrystalline composites have been produced on commercial basis using the spray conversion processing method" starting from the aqueous solution precursors such as ammonium metatungstate.As compared to gas condensation techniques, this process

requires less production cost as gas condensation technique require ultra high vaccum during processing which increases the cost of production. Mechanical alloying is a method of mass production of nanocrystalline powders but the problem of contamination restricts its widespread application. This problem can be overcome by spray conversion processing method.

Devitrification

Controlled crystallization of amorphous alloys, produced by other methods, leads to the synthesis of nanostructured materials. In fact, the most common method to produce nanocrystalline materials has been to obtain an amorphous phase by rapidly solidifying the melt of appropriate composition and then crystallizing the glassy phase at a relatively low temperature. This simple devitrification method has been commonly employed to study the magnetic properties of nano-crystalline materials because it can produce porosity free samples with different grain sizes by controlling the crystallization parameters and large quantities of materials.

Mechanical Alloying

Mechanical alloying produces nano structured materials by the structural decomposition of coarse grained structure as a result of severe plastic deformation using high energy ball mill. This process has produced nanocrystalline structures in pure metals, intermetallic compounds and immiscible alloy systems.

Physical Vapor Deposition

Physical vapor deposition (PVD) refers to coating processes where the transport of material to the substrate is affected by physical driving mechanism. Such mechanisms include evaporation, sputtering, iron plating, and ion assisted sputtering. Coating stability and performance is enhanced if they are fully dense and defect free.

Recent improvements in PVD techniques, in particular the use of plasmas and the unbalanced magnetron for the deposition process, have led to its wide application in industry. Such coating are used for corrosion protection, to provide hard surfaces for engineering applications, to form decorative coatings on a range of household and

industrial products, for energy saving window glass, for media storage systems such as compact discs and for a range of micro electronics applications. For example, for corrosive coating film density and tensile stress developed in coating during processing are very important factors affecting the corrosion behavior of coating. It hs been found that stress can be reduced via this process.

Sol Gel Method

Nanometer sized ceramic structures have been generated by means of a sol-gel technique. Both structural and compositional nanometer structures are obtained by "seeding "of a ceramic precursor with crystalline sols of the final equilibrium phase to catalyze nucleation.

A significant advantage of this method in comparison to methods involving high temperatures (e.g. calcinations, evaporations) is the low temperatures of the method. The preparation of stoichiometric compounds containing one or more components with a high vapor pressure, e.g. Pb in (BaPb) TiO_3 ferroelectrics poses serious problems due to the Pb loss. This difficulty can be avoided by the sol-gel approach. In fact, the specific surface areas of (BaPb) TiO_3 sol-gel derived powders have been found to be about 50 m²/g in comparison to 4 m²/g for powders prepared by calcined mixed oxides.

$CoFe_{2-x} Mn_xO_4$ (x=0-2.0) nanocrystalline thin films and powders were prepared by sol-gel process by Zhou et al. (2002). Ferrites are well known magnetic materials used as recording media. Cobalt ferrite, $CoFe_2O_4$, is one of the good candidates for high density recording media because of its high coercive force, moderate saturation magnetization, better chemical stability and mechanical hardness. For high density recording media, small grain size is very much is required. Such a kind of nanostructured material is often prepared by the sol-gel synthesis, which could offer the advantages of lowering annealing temperature for the crystallization process and controlling the grain size by varying the annealing temperature.

2.1.5 Structure

In order to understand the interrelationship between structure and properties, nanocrystalline materials need to be characterized on the both atomic and nanometer

scales. The micro structural features of importance include (a) Grain size, grain size distribution and morphology, (b) the nature and morphology of grain boundaries and interphase and morphology, (c) the perfection and nature of intra-grain defects, (d) composition profile across grains and interfaces, and (e) identification of residual trapped species from processing.

There is a gamut of experimental techniques that can yield structural information on nanocrystalline materials. These include 'direct; microscopic techniques such as transmission electron microscopy (TEM), scanning tunneling microscopy (STM), atomic force microscopy (AFM), field ion microscopy (FIM), and less direct electron, X-ray and neutron diffraction techniques. Indirect spectroscopic tools, such as EXAFS, nuclear magnetic resonance, Raman and Mossbauer spectroscopies, and positron annihilation spectroscopy, have also been used. Owing to the ultrafine scale of nanocrystalline materials, traditional characterization tools such as TEM and X-Ray diffraction technique are both necessary and useful to understand the structure of nanocrystalline materials.
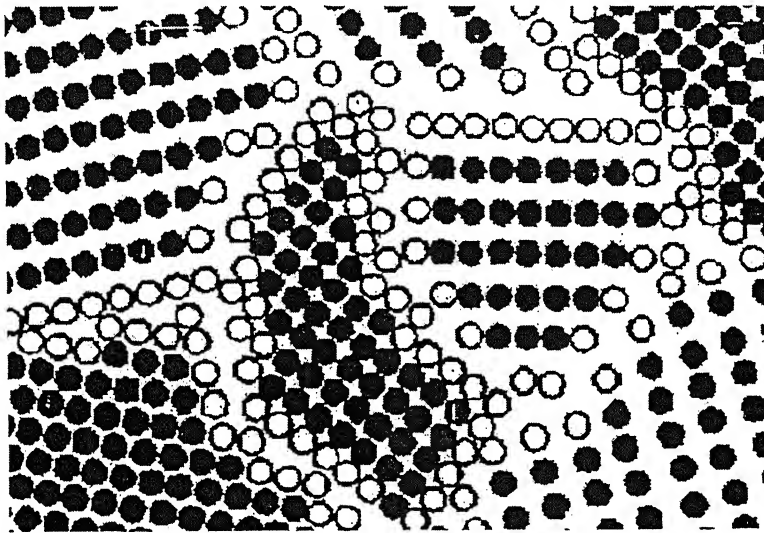
Figure2.5 Schematic arrangements of atoms in equiaxed nano crystalline metal

A nanocrystalline metal contains typically a large number of interfaces with random orientation relationship, and consequently a substantial fraction of the atoms lies in the interfaces (Figure 2.5). Assuming that grains have the shape of the spheres or cubes, the volume fraction of atoms associated with the boundaries can be calculated as follows [Andrievski 2002]:

$$V_f = 3S/D \qquad (1)$$

Where,

S= average grain boundary thickness

D= average grain diameter

It has been observed that volume fraction of atoms in the grain boundaries can be about 50% for 5 nm grains, decrease upto30% for 10 nm grains and 3% for 100 nm grains. Nanocrystalline metals can be considered to consist of two structural components – the numerous small crystallites with long range order and different crystallographic orientations constituting the "crystalline" component and a network of intercrystalline regions, the structure of which differs from region to region: which is referred as the "interfacial" component [Koch 1999].

Atomic Structure of Crystal Lattice and the Grain Boundary

The structure of the grains (crystallites) in nanocrystalline materials has been accepted to be the same as in a coarse-grained materials i.e long range order atomic structure [Gleiter2000]. Initially it was suggested that nanocrystalline grain boundary atomic structure has "gas like disorder". But after exhaustive studies on the nature of grain boundary structure, it has been established in most of the cases that interface structures are remarkably close, structure wise, to those in conventional crystalline materials with micron sized grains [Ranganathan etal 2001].

Triple Junction and Higher Order Grain Junction

In the ultra fine grained (nanocrystalline) materials, triple junctions and higher order junctions become an important component of the microstructure. The total intercrystalline region consisting of grain boundaries, triple junctions and four grained points is more important than just the grain boundary. The grain boundary area is inversely proportional to the grain size while triple line length is proportional to Inverse Square of the grain size. Thus the contribution of triple junction and higher order grain junction becomes important at very small grain size [Koch 1997].

2.1.6 Stability

Thermal stability is important for the consolidation of nanocrystalline powders with out coarsening of microstructure. Grain growth occurs in polycrystalline materials to decrease the system energy by decreasing the total grain boundary energy. Grain growth can be measured by following expression [Gleiter2000]:

$$D^{1/n} - D_0^{1/n} = kt \qquad (2)$$

Where,

D = length scale or mean grain diameter

n = empirical constant =<0.5

D_0 = length scale or mean grain diameter at t =0

K = temperature dependent rate parameter, t = annealing time

By applying, k= k_0 exp (-Q/RT), activation energy Q can be calculated and which in turn can be used to deduce the grain growth mechanism.

Nanocrystalline metals exhibit crystal growth at elevated temperatures. In metals with a crystal size of about 10nm, significant crystal growth (doubling the crystal size in about 24 hours) was noticed at ambient temperature or below equilibrium melting temperature, T was lower than about 600°C.However, if T was higher, the stability against grain growth seems to be enhanced [Gleter 1989]. The grain growth in mechanically alloyed solid solution has been found to decrease with increasing solute concentration, and heat release upon annealing indicates that solute segregates to the grain boundaries, thereby reducing the specific grain boundary energy and impeding the grain growth [Krill et al 1995].

2.1.7 Properties of Nano Structured Materials

Due to the fine grained structure, nanocrystalline materials have unique properties that are different and considerably improved in comparison with those of conventional coarse grained polycrystalline materials. These include increased strength and hardness, enhanced diffusivity, improved ductility and toughness, reduced density, reduced elastic modulus, higher electrical resistivity, increased specific heat, higher thermal expansion coefficient, lower thermal conductivity, and better soft magnetic properties in comparison with conventional coarse-grained materials.

Diffusion and Sinterability

Since nanocrystalline materials contain a very large fraction of atoms at the grain boundaries, the numerous interfaces provide a high density of short circuit paths for diffusion. As a consequence, they exhibit an enhanced diffusivity in comparison to with single crystal or conventional coarse-grained polycrystalline materials with the same chemical composition [Schumacher et al.1989, Holfer 1993].

This enhanced diffusivity can have a significant effect on mechanical properties such as creep and superplasticity, ability to dope efficiently nanocrystalline materials with impurities at relatively low temperatures, and synthesis of alloy phases in immiscible metals and the at much lower than those usually required in other systems. The enhanced

Self and impurity diffusivities in nanocrystalline materials appear to be strongly linked to the porosity present in the samples. However, in the light of recent results, the difference in diffusion coefficients seems to be caused by differences in relaxation states rather than by porosity [Holfer 1993].

Solid solubility limits are usually enhanced when the material is in the nanocrystalline state and this has been explained on the basis of elastic strains at the interfaces. The high diffusivity results in alloying, by diffusion along grain boundaries resulting in the formation of stable and metastable phases at relatively low temperatures. Another important consequence of the increased diffusivity is that sintering of nanocrystalline powders can occur at temperatures lower than those required for coarse-grained polycrystalline powders.

Mechanical Properties

The elastic constants of nanocrystalline materials have been found to be reduced by 30% or less. The presence of extrinsic defects e.g. pores and cracks, was suggested as the possible reason for low values of Young's modulus in nanocrystalline materials compacted from powders [Krstic 1993].

The Hall-Petch relation for conventional coarse-grained polycrystalline materials suggests that the yield strength (or hardness) of a material increases with a decreasing grain size according to the relationship,

$$\sigma = \sigma_0 + k_H d^n \tag{3}$$

where, d=grain size, σ = 0.2% yield strength (or hardness),

σ_0 = lattice friction stress to move individual dislocations (or the hardness of a single crystal specimen, d→ infinity)

n = the grain size exponent (generally -1/2), k_H = Hall-Petch intensity parameter

At extremely fine grain sizes, e.g. in the nanometer regime, the individual grains cannot support more than one dislocation; and thus, the Hall-Petch relation may not be valid. The deviation from the Hall-Petch relationship in nanocrystalline materials may be due to the following reasons:

a) Since in nanocrystalline materials, pile-ups can not form when the grain size is less than a critical value d_c, weaking mechanisms (e.g. viscous type flow) operate and leads to a decrease in hardness with decreasing grain size, i.e. a negative value for the slope k_H.

b) A large number of triple junctions may be a reason for negative slope in nanoarystalline materials as an increased triple junction volume fraction leads to softening and enhanced bulk ductility in polycryastlline materials [Palumbo et al. 1990 Nieh et al. 1991].

Summery of the mechanical properties of nanocrystalline materials can be given as follows [Suryanarayana and Koch 1999].

(1)   Except for very small grain nanocrystalline samples (<5 nm) the elastic properties are essentially identical to those of coarse-grained materials.

(2)   High hardness and yield strength values are observed for nanocrystalline materials.

(3)   Ductile coarse-grained materials are less ductile, perhaps brittle as nanocrystalline materials.

(4)   Brittle coarse-grained materials may exhibit slight ductility when nanocrystalline.

(5)   Superplasticity has not been observed at low temperatures (<0.4 to 0.5 Tm) for nanocrystalline materials, although it has been observed at somewhat lower temperatures and higher strain rates as grain size is decreases.

(6)   Shear bending and perfectly plastic behavior have been seen in some nanocrystalline materials analogous to plastic deformation in amorphous materials

Electrical Properties

The electrical resistivity of nanocrystalline materials has been found to be higher than that in coarse grained polycrystalline and amorphous alloys. The increased volume fraction of atoms lying at grain boundaries is considered responsible for the increase in electrical resistivity. The phenomena of giant magnetoresistance (GMR) (decrease in electrical resistance of materials when exposed to a magnetic field) has been reported in number of multilayer syatems. Where as the resistance drop is only 1-2% in conventional coarse-grained materials, the drop is as large as 50-80% in the case of nanocryastalline materials.

Specific Heat

The specific heat in the nanocrystalline state is much higher than that in the coarse grained material (by as much as 50% in some cases) and even in the amorphous material. The specific heat of a material is closely related to its vibrational and configurational entropy, which is significantly affected by the nearest neighbour configurations. Thus, the increase in specific heat of nanocrystalline materials has been attributed to the small crystal size (and consequent large interfacial component).

Magnetic Properties

Different magnetic properties of nanoscale ferromagnetic materials, as compared to conventional one, can be attributed to their small volume. It means that they are typically single domain, and a large fraction of atoms are associated with the grain boundaries/interfaces. If the single domain nanoscale ferromagnetic particles (e.g. Fe, Co, or Ni) are put in a non-magnetic matrix such that their magnetic interaction is negligible,

a superparamagnetic material is obtained. If the grain size is small enough, the structural distortions associated with the surfaces or interfaces can lower the Curie temperature, Tc , and reduce the magnitude of the saturation magnetization Ms.

While the very low losses of the nanocrystalline soft magnetic materials (FINEMET or Nanoperm) are depedent on the nanometer grain size for their properties, the hard magnetic nanocrystalline alloys with remanence enhancement provide flexibility in processing, especially with powder materials. These remanence enhanced nanocrystalline hard magnetic alloys may find many applications as permanent magnetic components. Two important requirements for alloys to exhibit remanence enhancement are a nanocrystalline grain size and a degree of coherence across interphase boundaries sufficient to enable adjacent phases to be exchanged coupled.

The magnetocaloric effect is another magnetic property that can be enhanced in nanocrystalline microstructures. Small magnetic particles in a non magnetic matrix exhibit alignment of the magnetic spins in a magnetic field. This increase in magnetic order lowers the magnetic entropy of the spin system. If this process is performed adiabatically the reduction in spin entropy is offset by an increase in lattice entropy and the specimen temperature will rise. This temperature rise ΔT is reversible – the specimen cools down on removal of the magnetic field – and is known as the magnetocaloric effect.

Chemical Properties

A majority of the processing methods to produce the nanocrystalline materials in the form of powder, and therefore the total surface area can be accurately tailored by controlling the particle and grain sizes through the processing parameters. Most important evidence of chemical reactivity of such material is demonstrated by their enhanced catalytic activity [Beck and Siegel 1992]. Recently, it has been emphasized that such catalytic activity is evolved in the environmental problems due to enhancement in the activity of aerosols due to their fine size.

The effect of particle size on gas-metal interaction has been utilized in the development of nanocrystalline materials for hydrogen storage application. Moreover, enhanced diffusion mechanism in nanocrysatlline materials may also be included in the navel chemical properties. Hydrogen absorbing alloys (FeTi, LaNi5, Mg_2 Ni, and other

Mg-based materials) in the nanocrystalline form show much better hydrogen sorption properties than their polycrastalline counterparts.

2.1.8 Applications and Present Potential

Being the new area, a lot of research is going on for potential use of nanostructured materials. Based on the properties of these materials, so many applications of these materials have been suggested. At present, bulk nanostructured soft magnetic iron based alloys and WC-Co composites have found industrial use.

Structural Applications

Higher hardness, strength and deformation than the conventional materials provide grounds for wide application of nanocrystalline materials.

- **Cutting Tools**

It has been shown that the hardness and strength of nanocrystalline materials is 4-5 times higher than that of coarse grained materials of same composition. For example, in WC-Co composites it has been found that hardness of WC-Co composites, with WC grains in nanometer size range, increases with decreasing grain size reaching values as high as 2,200 VHN. Scratch test suggests that higher hardness in nanograined WC-Co is also accompanied by increased toughness. Thus, the abrasive resistance of nanostructured WC-Co is higher than that of conventional WC-Co when comparison is made at equal hardness. Thus, nanocrystalline WC-Co cutting tools are expected to have more than doubled the life time than conventional coarse grained composite. These materials could be used as fine drill bits for drilling holes in PCBs and as rotary cutting tools [McCandlishet al. 1994].

- **Nanocomposites**

Nanocomposites are those materials in which either the reinforcement or the matrix or both are on a nanometer scale. Further, Nanocomposites may be such that the reinforcement may be distributed either in the grain boundaries or inside the garins. It has been known that dispersing a second phase on a microscopic scale can considerably

enhance the fracture toughness of ceramics. Since reducing the grain size to nanometer dimensions can provide increased strength and hardness, it is suggested that fabrication of micro/nanohybrids will lead to class of supertough and superstrong ceramics. In these hybrids, a Nanocomposite matrix is reinforcement with sub micron sized particles like whiskers, platelets, and long fibers and these hybrids show enhanced fracture toughness and strength up to very high temperatures, where the properties of coarse grained composites normally degrade.

Further, nanoreinforcements increase creep resistance by suppressing grain boundary sliding. Consequently, nanoreinforcements are now being used to boost the performance of a growing number of composites. Nanocrystalline fibers also are used to reinforce composites [Bhaduri and Bhaduri 1998]. While high hardness and strength are usually associated with low ductility, it has been shown that a uniform dispersion of about 20 vol% of a Nanocrystalline phase in an amorphousmatrix increases the strength of the material significantly while maintaining an adequate level ductility in the composite [Inoue al. 1994].

- **Superplastic Materials**

Materials in the nanocrystalline state show tendencies if superplastic deformation at temperatures lower and strain rates higher than conventional coarse-grained materials. Since ceramics and conventionally brittle intermetallics can be rendered ductile at elevated temperatures (at least in some cases) by nanostructure processing, these materials can be formed to near-net shapes by means of deformation processing methods previously applicable only to produce ductile metal parts.

- **Coatings**

As we have been seen earlier that nanocrystalline materials have high hardness and strength than that of conventional ones, these properties can be utilized to produce wear resistance coatings. Thermal barrier coatings of a metallic bond coat, usually MCrAlY, a thermally grown $Al_2 O_3$ film, and s ceramic layer, usually yttria stabilized zirconia. These coatings reduce superalloy metal temperatures by as much as 300F, and there by provide durability to combustors, transition ducts, and turbine vanes. With the

gas turbine industry's demand for higher operating temperatures to provide enhanced fuel efficiency, thermal barrier coatings with reduced thermal conductivity provide the highest pay-off coating application. One can also deposit nanocryastalline coatings to improve the wear resistance while retaining a tough interior for low-temperature application.

Magnetic Applications

The exceptional soft magnetic properties of the "FINEMET" and "Nanoperm" Nanocrystalline/amorphous Fe-base alloys promise applications in transformer cores for power frequencies, saturable reactors, high frequency transformers, and magnetic heads. Additional probable applications are for data communication interface components, sensors, and common mod choke coils and magnetic shields.

Magnetic recording materials to some extent already use nanostructured materials. Magnetic materials are used in both the information storage media and in the "write" and "read" heads. It is predicted that in the future essentially all media and heads will contain nanostructured materials. There is now a large market for strong rare earth-based permanent magnets in a wide variety of applications, and flexibility in manufacturing and lower materials costs (less expensive rare earth metals needed in remanence enhanced magnets) should encourage use of nanostructured materials

Electronic Applications

"Functional "electronic and optical nanostructures are typically fashioned from single crystal semiconductor materials using a variety of possible pattern formation (e.g., electron beam lithography) and pattern transfer processes (e.g., reactive ion etching), which can create structures at the nanoscale. By replacing inks with nanoparticles solutions, it is also conceivable that we could print structures onto surfaces e.g., printing electronic circuits. This is large area of research and development of importance to the mocroelectronics industry for the future directions such as quantum circuits and systems, massive memory, architecture and interconnected systems.

Catalysis and Hydrogen Storage Materials

When a sample is divided into small portions, high specific area is obtained. A lot of studies show that catalytic activity and selectivity can be dependent on particle size that is why finely dispersed materials are used in catalysis. Metal hydrides are the best option available for storage of hydrogen for use as a fuel. It was believed that a way to enhance their properties is to produce the materials in Nanocrystalline form. The high density of grain boundaries/interfaces might increase diffusion. Nanocrystalline Mg_2Ni inclusions in a two phase Mg/Mg_2Ni alloy showed improved hydrogen storage behaviour in term of Mg_2Ni catalyzing the decomposition of the molecular hydrogen, greatly increasing the hydrogen absorption/desorption kinetics.

Bio-Medical Applications

Magnetic nanoparticles are being used in biomedical research on cell separation, for magnetically targeted drug delivery, for protein and DNA purification, and for contrast enhancement in magnetic resonance imaging (MRI). Functionalization of the nanoparticle surface could enable the selective attachment to particular type of cells. Magnetic nanoparticles for selective tag could someday be used in HIV immune therapy or the treatment of blood diseases.

If magnetic nanoparticles were attched to cancer cells, they could be for hypothermia; raising the local temperature about 420^0 C increases their sensitivity to radiation and chemotherapy, and heating above 420^0 C causes a significant amount of cell death. Nanoparticles additions can be used in suns creams and cosmetics to protect our skin against UV rays in plastics for out door applications to prevent UV-induced weathering and in bottle coatings to protect beer, wine and olive oil against photo degradation.

2.1.9 Consolidation Strategy for Nano Structured Materials

The potential application of nanoscale materials as novel structural or functional engineering materials largely depends on the consolidation of powders into bulk nanoscale solids. The retention of metastable microstructure in the course of this consolidation process is essential for preserving the often superior mechanical, magnetic,

or catalytic properties of the material [Gleiter 2000]. Consolidation of the nanocryatlline powders has been achieved by **electro-discharge compaction; plasma activated sintering , explosive consolidation, hot isostatic processing, hydrostatic extrusion, strained powder rolling and sinter forging** [Suryanarayana 1999, Siegel 1994].

Optimization of consolidation parameters is important because retention of nanostructures requires use of low consolidation temperatures while achieving full (theoretical) density requires use of high temperatures [Ma and He 2000]. However, it should be noted that because of the increased diffusivities in nanocrystlline materials, sintering takes place at a temperature much lower than in coarse-grained materials. This is likely to reduce the grain growth. It is typically difficult to obtain full density while retaining the nanoscale microstructure. The high driving force and enhanced kinetics due to large curvature facilities may cause full densification of nanocrystalline materials at temperatures below those of coarse grained materials of the same composition by few hundred degrees [Ma 2000, Ma and He 1996]. Retention of fine grain sizes and elimination of sintering aids are specific advantages of the lower processing temperatures [Liu 1998, Suraynarayana and Hofler et al 1993].

Effect of Temperature on Consolidation

For conventional materials, pores are removed through sintering at high temperatures for long times, driven by the reduction in surface energy where as for nanophase materials, consolidation temperature needs to be kept low to maintain nanoscale grain sizes. Full densification is possible at some intermediate elevated temperatures because nanophase powders are expected to show increased sinterability compared with their conventional coarse-grained counterparts. A reduction in sintering temperature can reduce contamination and compositional changes, and stresses and cracking during cooling. A number of factors contribute to this possible processing advantage. For mechanically milled powders, particles with varying sizes may lead to easier filling of pores of different sizes. Fine grain sizes provide shorter diffusion paths and much increased densification rate during sintering [Ma 2000].

It is obvious that the diffusional processes that mediate sintering also lead to undesired grain growth. The driving force for grain growth also increases, as grain size

decreases such that the advantage nanophase materials have in sinterability can be partly lost due to concomitant grain growth that destroys the desirable nanoscale grain size. Therefore, consolidation temperature needs to be maintained sufficiently low, and other mechanisms (such as stress assisted densification) must be invoked to allow full consolidation and retention of nanostructure.

Effect of Pressure on Consolidation

To compensate for the low consolidation temperature the strategy usually adopted is to use hot pressing and forging employing high pressure (of the order of 0.5-1.0 GPa) to enhance the contribution of plastic deformation and bonding. The high stress enhances the plastic strain controlled pore closure. Also, the stress plays a significant role in stress assisted densification (diffusion) mechanisms. Possible stress effect on deformation and densification can be seen from the established formula for creep, in general.

$$\partial\varepsilon/\partial t = A\ \sigma^n/RTd^{q^*}\exp\ (-Q/RT)\ f\ (\rho) \tag{4}$$

Where, σ is the applied stress, d the grain size, $\partial\varepsilon/\partial t$ the strain rate, n= the stress exponent, q the grain size dependent exponent, A, a coefficient involving diffusivity prefactor, Burger vector, shear modulus etc., Q the activation energy for the accommodation process, ρ the density, R the gas constant, and T the temperature. In this expression, A,n,q, and Q can have different values for different creep mechanisms (Nabarro-Herring creep, Coble creep, Dislocation climb power law creep etc.) and f(ρ) accounts for density effects.

The equation indicates that the high pressure applied and the strong grain size dependence of creep deformation can contribute significantly to densification by plastic deformation at relatively low temperatures. In addition, the extensive plastic deformation under high stress results in disruption of any continues surface oxides on powder particles, which may degrade bonding and properties. The high pressure applied may also have the beneficial effects of slowing down grain growth because of the reduction of free volumes in grain boundaries, which facilitate atomic jump across the boundary.

Effect of Contamination

Surface contamination is inevitable for any powder material and may become significant in nanopowders due to their large surface area. Metastable powders obtained by mechanical alloying or milling are special case. Their structure is either amorphous or nanocrystalline but the powder particle size is in the micron range. In this case, the surface area is less than for nanometer powder particles but contamination is due to large impurity intake during the milling process. Oxides, nitrides and other compounds are often found in consolidated parts made of attrition-milled nanopowders.

Studies show that ultra clean nanoparticles sinter very rapidly even at room temperature. The oxygen contamination decreases the surface energy and slows down the sintering kinetics. To reduce contamination, all mechanical alloying and consolidation should be performed under inert atmosphere. To reduce metallic impurities acquired during milling, milling media and materials being milled should match in composition.

Suppression of Grain Growth

Compared with the grain sizes in as milled powder, grain growth is observed in all consolidation techniques. There could be several possible ways for suppression of runaway grain growth during consolidation. First of all, sinter forging scheme allows full density processing at relatively low temperatures, significantly below 0.5Tm, resulting in less grain growth than other consolidation methods, second, a minute amount of impurities picked up during milling, although often below the detection limit, may have also contributed to the success in suppressing grain growth through solute drag or Zener drag mechanism. These trace impurities are uniformly distributed by the milling action, reducing the possibility of abnormal grain growth.

Grain size stability is especially high when a second element, copper is added into iron. In this case, additional factors contribute to the retention of nanoscale grain sizes in consolidated composites. First of all, the powder after mechanical milling consists of a super saturated solid solution, with iron and copper alloyed on the atomic scale due to the non-equilibrium nature of the milling process. The solute drag effect, due to the solute atoms segregating to grain boundaries, retards grain growth. Second, upon heating during consolidation, phase separation into f.c.c. copper and b.c.c. iron occurs inside the

nanograins or along the abundant grain boundaries. The new grains thus start out with sizes smaller or atleast similar to those in the nanocrystalline precursor phase. Third, resultant two phase mixture configuration helps to isolate grains and/or domains of the same structure and there by reduce grain growth boundary migration. In other words, incorporating a second phase or elements helps to retain nano phase grain size when reaching full density.

2.1.10 Kinetics of Nano Crystalline (Metastable) Phase Transformations

Many metastable phases are found in the nature and also have been produced by the recently developed novel materials processing techniques. According to the thermodynamics, there is a possibility for both stable and metastable phases to form [Ishihara 1999]. There are two reasons as to why metastable phases form. These are:

1) Metastable phses can nucleate before the stable phases can nucleate

2) The crystal growth rate of the metastable phase exceeds that of the stable phase.

Nucleation of the Metastable Phases

It is well known that according to the Ostwald step rule (Ostwald 1897) that the first phase to appear will be a metastable phase which has a higher free energy than the stable phase. The excess free energy of critical nucleus (ΔG^*) can be expressed as:

$$\Delta G^* = (16/13)*\pi*(0.065)^3 *\Delta H_f*[T_m^2/(T_m-T)^2] \tag{5}$$

Where ΔG^* = the excess free energy of critical nucleus,

ΔH_f = the enthalpy of fusion,

T_m and T are melting temperature and temperature of cooling ($T<T_m$)

. The condition (B<1) should usually be satisfied because ΔH_f approaches ΔG at low temperatures and ΔG^* for the metastable phase is always less than that of the stable phase. Therefore, it may generally be expected the nucleation frequency of the metastable phases is larger than that of the stable phase if the under-cooling is large enough.

The Crystal Growth Rate of the Metastable Phase

There have been only a few schematic studies of the growth rate. In general, the growth rate can be expressed as a function of the undercooling by the equation (Jackson 1984).

$$S = S_0 (\Delta T)^\beta \qquad\qquad (6)$$

Where S_0 and constants, and ΔT is the degree of undercooling. S_0 and β have no physical significance. However when β of the metastable phase become larger than that of the stable phase at a undercooling . Such a situation can occur when the stable phase has a faceted solid liquid interface while the metastable phase has a molecularly rough interface. β of stable and metastable phases is 1.4 and 2.0 respectively. For S_0, the metastable phase is three times larger than that of the stable phase.

2.2 Mechanical Alloying
A Possible Route for Preparing Nano Structured Materials

Almost the different options for preparations, the mechanical alloying of powders with high energy ball milling has been considered the most powerful method for nanostructured materials because of its simplicity, relatively inexpensive equipment ,and the possibility of producing large quantities, that can be scaled up to several tons. Mechanically processed micron sized powders have been shown to posses nanosized substructures or even to become amorphous with appropriate milling parameters. In most systems, the nano grains or amorphous structure represents a far from equilibrium condition that is generally quite metastable in nature.

Mechanical alloying is normally a dry, high energy milling technique and has been employed to produce a variety of commercially useful and scientifically interesting materials. This technique was developed around 1966 by john S. Benjamin and his colleagues at the Paul D. Merica Research laboratory of the international nickel company (INCO). Mechanical alloying is a powder processing technique that allows production of homogeneous material starting from blended elemental powder mixtures. This solid state powder processing technique· involves repeated welding, fracturing, and rewelding of powder particles in high energy ball mill. Originally developed to produce oxide dispersion strengthened nickel and iron base super alloys for applications in aerospace

industry, MA has been shown to capable of synthesizing a variety of equilibrium and non-equilibrium alloy phases starting from blended elemental or prealloyed powders. The non-equilibrium phases synthesized include supersaturated solid solutions, metastable crystalline and quasicrystalline phases, nanostructures, and amorphous alloys [Suryanarayana 1999, 2001].

The actual process of MA starts with mixing of the powders in right proportion and loading the powder mixture in to the mill along with the grinding medium (Generally steel balls). This mix is then milled for desired period of time until a steady state is reached when the composition of every powder particle is same as the proportion of the elements in the powder mix. Some of the attributes of the MA process are as follows

- Extension of solid solubility limits
- Development of amorphous phases
- Production of fine dispersion of second phase(usually oxide) particles
- Refinement of grain size down to nanometer range
- Synthesis of novel crystalline and quasicrystalline phases
- Disordering of ordered intermetallics
- Inducement of chemical reactions at low temperatures
- Possibility of alloying of difficult to alloy elements
- Scaleable process

2.2.1. Raw Materials

The raw materials used for MA are widely available commercially pure powders that have particles sizes in the range of 1-200μm. But, the powder particle size is not very critical, except that should be smaller than the grinding ball size. This powder particle size decreases exponentially with time and reaches a small value of a few microns only after a few minutes of milling. The raw powders fall in to the broad categories of pure metals, master alloys, prealloyed powders, and refractory compounds. Ductile-ductile, ductile- brittle, and brittle-brittle powder mixtures are milled to produce navel alloys.

Occasionally, metal powders are milled with a liquid medium and this is referred as wet grinding. If no liquid is involved then it is referred as dry grinding. It has been reported that wet grinding method is more suitable method than dry grinding to obtain

fine-ground products because the solvent molecules are adsorbed on the newly formed surfaces of particles and lower their surface energy. The less-agglomerated condition of the powder particles in the wet condition is also a useful factor. It has been reported that the rate of amorphization is faster during wet grinding than during dry grinding. A disadvantage of wet grinding is the increased contamination of powder.

2.2.2 Types of Mills

Different types of high energy milling equipments are used to produce mechanically alloyed powders. They differ in their capacity, efficiency of milling and additional arrangements for cooling, heating, etc. A brief description of different mills is provided below.

SPEX Shaker Mills

Shaker mills such as SPEX mills which mill about 10-20 grams of powder at a time, are most commonly used for laboratory investigations and for alloy screening purposes. The common variety of the mill has one vial, containing the sample and grinding balls, secured in the clamp and swung energetically back and forth several thousand times a minute.

The back and forth shaking motion is combined with lateral movements of the ends of the vial, so that the vial appears to be described in the fig   or infinity sign as it moves. Because of the amplitude (about 5cm) and speed (about 1200 rpm) of the clamp motion, the ball velocities are high (of the order of 5m/s) and consequently the force of ball's impact is great. Therefore these mills are considered as high energy variety.

Planetary Ball Mills

Another popular mill for conducting MA experiments is the planetary ball mill (referred to as pulverisette) in which a few hundred grams of powder can be milled at a time. The planetary mill owes its name to the planet-like movement of its vials. These are arranged on a rotating support disk and a special drive mechanism causes them to rotate around their own axes. The centrifugal force produced by vials rotating around their own axes and that produced by the rotating support disk both act on the vial contents,

consisting of material to be ground and the grinding balls. Since the vials and the supporting disk rotate in the opposite directions, the centrifugal forces alternatively in like and opposite directions. This causes the grinding balls to run down the inside wall of the vial – the friction effect, followed by material being ground and the grinding balls lifting off and traveling freely through the inner chamber of the vial and colliding against the opposite inside wall – the impact effect (fig 2.6a and 2.6b)

(a)
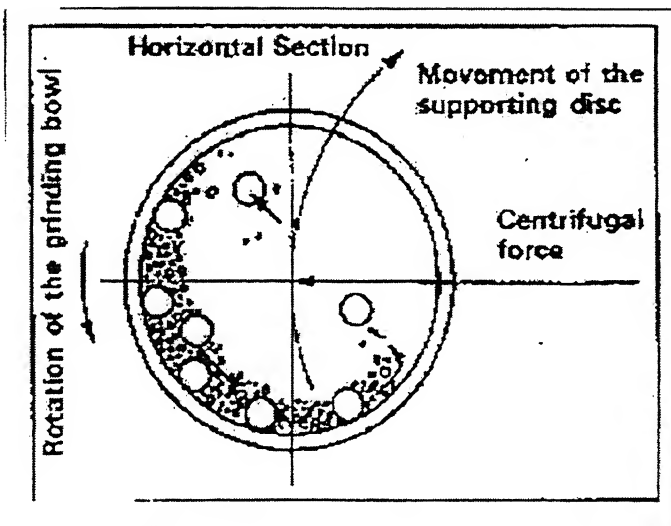
(b)

Figure2.6 (a) Fritch Pulverisette P-5 four station ball mill.(b) Schematic depicting the ball motion inside the ball mill(Courtesy of Gilson company. Inc.Washington, OH.)

Attritor Mills

A conventional ball mill consists of rotating horizontal drum half-filled with small steel balls. As the drum rotates the balls drop on the metal powder that being ground. The rate of grinding increases with the speed of rotation. Attritors are the mills in which large quantities of powder (from about 0.5 to 40 kgs) can be milled at a time.

New Designs

Several new designs of mills have been developed in the recent years for specialized purposes. These include the rod mills, vibrating frame mills, and the equipment available from Dymatron Cincinnati, OH; Super Misuni NEV -- MA -- 8 from Nisshin Giken, Tokyo, Japan (with ability to control the temperature of milling from very low temperatures by spraying liquid nitrogen up to a high temperature 300°C by electrical heating); Uni-ball-mill from Australian Scientific Instruments (it is possible to control the nature and magnitude of impact of the balls in this machine by controlling the field strength with the help of adjustable magnets) etc.

2.2.3 Process Variables

Mechanical alloying is a complex process and hence involves optimization of a number of variables to achieve the desired product phase and/ or microstructure. Some of the important parameters, that have an effect on final constitution of the powders, are

- Type of mill
- Milling container
- Milling speed
- Milling time
- Type, size, and size distribution of grinding medium
- Ball to powder weight ratio
- Extent of filling the vial
- Milling atmosphere
- Process control agent, and
- Temperature of milling

All these process are not completely independent. Even then, we will discuss the effect of these variables, assuming mostly that the other variables have no significant effect on the specific variable being discussed, on the final product obtained after MA.

Type of mill

There are number of different types of mills for conducting the MA. These mills differ in their capacity, speed of operation, and their ability to control the operation by varying the temperature of milling and the extent of minimizing the contamination of the powders. Depending on the type of the powder, and the final constitution required, a suitable mill can be adopted.

Milling Container

The material used for the milling container is important because if the material of the grinding vessel different from that of the powder, then the powder may be contaminated with the grinding vessel material during grinding. The shape of the container also seems to be important, especially in the internal design of the container. Alloying was found to occur at significantly higher rates in the flat ended vial than the round ended container

Milling Speed

It is easy to realize that the faster the mill rotates the higher would be the energy input in to the powder. But, depending on the design of the mill there are certain limitations to the maximum speed that could be employed. In the conventional mill there is an upper speed limit and that could be employed. In the conventional mill there is an upper speed limit and if the speed is increased above this critical speed (upper limit), the balls will be pinned to the inner walls of the vial and do not fall down to exert any impact force on the powder. Therefore, the maximum speed should be well below the critical speed so that balls fall down from the maximum height to produce maximum collision energy.

Another limitation is that at high speeds, the temperature of the vial may reach a value. This may be advantageous in some cases where diffusion is required to promote

homogenization and/ or alloying in the powders. But, in some cases, this increase in temperature may be disadvantage because the increased temperature accelerates the transformation process and results in the decomposition of supersaturated solid solutions or other metastable phases formed during milling. Additionally, the high temperature generated may also contaminate the powders. It has been reported that during nanocrystal formation, the average crystal size increases and the strain decreases at higher milling intensities due to the enhanced dynamical recrystallization [Surayanarayana 1999, 2001].

Milling Time

The milling time is the most important parameter. Normally the time is so chosen as to achieve a steady state between the fracturing and cold welding of the powder particles. The times required vary depending on the type of the mills used, the intensity of the milling, the ball-to-powder ratio, and the temperature of milling. It should be noted that the level of contamination increases as the milling time is increased hence it is desirable that the powder is milled just for the required duration and not any longer.

Grinding Medium

The density of the grinding medium is high enough so that the balls create enough impact force on the powder. It is always desirable to have the grinding vessel and the grinding medium made of the same material as the powder being milled to avoid cross contamination. The size of the grinding medium also has an influence on the milling efficiency. A larger size (and high density) of the grinding medium is useful since the larger weight of the balls will transfer more impact energy to the powder particles. It has been reported that the final constitution of the powder is dependent upon the size of the grinding medium used.

Ball-to-Powder Weight Ratio

The ratio of the weight of the balls to the powder (BPR),some times referred to as charge ratio (CR), is an important variable in the milling process. This has been varied by different investigators from a value as low as 1:1 to as high as 20:1 . The higher the BPR, the shorter is the time required to achieve a particular phase in the powder being milled.

At high BPR more energy is transferred to the powder particles and so alloying takes place faster. It is also possible that due to higher energy, more heat is generated and this could change the constitution of the powder. The amorphous phase may even crystallize if the temperature rise is substantial [Suryanarayana 2001].

Extent of Filling the Vial

Since alloying among powder particles occurs due to impact forces exerted on them, it is necessary that should be enough space for the balls and powder particles to move around freely in the milling container.

Milling Atmosphere

The major effect of the milling atmosphere is on the contamination of the powder. Therefore, the powders are milled in the container that have been either evacuated or filled with an argon gas such as argon or helium.

Process Control Agents

The powder particles get cold welded to each other, especially if they are ductile, due to the heavy plastic deformation experienced by them during milling. But, true alloying among the powder particles can occur only when balance is maintained between cold welding and fracturing of the particles. A process control agent (PCA), also referred to as lubricant or surfactant, is added to the powder mixture during milling to reduce the effect of cold welding.

The PCAs can be solids, liquids or gasses. They are mostly organic compounds, which act as surface active agents. The PCA adsorbs on the surface of the powder particles and minimizes cold welding between powder particles and thereby inhibits agglomeration. The surface-active agents adsorbed on the particle surfaces interfere with cold welding and lower the surface tension of the solid material. Since the energy required for the physical process of size reduction, E is given by

$$E = \gamma \, \Delta S \qquad\qquad\qquad (7)$$

Where γ is the specific surface energy and ΔS is the increase of surface area, a reduction in surface energy results in the use of shorter milling times and/or generation of finer powders [Suryanarayana 2001].

A wide range of PCAs has been used in practice at a level of about 1-5 wt% of the total powder charge. The most important of the PCAs include stearic acid, hexane, methonal, ethanol, and acetone. The choice of a PCA for milling depends on the nature of the powder being milled and the purity of the final product desired.

Temperature of Milling

The temperature of the milling is another important parameter in deciding the constitution of the milled powder. Since diffusion process are involved in the formation of alloy phases irrespective of whether the final product phase is solid solution, intermetallics, nanostructure, or an amorphous phase, it is expected that the temperature of milling will have a significant effect in any alloy system.

During the formation of nanocrystals, it was reported that the root mean square (rms) strain the material was lower and the grain size larger for materials milled at higher temperatures. For example, during planetary ball milling of a Cu-37at% Ag powder mixture, it was noted that the mixture of an amorphous and crystalline (supersaturated solid solution) phases was obtained on milling at room temperature; instead, only a Cu-8at%Ag solid solution was obtained on milling the powder at 200°C. Similar results were also obtained in the Cu-Ag, Zr-Al, and Ni-Ag alloy systems and were explained on the basis of the increased diffusivity and equilibrium effects at higher temperatures of milling.

2.2.4   Mechanism of Mechanical Alloying

During high-energy ball milling the powder particles are repeatedly flattened, cold-welded, fractured and rewelded. Whenever two balls collide, some amount of powder is trapped in between them. Typically, around 1000 particles with an aggregate weight of about 0.2 mg are trapped during each collision. The force of impact plastically deforms the powder particles leading to work hardening and fracture (Figure 2.7). The new surfaces created enable the particles to weld together and this leads to an increase in

particle size. Since in the early stages of milling, the particles are soft (if we are using either ductile to ductile or ductile-brittle material combination), their tendency to weld together and form large particles is high. A broad range of particle sizes develops, with some as large as three times bigger than the starting particles. The composite particles of
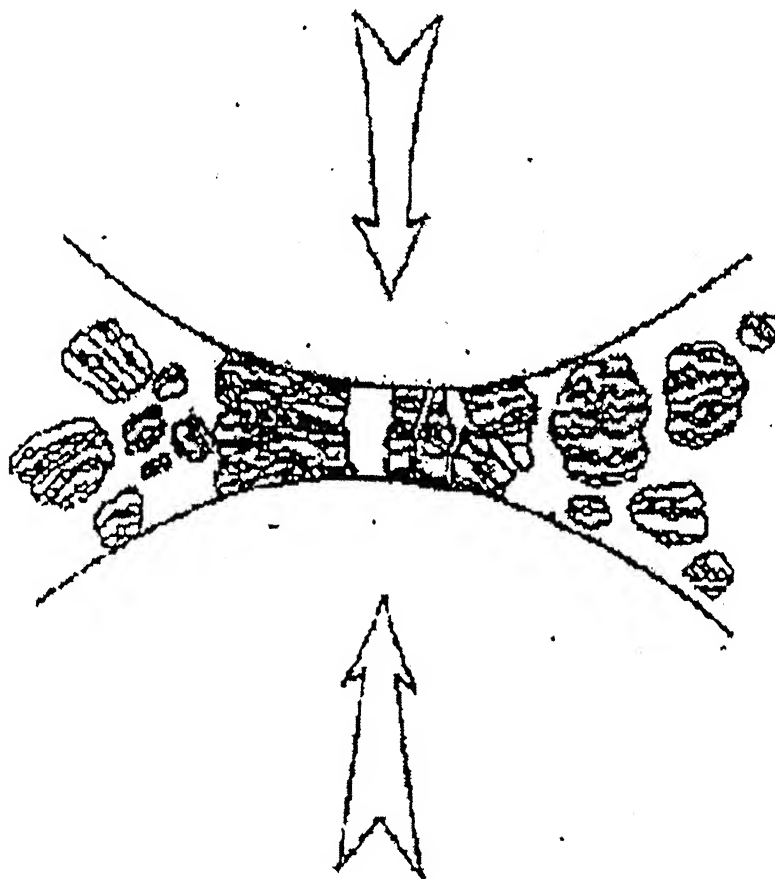

Figure2.7Ball powder ball collision of powder mixture during Mechanical alloying
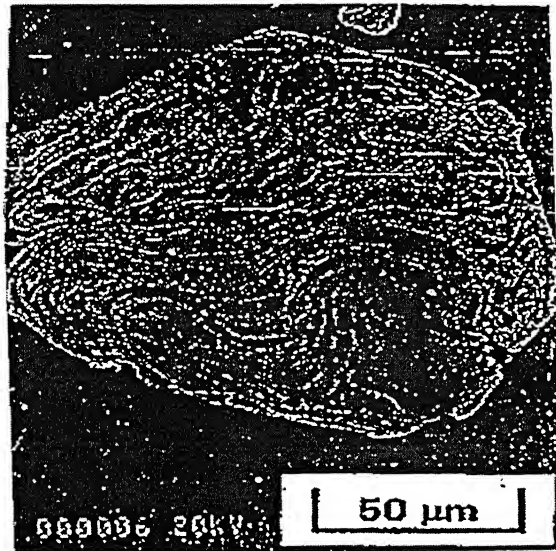
Figure2.8 Scanning electron micrograph depicting the convoluted lamellar structure obtained during milling of a ductile-ductile component system (Ag-Cu).

This stage have a characteristics layered structure consisting of various combinations of starting constituents (Figure 2.8) [Surayanarayana 1999, 2001]. With continued deformation, the particles get work hardened and fracture by fatigue failure mechanism and/ or by the fragmentation of fragile flakes.

Fragments generated by this mechanism may continue to reduce in size in the absence of strong agglomerating forces. At this stage, the tendency to fracture predominates over the cold welding. Due to the continued impact of the grinding balls, the structure of the particles is steadily refined, but the particle size continues to be same. Consequently, the interlayer spacing decreases and the number of layers in the particle increases. However, it should be noted that the efficiency of the particle size reduction is very low, about 0.1% in a conventional ball mill. The efficiency may be somewhat higher

in high-energy ball milling processes, but is still less than 1%. The remaining energy lost in the form of heat, but a small amount is also utilized in the elastic and plastic deformation of the powder particles.

After milling for a certain period of time, steady state equilibrium is attained when a balance is achieved between the rate of welding, which tends to increase the average particle size, and the rate of fracturing, which tend to decrease the average composite particle size. Similar particles are able to with stand deformation without fracturing and tend to be welded in larger pieces, with an overall tendency to drive both very fine and very large particles towards intermediate size. At this stage each particle contains substantially all of the starting ingredients, in the proportion they were mixed together and the particles reach saturation hardness due to the accumulation of the strain energy. The particle size distribution at this stage is narrow, because particles larger than average size at the same rate that fragments smaller than average grow through agglomeration of smaller particles (Figure 2.9).

From the foregoing it is clear that during MA, heavy deformation is introduced in to the particles. This is manifested by the presence of a variety of crystal defects such as dislocations, vacancies, staking faults, and increased number of grain boundaries. The presence of this defect structure enhances the diffusivity of solute element in to the matrix. Further, the refined micro structural features decrease the diffusion distances. Additionally, the slight rise in temperature during milling further aids the diffusion behavior, and consequently, true alloying takes place amongst the constituent elements. While this alloying generally takes place normally at room temperature, sometimes it may be necessary to anneal the mechanically alloyed powder at elevated temperature for alloying to be achieved. This is particularly true when formation of intermetallics is desired.

The specific times required to develop a grain structure in any system would be a function of the initial particle size and characteristics of ingredients as well as the specific equipment used for conducting the mechanical alloying operation and the operating parameters of the equipment. But, in the most cases, the rate of refinement of the internal structure (particle size, crystallite size, lamellar spacing, etc.) is roughly logarithmic with

processing time and therefore the size of the starting particles is relatively unimportant. In a few minutes to an hour, the lamellar spacing becomes small and the crystallite(or grain) size is refined to nano dimensions (Figure 2.10). The ease with which nanostructured material can be synthesized is one reason why MA has been extensively employed to produce nanocrystalline materials.
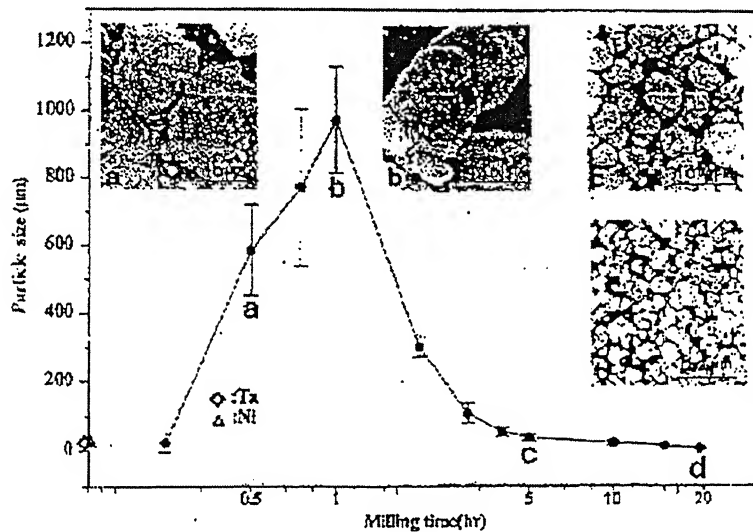

Figure2.9 Narrow particle size distribution caused by tendency of small   particles to weld together and large particles to fracture under steady-state conditions
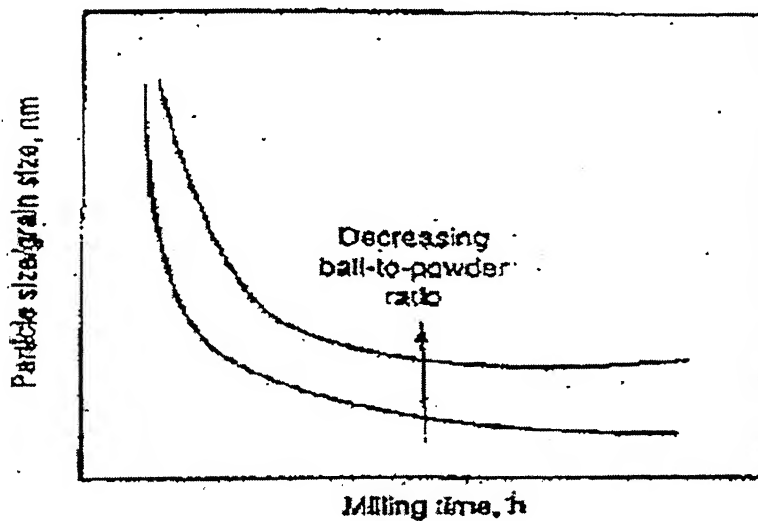

Figure2.10 Refinement of particles and grain sizes with milling time

43

2.2.4 Applications of Mechanical Alloying

The technique of MA has been shown to produce a variety of materials. The most important reason for the invention and development of the MA process was the production of oxide dispersion strengthened (ODS) materials in which fine particles of Y_2O_3 or ThO_2 were uniformly dispersed in a nickel or iron based super alloy. Investigations have revealed that MA can synthesize metastable phases such as super saturated solid solutions, nonequilibrium crystalline or quasicrystalline intermediate phases and amorphous alloys. In addition, nanostructures with grain size of a few nanometers, typically <100nm, are produced. These metastable phases have interesting combinations of physical, chemical, mechanical, and magnetic properties and are being widely explored for potential applications.

Mechanically alloyed materials find applications in variety of industries. The applications include synthesis and processing of advanced materials (magnetic materials, superconductors, and functional ceramics), intermetallics, nanocomposites, catalysts, hydrogen storage materials, food heaters, gas absorbers, and also in the modification of organic compounds, waste management, and production of fertilizers. But, the major applications of mechanically alloyed materials have been in the areas of thermal processing, glass processing, energy production, aerospace, and other industries

2.3 Fe-Cr System

The system Fe-Cr has been repeatedly investigated, and its interest lies both in its complexity and in the major importance of Fe-Cr alloys to the industry.

2.3.1 Fe-Cr phase diagram

Fe-Cr phase diagram showing that the liquidus and solidus lines of the system intersect, forming a minimum on the melting point curve some what above 1400° at 10 – 15 % Cr. The liquidus temperature minimum in the system is at 20% Cr and 1510°, as shown in the Fig. Between 40 and 100% Cr showed narrower solidification range. The maximum solubility of chromium in γ-Fe is 12%.
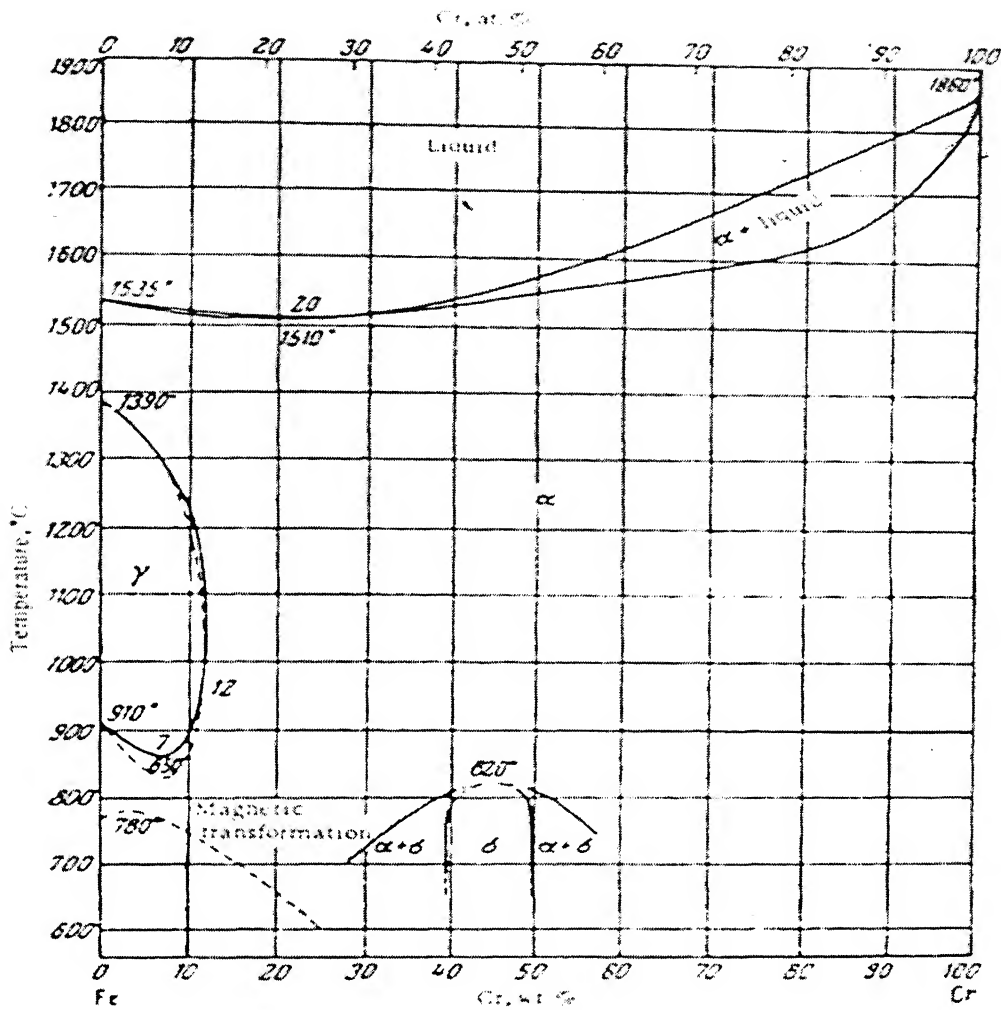
Figure 2.11 Fe-Cr binary Phase diagram

However carbon and nitrogen increases the chromium solubility in γ-Fe. The transformation α→γ is accomplished by considerable hysteresis, especially at low temperatures. The curve in the diagram represent this hysterisis and not the boundaries of the bi phase field (α+γ), the continuous line represents the data obtained on heating, while the dotted line represents the data obtained on cooling. Alloy containing 8.25% Cr the structure observed to be body centered cubic lattice (α-Fe) at this temperature. In alloys with 16.8% Cr the lattice is preserved up to 800°, and between 810° and 900° it has biphase structure. The transformation of α→γ is diffusionless. There is a possible formation of superstructures of the compound FeCr(48.22% Cr) as a result of ordering of α-solid solution. It was also established that the compound FeCr has the structure of a σ-phase, and the rate of formation is very slow. The alloys obtained powder metallurgy, a

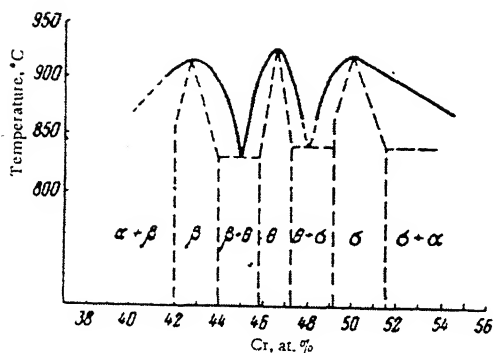complete transition of α- into σ phase may be attained by 10 days holding at 650° in evacuated tubes.

Figure2.12. Solid state Transformations in Fe-Cr binary phase diagram

Alloys containing 36.1 – 54.5.at % Cr were observed for microscopic and magnetic analysis, and also by determining the rates of conversion (from the change in the saturation magnetization), there is evidence in favor of the existence of three superstructures in the system: β, θ, and σ. The homogeneity fields of these phases correspond, respectively, to 41.9 – 44.2 at. % Cr, 45.7 – 47.2 at. % Cr and 49.2 – 51.5 at.% Cr. It is also claimed that the system contains also the biphase eutectoid field (β+θ) and (θ+σ).   In addition to non magnetic σ-phase, three metastable ferromagnetic superstructures are also formed in the system:Fe_3Cr, FeCr and $FeCr_3$, and two metastable compounds: Fe_2Cr and $FeCr_2$.   Of all these FeCr is metastable phase, intermediate between the disordered α- solid solution and the stable σ- phase. The solubility at room temperature of chromium in α-Fe and of iron in Cr is insignificant. σ – Phase was unstable below room temperature.

2.3.2 Crystal structure of Fe-Cr alloys

The variation of lattice spacing of the α-Fe-base solid solution was increased with increase in composition of the Cr. Crystal structure of the α solid solution is BCC. And crystal structure of the σ-phase was reported as cubic[88] and orthorhombic[89].It may, however, be taken as definitely established at present that the structure is tetragonal, similarly to the corresponding phases of other systems, with 30 atoms in the elementary cell. Lattice constants of the σ-phase determined by several workers and are reported a=8.7995 A°, c= 4.5442 A° and c/a = 0.5164.

2.3.3 Physical Properties

Density

With increase in the chromium content the density of Fe-Cr alloys decreases linearly from 7.86g/cm^3 for iron to 7.19g/cm^3 for chromium. The density of the alloy containing 49.68 at. % Cr and having the structure of the α- phase is 7.50g/cm^3, while the density of the alloy having the structure of the σ-phase is 7.55g/cm^3, the specific volume of the σ-phase near the transformation temperature is 0.24% less than the specific volume of an alloy of the same composition in a disordered state.

Mechanical Properties

The hardness of alloys increases considerably as a result of the ordering of the α-Solid solution and formation of the σ- phase. Vickers hardness of an alloy with 48% Cr is 220kg/mm^2 when disordered, and 950kg/mm^2 in ordered state(σ-phase), an alloy containing ~50at.%Cr the Vickers hardness of the α- phase is 240, while that of the σ-phase is ~800kg/mm^2. The hardness of the σ-phase depends on the conditions of the thermal treatment of the alloy and may vary from 230 to 3000kg/mm^2

Chromium present in concentrations of up to 3% has almost no effect on the tensile strength of ferrite. The tensile strength and yield strength of iron decreases on the addition of up to ~4% Cr as shown in the Table 2.3 and 2.4 in the presence of 5% Cr these values are slightly higher than and very close to the corresponding parameters of the initial iron reduces the temperature threshold of brittleness of iron. All the alloys with less than 12.8% Cr acquire increased hardness when quenched from the γ-field as shown in Figure 2.13. Thus, the yield strength of iron alloyed with chromium increases from 28 to 76kg/mm^2 as a result of quenching, and lateral reduction decreases from 20 to 2% at the same time.
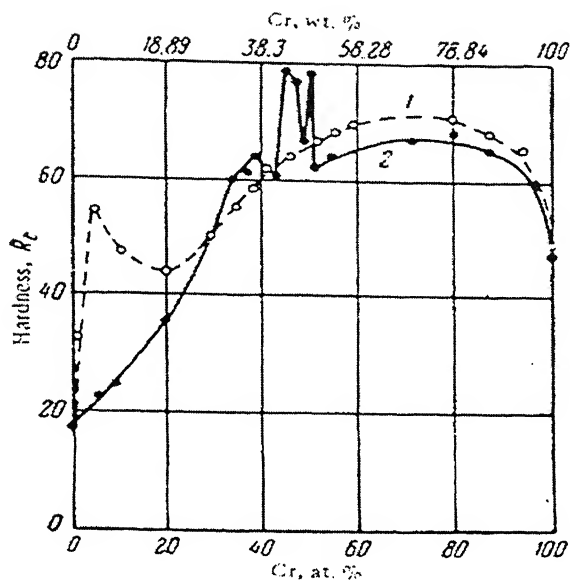
Figure 2.13 Effect of Cr on hardness of cast Fe-Cr alloy

Table 2.3 Effect of Cr on the strength properties of Fe-Cr alloy

Cr ,%	Proportional limit, kg/mm^2	Yield strength, kg/mm^2	Tensile strength ,kg/mm^2	Relative elongation, %	Relative reduction, %	Impact strength, kgm/cm^2		Vicker's Hardness, kg/mm^2
						At 0^{0}C	At - 80^{0}C	
Fe	19.8	21.5	38.8	32.5	74.7	25.6	1.6	92
0.84	22.8	22.3	38.5	34.0	83.4	33.0	0.9	93
1.24	21.1	22.0	36.8	34.5	81.8	28.36	1.6	89
3.20	20.0	21.4	37.3	34.3	83.5	28.7	0.9	97
4.17	22.7	25.5	40.7	35.3	81.7	23.7	14.8	115

48

Table 2.4 Effect of Cr on the strength properties of Fe-Cr alloy

Cr,%	Yield strength, kg/mm^2	Tensile strength, kg/mm^2	Relative elongation,%	Relative reduction,%	Elastic modulus, kg/mm^2
49.0	55.3	63.7	27	83	22,500
61.2	68.8	91.7	12	10	23,400
Cr	36.8	42.0	44	78	29,400

Table 2.5 Effect of Cr on the Elastic Modulus and Shear modulus of Fe-Cr alloy

Cr, at%	Elastic modulus, kg/mm^2		Shear modulus, kg/mm^2	
	annealed	quenched	annealed	Quenched
0.92	21,690	21,560	8,330	8,440
1.93	21,720	21,740	8,380	8,480
3.99	21,940	21,610	8,440	8,480
5.02	22,000	21,780	8,480	8,380
7.22	22,040	22,110	8,560	8,515
14.78	22,260	22,140	8,640	8,040

Table 2.6 Effect of Cr on the Fatigue limit and ratio of fatigue limit to tensile strength

Cr, at%	Fatigue limit,kg/mm^2	Tensile strength,kg/mm^2	Ratio of fatigue limit to tensile strength
0.00	11.2	23.8	0.47
1.07	11.6	24.8	0.47
5.30	12.6	27.0	0.47

Elastic modulus increases with increase in % Cr in the Fe-Cr alloy. Shear modulus increases with increase in % Cr for the Fe-Cr alloy in annealed condition as shown in the Table 2.5, as it was fluctuating in the quenched condition. When present in concentrations of up to 5.3 at % chromium has only an insignificant effect on the fatigue limit of the alloys as shown in Table 3.4. Addition of 0.5 % Cr produces a sharp increase in the creep strength of iron. Further increase in the content of chromium results in a small, smooth increase of this parameter in the alloys. The presence of chromium increases the heat resistance of iron. At 850° the most heat resistant alloys in the system are those containing more than 35% Cr. Addition of small amount of Fe to the Cr increases the temperature of the brittle transition. The mechanical properties of Fe-Cr alloys strongly depend both on the quality of the initial components and on the conditions of preparation. Thus for instance, an alloy containing 25% Cr, melted in an electrical furnace, after being forged at 600-800° and quenched from 1200° had an impact strength of 1.2 kgm/cm^2; after remelting in vacuo and similar treatment, its impact strength increased to 31.6 – 33.8 kgm/cm^2.

Heat capacity

The specific heat of Fe-Cr alloys increases with increase in %Cr. The specific heat of a carbon free alloy of 30% Fe with 70% Cr between 273-300°,273-700°, and 273-1000°K is 0.1135, 0.1275, and 0.1365 cal/g . °C respectively.

Thermal conductance

Thermal conductance decreases of Fe-Cr alloys decreases with increase in %Cr up to 18% Cr and it is again increases as the %Cr increased. It was shown in the Figure 2.14

Thermal Expansion

The thermal expansion of Fe-Cr alloy was shown in the Fig., indicates that there is slight increase in linear expansion coefficient of iron on the addition of ~ 1.5 at. % Cr, and a considerable drop in this parameter when the chromium content is increased to 6

at.%. The average linear expansion coefficient between 0 and 700° of alloys with 0, 1.0 and 25%Cr is $14.9*10^{-6}$, $12.9*10^{-6}$ and $12*10^{-6}$ respectively
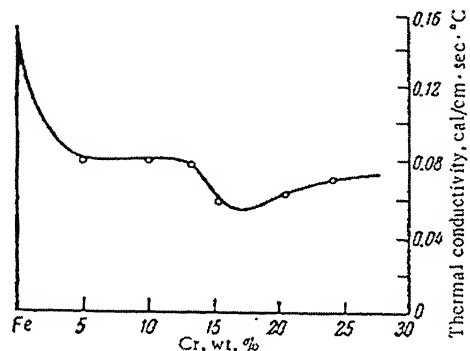

Figure 2.14 Effect of Cr on the thermal conductivity of Fe-Cr alloy

Electrical resistance and its temperature coefficient

With increase in chromium content in iron-rich alloys and of the iron content in chromium-rich alloys, their electrical resistance increases rapidly. The maximum resistivity in the homogeneous state is displayed by alloys with about 50 at.%Cr. The electrical resistivity and the temperature coefficient of electrical resistance of more strongly contaminated alloys between 25 and 100° is shown in the Figure 2.15
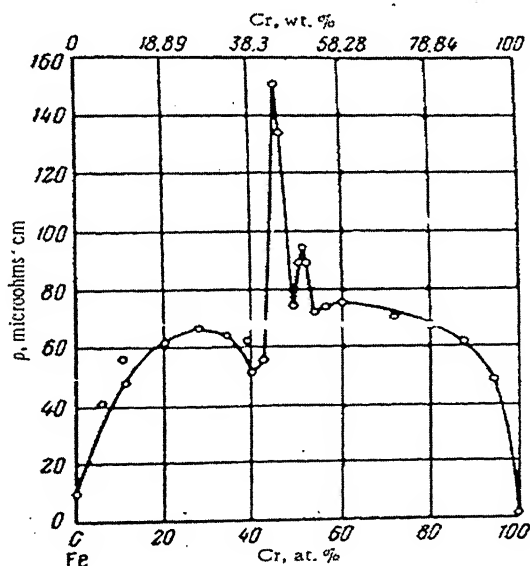
Figure 2.15 Effect of Cr on the Electrical resistivity of Fe-Cr alloy

Magnetic properties

The variation of the coercivity of Fe-Cr alloys with the composition shown in the Figure 2.16. It follows from the curve that the presence of up to 8% Cr in the alloys produces a very small increases in their coercivity as compared with the initial iron, when quenched to martensite, chromium considerably increase the coercivity of iron. When the iron content increased to 10 at. %, the magnetic suceptability of chromium rich alloys in the system increases. The curie point of the alloys decreases from 769 to 95° with increase in chromium content from 0-58.61%. In the range 42.72-55.72 at.% Cr (41-53.93% Cr) Fe-Cr alloys are nonmagnetic. The variation of the curie point of the alloys with the composition will be found in the phase diagram. The curie point of the σ-phase at 46.4 at.% Cr is at 163°K. Magnetic permeability decreases with increase in % Cr as shown in the Figure 2.17
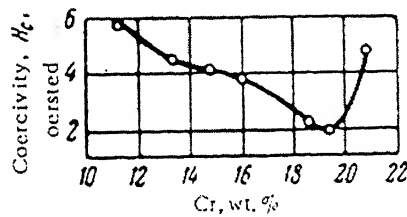
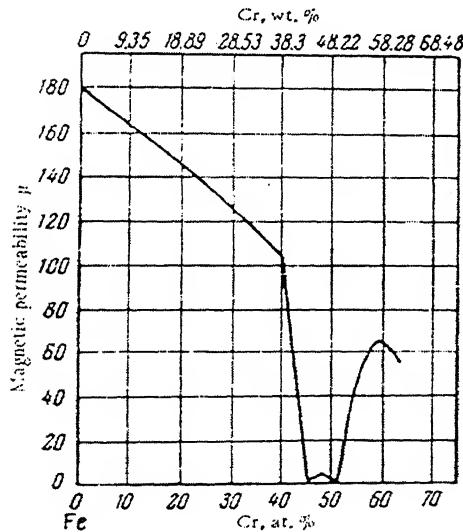Figure 2.16 Effect of Cr on the Coercivity of Fe-Cr alloy

Figure 2.17 Effect of Cr on the magnetic permeability of Fe-Cr alloy

2.3.4   Chemical properties

Resistance to atmosphere corrosion at ordinary and elevated temperature

An increase in the chromium content from 0 to 18% results in a rap increase of the resistance of the alloys to atmospheric corrosion, both at ordinary and at elevated temperatures. The increase in chromium content has a similar effect on the resistance of the alloys to corrosion at elevated and high temperature. When alloys with 5-30% Cr were held at 900° for several hundred hours, there was no significant oxidation. A fine oxide film was formed on the alloys, which adhered firmly to the metal and protected it from further oxidation. The rate of oxidation of Armco iron at 850° in an atmosphere of water vapor decreased to one-half in the presence of 3.2% Cr, and in the presence of 16% Cr it was 25 times slower; in the presence of 31.3% Cr the oxidation process was ceased altogether.

Corrosion resistance in solutions of salts, acids and alkalis

An alloy containing 28% Cr had a high resistance to corrosion in an atmosphere of SO_2. The surface layer on Armco iron, which had been obtained by diffusion chrome plating and containing 13% Cr was resistant to corrosion in soft water. Alloys containing more than 12% Cr have a satisfactory corrosion resistance in the oxygenated media. Alloys with more than 11.5% Cr are passive in 4% NaCl, if contaminated with hydrogen, passivity begins with more than 15% Cr. Alloy containing 12.5% at.% Cr is not corroded by nitric acid of any concentration at 20°, but was not stable in boiling nitric acid. Iron – Chromium alloys have a satisfactory stability in alkali solutions at ordinary temperatures, but at elevated temperature corrode more strongly than iron. In solutions of salts, even neutral or basic salts, containing large concentrations of halides, especially chlorides, Fe-Cr alloys show pitting, and in some media corrosional cracking under stress.

Solubility of hydrogen, oxygen and nitrogen

The capacity alloys to absorb hydrogen decreases with the increase in chromium content, and attain maximum values between 15 and 30% Cr. When the Cr content increased from 0-6%, the solubility of oxygen in the liquid alloys decreases, and then gradually increases as the chromium content is raised to 50%. The solubility of nitrogen in both liquid and solid alloys increases with the increase in content of chromium. The presence of dissolved nitrogen increases the area of the γ-field in the system, nitrogen forms with chromium the nitride CrN at 600°.

EXPERIMENTAL PROCEDURES

3.1   POWDER MILLING

Iron and chromium powders of greater than 99.99 % purity were used for the purpose of mechanical alloying. Powders had been sealed and stored in the argon glove box thus had no oxygen contamination during their storage. Fe as well as C powders corresponding to Fe – 5 wt % Cr, Fe – 10 wt % Cr, Fe – 15 wt % Cr and Fe – 20 wt % Cr were separately weighed in the argon glove box itself. Each milling batch for the above compositions comprised of 50 – 55 gms. Weighed powders for each composition, along with grinding media steel balls, were transferred in the steel jars within the argon glove box itself. The milling charge could thus be maintained under the argon atmosphere. Charge to ball ratio for each milling operation was maintained as 1:8. Size of the balls used was 10 mm. Powder milling was carried out in a Retsch type planetary ball mill. The milling speed was kept at 250 rpm

For the purpose of monitoring the nature of milling and alloying in Fe – 10 wt % Cr and Fe – 20 wt % Cr alloy compositions, the milling operation was intermittently stopped after milling time of 5 hrs, 10 hrs, 15 hrs, 20 hrs, 40 hrs, 65 hrs and 100 hrs. After each of such operations milling jars were transferred to the argon glove box and small amounts of powder samples (roughly 1 – 1.5 gms) were taken out for the purpose of their characterization. For powders corresponding to the compositions of Fe – 5 wt % Cr and Fe – 15 wt % Cr, the milling was done for the periods of 65 hrs and 100 hrs.

Powders of all the four Fe – Cr compositions were taken out in the argon glove box after the milling time of 100 hrs. They could thus be sealed in plastic bottles under the argon atmosphere.

Figure3.1 showing the Retsch planetary ball mill

3.2   X-RAY DIFFRACTION

Powder samples taken out of the planetary ball mill after different time intervals, and were characterized using X-ray diffraction technique. The bulk compacted samples were also characterized by this method. This instrument used was Seifert ISO-DEBYFLEX 2002 diffractometer with copper target. The tube was operated at 30kV and 10mA. The radiation used was Cu Kα having wavelength of 1.540598 A°. The scanning rate in the X-ray powder diffraction was kept at 3°/min and 0.3°/min.

3.2.1   Phase Identification

Phase identification of the XRD patterns of the milled powders were done by using JSPDS standard files.

3.2.2   Crystallite Size Determination of Mechanically Alloyed Fe-Cr Powders

The grain sizes of the powder samples were determined by using "PEAKOC" software. The details about this software are as follows:

PEAKOC Software

"PEAKOC" is a general profile fitting computer program written in C++ programming language. It is particularly suitable for the INEL CPS detector data as it runs with the INEL data format and performs CPS calibration (files). But it can treat any other raw data in ASCII format too (from Bragg Brentano setting for instance). Peakoc allows fitting peak-by-peak diffractogram under windows. Six peak shapes are proposed in this software: Gaussian, Lorentzian, pearson VII, Voigt, Pseudo Voigt (PV) and split Pseudo (SPV). " Peakoc" is able to perform background removing, smoothening or Kα_2 stripping.

Analysis of Crystallite Size and Nano Structure:

The data collected from the diffractometer were converted in to the required format for the software. The X-ray diffraction pattern was fitted with a Gaussian

function convoluted with an asymmetric function using the "PEAKOC" software for diffraction. The whole pattern was fitted in multiple steps along with a parabolic varying background. A nonlinear least square-fitting algorithm was used to minimize the residuals. Usual correction for the q-dependent part of the diffraction pattern was applied. The effect of diffraction of $K\alpha_2$ line was removed with the correction for the instrumental broadening. Both the profile shape parameters (viz. peak position 2q, maximum intensity I, half width w and pV mixing parameter h) along with the background were refined simultaneously.

The grain size was calculated using Pseudo-Voigt function. The PEAKOC software gives the values of 2θ and FWHM (full width at half maximum). To remove the instrumental broadening effects from the FWHM, the following procedure was adopted. We eliminated the FWHM value (of the peak at same position as in our sample under investigation) of standard Si sample from the FWHM value of sample under investigation by following approximation:

$$B = (W^2 - W_s^2)^{1/2} \qquad (8)$$

where, B is full width at half maximum after suitable correction, W is the FWHM of the sample under consideration and W_s is the FWHM of standard, Silicon in the present case.

The value of B thus obtained is put in the Scherrer's formula to calculate the value of crystallite size which states that .

$$D = K\lambda/(B*Cos\theta) \qquad (9)$$

where K is Scherrer's constant, λ is wavelength of copper $K\alpha$ radiation, θ is half of the value of 2θ in radians.

3.3 MICROSCOPY

3.3.1 Optical Metallography

Sample preparation for the microstructural studies consisted of standard emery paper polishing followed by fine cloth polishing with 0.3 μm alumina abrasive

in suspension with water. Compacted sample was first polished on the polishing wheel, followed by polished on the emery papers from coarse to fine papers of having numbers 1-4 respectively. These samples are then polished on the cloth-polishing machine with 0.3μm alumina abrasive in suspension with water. Samples were cleaned and dried, followed by imaging in the optical microscope.

3.3.2 Scanning Electron Microscopy

Powder morphology of mechanical alloyed powders was analyzed under a JOEL JSM 840A Scanning Electron Microscopy (SEM). The milled powder morphologies were observed by dispersing the powders with acetone on finely polished brass stubs prepared especially for this purpose.

3.3.3 Atomic Force Microscopy

The samples were imaged with atomic force microscopy (Molecular Imaging, USA), operated on Acoustic AC mode (AAC) with the aid of cantilever (NSC 12 (c) from MikroMasch). The force constant was 2.4 N/m, while the resonant frequency was 150 kHz. The images were taken in air at room temperature, with the scan speed of 1.5-2.2 lines/sec. Data acquisition was done by using PicoScan5 software, while the data analysis was done with the aid of visual SPM. The Fe_{100-x}-Cr_x x=10 mechanically alloyed powders of different milling time of 5hr, 20hr, 40hr, 65hr; 100hr are sprinkled over the freshly cleaved mica surface, and uniformly spread with the aid of spin-coater. Then mica was dried for 30 min, at room temperature, followed by immediately imaged with AFM.

3.4   MÖSSBAUER SPECTROSCOPY

The technique of Mössbauer spectroscopy involves using the gamma rays emitted from the nuclei of a radioactive source [57]Co to probe those in the sample to be studied. The source contains the parent nucleus of the Mössbauer isotope, embedded in a rigid matrix to ensure a high f factor. The gamma rays emitted from this are passed through the material being investigated and those transmitted through the absorber are detected and counted.

If the nuclei in the source and absorber are in the exact same environment (i.e. the energy of the nuclear transition is equal in both nuclei) the gamma rays will be resonantly absorbed and an absorption peak will be observed. In order to probe the energy levels in nuclei in different environments we must scan the energy of the Mossbauer gamma ray. This is achieved by moving the source relative to the absorber. The Doppler effect produces an energy shift in the gamma ray energy allowing us to match the resonant energy level in the absorber.

3.5 DIFFERENTIAL THERMAL ANALYSIS

Differential Thermal Analysis was done using PYRIS DIAMOND TG/DTA. 150 mg weight of the milled powder was taken for the analysis. The sample was heated from room temperature to 1150°C under the H_2 atmosphere at a heating rate 10°C/min. The thermocouple (platinum-platinum rhodium13%) for DTA measurement was incorporated in the end of each of the balance beam ceramic tubes, and the temperature difference between the holder on the sample side and the holder on the reference side was detected.

3.6 HARDNESS TESTING

Hardness values of the powders were determined by using CARL ZEISS JANA GERMANY 160 Microhardness Tester. The hardness values of the powders were determined under 20gm of load. Microhardness, μH, was calculated by

$$\mu H = 1854 \, P/D^2 \text{ in Kg/mm}^2 \tag{10}$$

where P is the load in gms and D is the diameter of the two diagonals in μm.

3.7 POWDER COMPACTION AND SINTERING

The consolidation of milled powders were done in stainless steel cylindrical die and the applied pressure of 4 tons under the APEX Hydraulic Press for the powders $Fe_{100-x}Cr_x$ x=5, 10, 15, 20. milled for 100hours. The size of the compacts was 5mm diameter and 5mm height. Green compacts were subjected to sintering at 650°C for 45min and heating rate of 5°C/min under the argon atmosphere.

RESULTS AND DISCUSSIONS

4.1. CHARACTERIZATION OF THE MECHANICALLY ALLOYED Fe-Cr POWDERS

4.1.1 X-Ray Diffraction

The progress of alloying in mechanically alloyed powders during the course of milling can generally be inferred by taking the X-ray diffraction patterns from powders milled for different time intervals. For this purpose, high intensity peaks corresponding to diffraction from the constituent elements (in the present case Fe and Cr) are monitored with respect to milling time and it is seen whether other peaks corresponding to new phases formed by mechanical alloying develop or not. The standard 2θ values and the corresponding planes of diffraction for pure Fe, pure Cr and Fe-Cr solid solutions, as obtained from the JCPDS files, are shown in Table 4.3. Identification of phases formed during the course of milling was done using these values as the standard values. It is seen that pure Fe, pure Cr and solid solutions of Fe and Cr give first three highest intensity peaks from planes (110), (211) and (200) respectively. Further, it should be noted down that peaks corresponding to all the three planes occur at very close 2θ values for pure Fe, pure Cr and solid solutions of Fe-Cr.

The XRD patterns of MA $Fe_{90}Cr_{10}$ and $Fe_{80}Cr_{20}$ milled for 5 hrs, 10 hrs, 20 hrs, 40 hrs, 65 hrs and 100 hrs are shown in Figures 4.1 and 4.2 respectively. The corresponding data for the diffraction from these powders are also shown in Tables 4.1 and 4.2. As expected from the standard data, these XRD patterns of 100 hrs milled $Fe_{100-x}Cr_x$ [x = 10, 20] alloys show three prominent peaks at 2θ values of 44.73, 65.26, and 82.51 (for x = 10) and 45.05, 65.6, and 82.7 (for x = 20) respectively, in the order of decreasing intensity. By comparing 2θ values and peak

intensities obtained from MA $Fe_{100-x}Cr_x$ [x = 10, 20] powders it was concluded that these peaks corresponded to planes (110), (200) and (211) respectively. Absence of any other peak(s) in the XRD patterns, as obtained from the milled powders, shows that no oxides or other phases were formed during alloying by oxidation or contamination of powders coming from either the milling vials or the balls. This was expected because, as explained in Section 3.1 of chapter 3, the powders as well as the milling balls were loaded in the vials inside the glove box itself under the argon cover. The milling of powders could thus be done under an inert atmosphere cover.

It is to be noted that both Fe and Cr crystallize in the body-centered cubic (bcc) structure and the difference in their lattice parameters is only 0.5%. Because the diffraction peaks from Cr and Fe overlap, the progress of mechanical alloying, i.e. consumption of elemental Cr and Fe powders by the formation of their solid solution, in terms of decrease in peak intensities corresponding to Fe and Cr and formation of new peaks was very difficult to be inferred through XRD technique. Similar difficulties have also been faced by earlier investigators [Murugesan et al]. The progress of mechanical alloying with increase in milling time was thus very difficult to be inferred by X-ray diffraction studies. As discussed in Section 4.1.3, this could be done by Mossbauer spectroscopy.
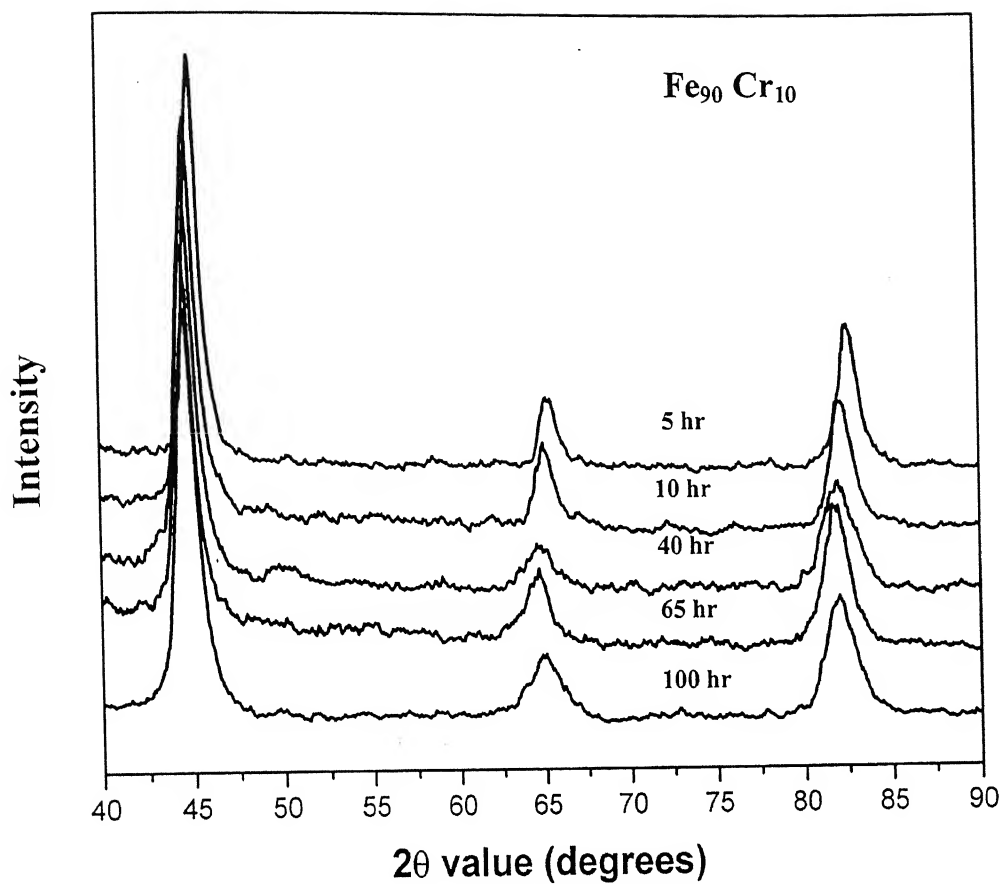
Figure 4.1: XRD showing $Fe_{80} Cr_{10}$ milled powders corresponding to different milling time
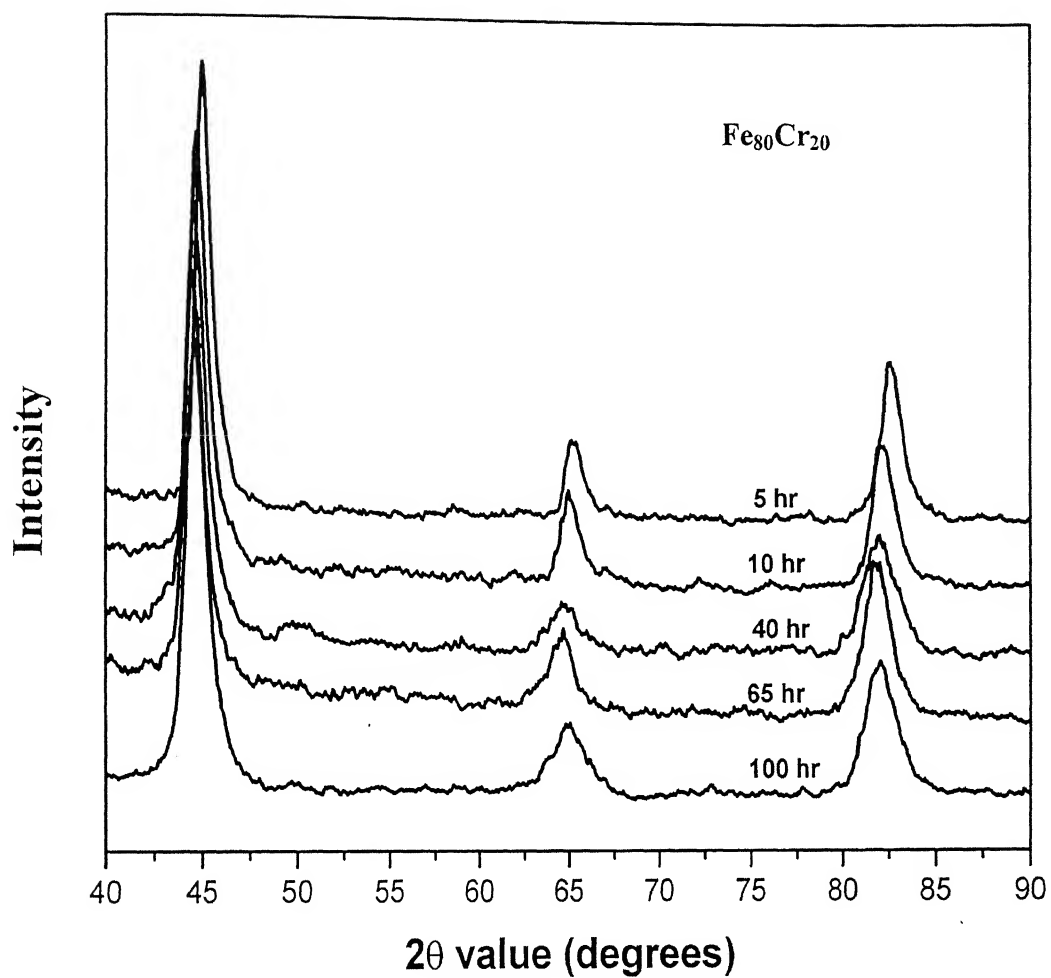
Figure 4.2.: XRD showing $Fe_{80} Cr_{10}$ milled powders corresponding to different milling time

Table4.1. Intensities and 2θ values of different peaks of MA $Fe_{90}Cr_{10}$ powder milled for various period of time.

S.No	Alloys/ Systems	Peak Intensities (%)	Angle (2θ)
1.	$Fe_{90}Cr_{10}$ (5 hrs milled)	100	44.72
		18	65.05
		36	82.37
2.	$Fe_{90}Cr_{10}$ (10 hrs milled)	100	44.79
		22	65.27
		32	82.48
3.	$Fe_{90}Cr_{10}$ (40 hrs milled)	100	44.61
		12	64.84
		28	82.21
4.	$Fe_{90}Cr_{10}$ (65 hrs milled)	100	44.55
		22	64.94
		31	81.99
5.	$Fe_{90}Cr_{10}$ (100 hrs milled)	100	44.73
		16	65.26
		30	81.51

Table4.2. Intensities and 2θ-values of different peaks of MA $Fe_{80}Cr_{20}$ powder milled for various period of time

S.No	Alloys/ Systems	Peak Intensities (%)	Angle (2θ)
1.	$Fe_{80}Cr_{20}$ (5 hrs milled)	100	44.75
		19	65.15
		32	82.50
2.	$Fe_{80}Cr_{20}$ (10 hrs milled)	100	44.64
		21	65.25
		32	82.44
3.	$Fe_{80}Cr_{20}$ (40 hrs milled)	100	44.68
		14	64.27
		32	81.91
4.	$Fe_{80}Cr_{20}$ (65 hrs milled)	98	44.67
		21	65.29
		32	82.15
5.	$Fe_{80}Cr_{20}$ (100 hrs milled)	99	45.05
		19	65.60
		28	82.70

Table 4.3 Intensities, 2θ values, and corresponding planes of compounds of Fe-Cr system, collected from 2001 JCPDS.

S.No	Alloy System/ compound	Intensity	Angle (2θ)	(hkl)
1	Fe	100	44.71	(110)
		30	82.41	(211)
		20	65.08	(200)
2	Cr	100	44.43	(110)
		30	81.80	(211)
		16	64.64	(200)
3	FeCr (solid solution)	100	44.52	(110)
		50	82.06	(211)
		20	64.83	(200)

4.1.2 Effect of milling time on the Crystallite size reduction in Fe-Cr alloy:

In view of the crystallite size of mechanically alloyed powders generally being of the nano-scale, the crystallite size of milled Fe-Cr powders and its reduction with milling time was monitored by analyzing the XRD data obtained from powders milled for time intervals of 5 hrs, 10 hrs, 20 hrs, 40 hrs, 65 hrs and 100 hrs respectively. As shown in the X-ray diffraction patterns (Figures 4.1 and 4.2), the three peaks were found to undergo their broadening with increasing milling time. Crystallite size of milled Fe-Cr powders was analyzed by studying the broadening occurring in the maximum intensity peak in each X-ray diffraction pattern. For this purpose, the profile shape function of the Pseudo-Voigt type was filled on the smoothened X-ray data of Figures 4.1 and 4.2.

Figures 4.1 and 4.2 compare the XRD patterns of $Fe_{100-x}Cr_x$ [x = 10, 20] powders milled for various periods of time. It can be seen that broadening of peaks increases as the milling time is increased. Such an observation confirms that the crystallite size of mechanically alloyed Fe-Cr powders gets decreased with increase in milling time. Broadening of XRD peaks, however, occurs also due to instrumental broadening. Therefore, in order to get the real FWHM of the samples, the effect of instrumental broadening was eliminated by taking XRD patterns of standard sample of pure silicon using the same experimental parameters as used in the sample of milled Fe-Cr powders. From this data of silicon, instrumental broadening effect in the XRD pattern of the mechanically alloyed Fe-Cr powder was removed. The FWHM obtained after removal of instrumental broadening effect, was used to determine crystalline size using Scherrer's formula.

The effect of milling time on the crystallite size corresponding to (110) plane of the resulting $Fe_{100-x}Cr_x$ [x = 10, 20] powder is shown in Figure 4.3 and Table 4.4. It can be seen that the rate of decrease in crystallite size was very rapid up to the milling time of 10 hrs. Subsequently the rate of decrease of crystallite size was found to be less rapid up to the milling time of 65 hrs. Beyond the milling time of 65 hrs, the

crystallite size of mechanically alloyed powder for both the compositions was found to be almost constant. The reason for this trend is that in the initial phase of milling powder particles are deformed and fractured severely which causes accumulation of defects, dislocations, stacking faults etc. and these features cause severe distortions in the lattice. [Suryanarayana 1999] These defects become localized in the shear bands formed and then disintegrate into small grains due to higher instability of the structure [Suryanarayana 1999].

It is to be noted that the nano-scale crystallites could be directly observed while examining the milled powders under Atomic Force Microscope. The crystallite size obtained from the X-Ray diffraction data were found to be matching with the size obtained from Atomic Force Microscopy [See Section 4.1.6]

Table4.4. Effect of Milling time on the crystallite size

Milling time (Hrs)	Crystallite size of Fe 10Cr, nm	Crystallite size of Fe 20Cr, nm
5	10.15	9.62
10	8.74	8.56
40	7.5	6.59
65	7.41	6.46
100	7.02	6.19
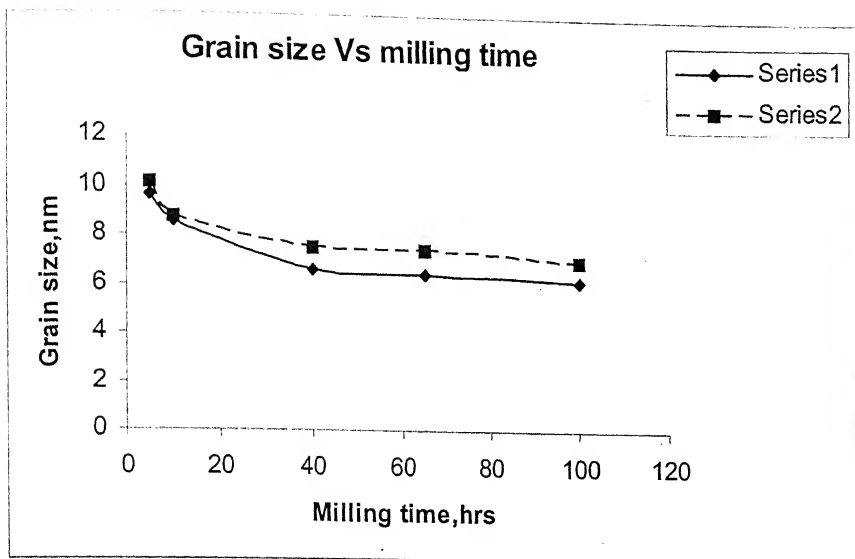
Series 1 ---------- Fe – 10 Cr
Series 2 ---------- Fe – 20 Cr
Figure4.3: Effect of milling time on the crystallite size

4.1.3 Mössbauer Spectroscopy

Mössbauer spectroscopy is a very precise tool for getting the chemical, structural and magnetic properties of the iron base alloys. In this method γ-rays coming from the ^{57}Fe isotope source pass through the sample to be tested and, depending on the hyper-fine magnetic field (HMF) interaction between ^{57}Fe isotope nuclei and their nearest neighbour environment in the lattice of the milled Fe-Cr solid solutions, get absorbed. Remaining rays come out from the sample and are counted. In the present research the hyper-fine magnetic field (HMF), which is the property of the nucleus will change nearest neighbor environment around iron atom continuously as the alloying is taking place with in the material.

When sample placed in the magnetic field a nucleus with a magnetic moment has a dipole interaction with the field, which raises the degeneracy of nuclear states. As in the case of ^{57}Fe ground state I=1/2 splits into two, and excited state I=3/2 splits in to

70

four energy states, which gives the six possible transitions, as observed in our present Mossbauer spectrum. The splitting is directly proportional to the magnetic field applied.

Effect of Milling Time on Alloying in $Fe_{100-x}Cr_x$ Milled Powders

Mossbauer spectra at room temperature of $Fe_{100-x}Cr_x$ [x = 10, 20 wt.%] after different milling times are reported in the Figures 4.4 and 4.5. Showing that up to 20 hr of ball milling there is no change in spectrum as shown in the Figures 4.4(a)-(c) and 4.5(a)-(c).As the milling time increases to 40hrs spectrum is changed, because of the hyperfine field at the ^{57}Fe nucleus (HMF) decreases with the milling time due to the milling of the Cr atoms with Fe atoms as shown in the figures 4.4(d)-(f). and 4.5 (d) and (e). At the same time, the peak width of the sextuplets increases due to the different ^{57}Fe environments. The hyperfine field distributions (HFD) shows up to 20 hrs of milling the HFD shows a narrow peak centred on 33T which is characteristic of Fe not yet alloyed with Cr as shown in the figure 4.4 (c) and figure 4.5(c). With an increased milling time to further, this peak widens until a Gaussian type distribution shape is reached as shown in the figrures4.4 (d)-(f) and 4.5(e) and (f) which is characteristic of the bulk FeCr solid solution with Fe and Cr randomly distributed on the bcc lattice. From the above argument it was concluded that mechanical alloying of Fe and Cr powders were progressed between 20-40 hrs of milling time for both the composition of x = 10, 20 respectively.

(a)

(b)

(c)

(d)

(e)

(f)
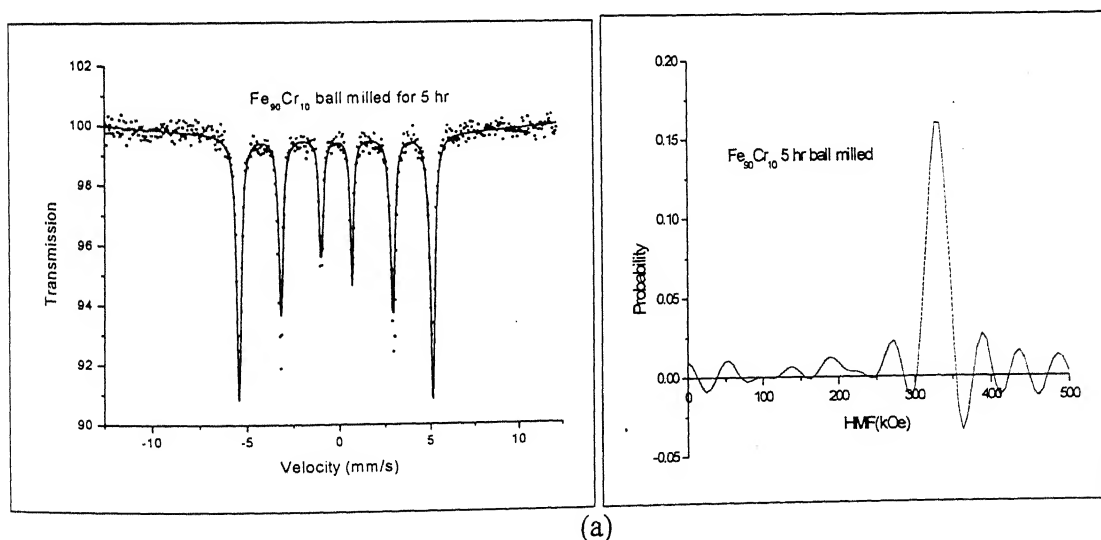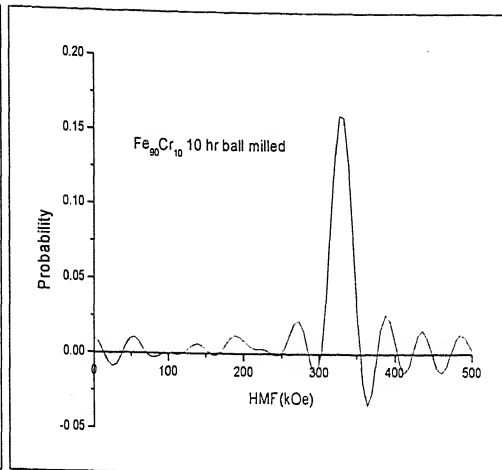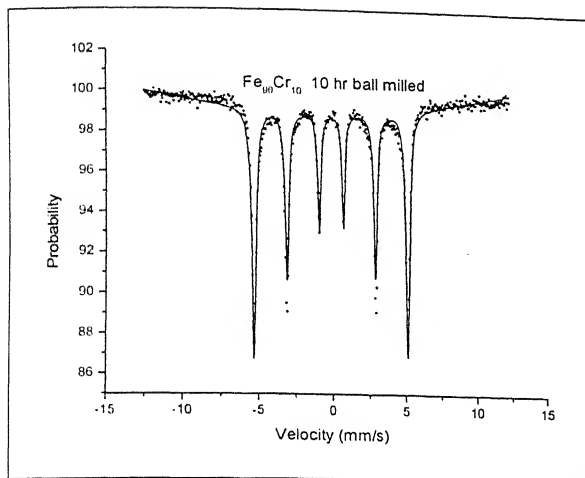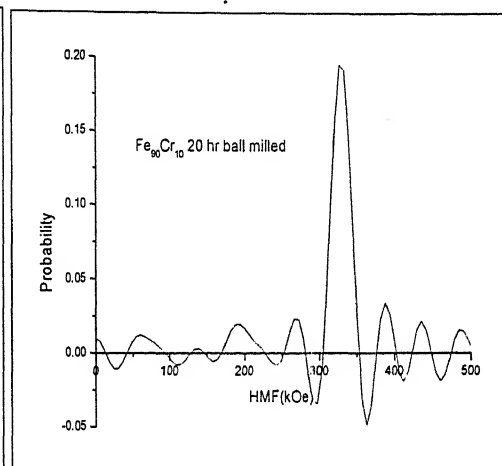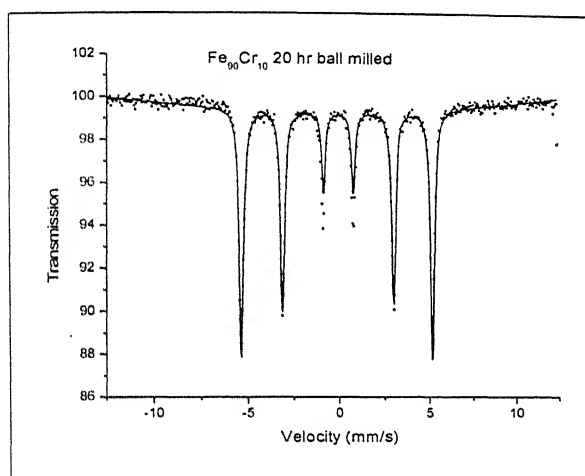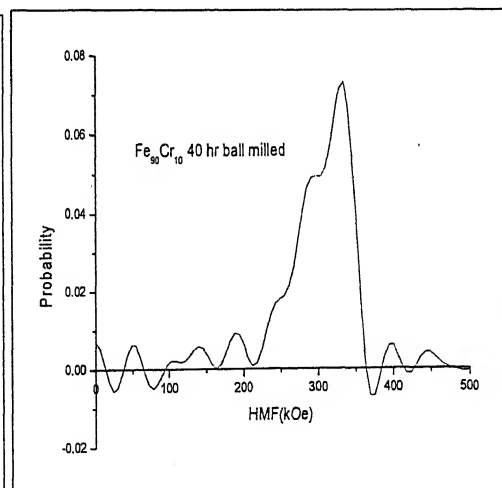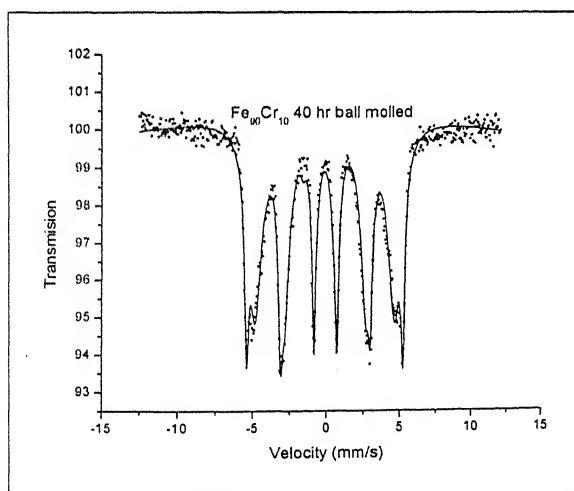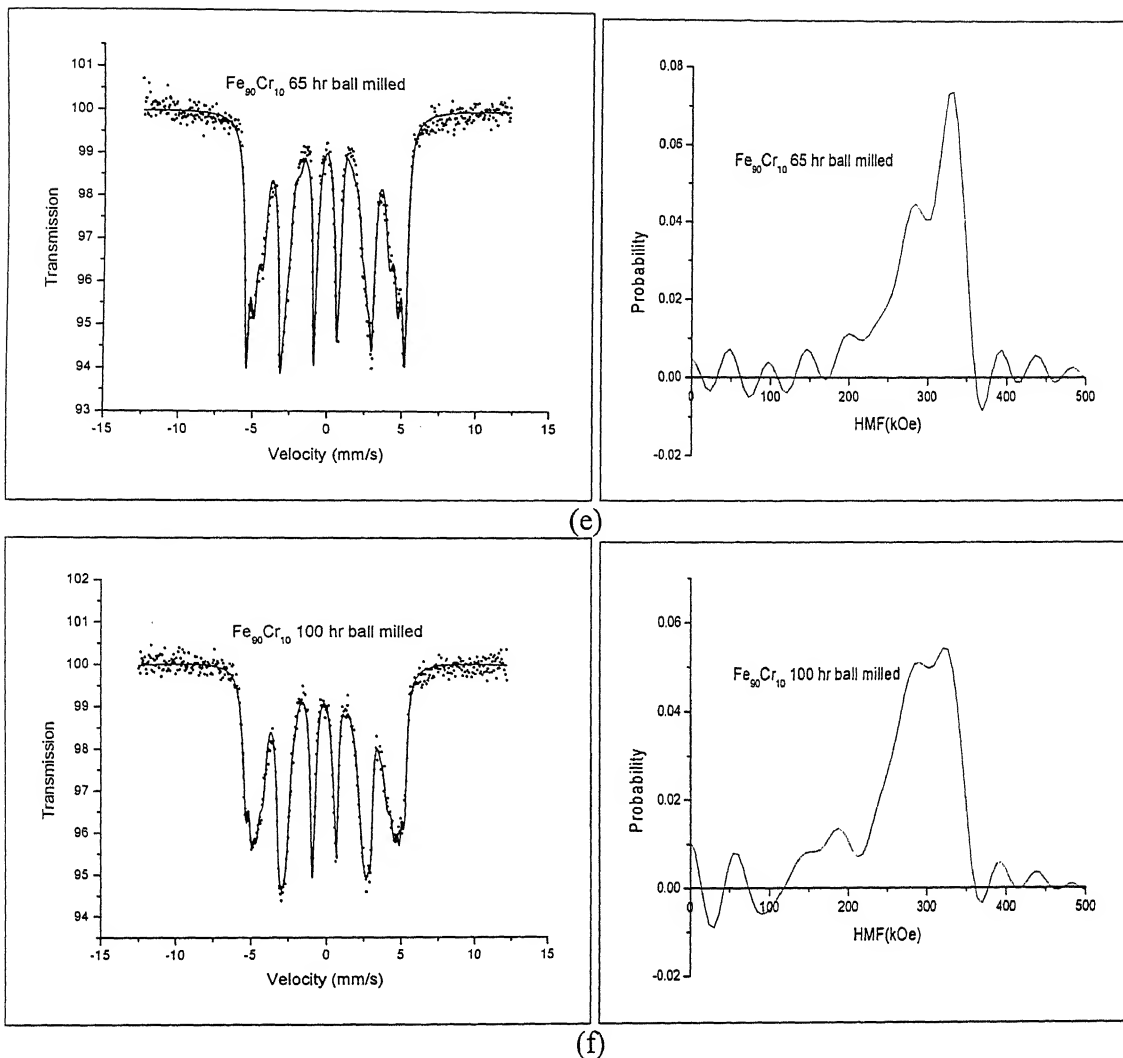
Figure4.4: Mossbauer spectra showing the effect of milling time on the alloying of $Fe_{90}Cr_{10}$ mechanically alloyed powder. (a) 5hrs (b) 10hrs (c) 20hrs (d) 40hrs (e) 65 hrs (f) 100hrs

(a)

(b)

(c)

(d)

(e)

Figure 4.5 Mossbauer spectra showing effect of milling time on the on the alloying of $Fe_{80}Cr_{20}$ ball milled powder. (a) 5hrs (b) 10hrs (c) 20hrs (d) 40hrs (e) 65 hrs (f) 100hrs

75

Effect of Composition on the Alloying of the $Fe_{100-x}Cr_x$ [x = 5, 10, 15, 20] Powders Ball Milled for 100 hrs

Mossbauer spectra at room temperature of $Fe_{100-x}Cr_x$ with x=5,10,15,20 wt % Cr at constant milling time of 100hrs reported in the figure 4.5.hyperfine field at the [57]Fe nucleus (HMF) decreases with the increased %Cr due to the alloying of the Cr atoms with Fe atoms as shown in the figures 4.5(a)-(d)

At the same time, the peak width of the sextuplets increases due to the different (HMF) corresponding to different [57]Fe environments. It was reported that with an increased % Cr, hyper field distributions (HFD) peak widens until a Gaussian type distribution shape is reached as shown in the figures 4.5(a)-(d), which is characteristic of the bulk FeCr solid solution with Fe and Cr randomly distributed. From the above argument it was concluded that formation of solid solution is increasing with increase in % of Cr.
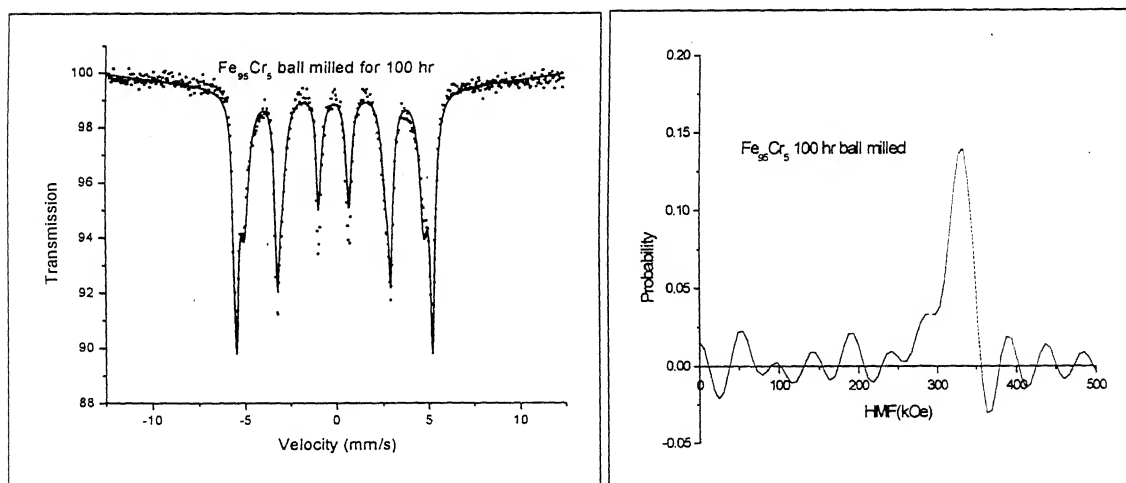
(a)
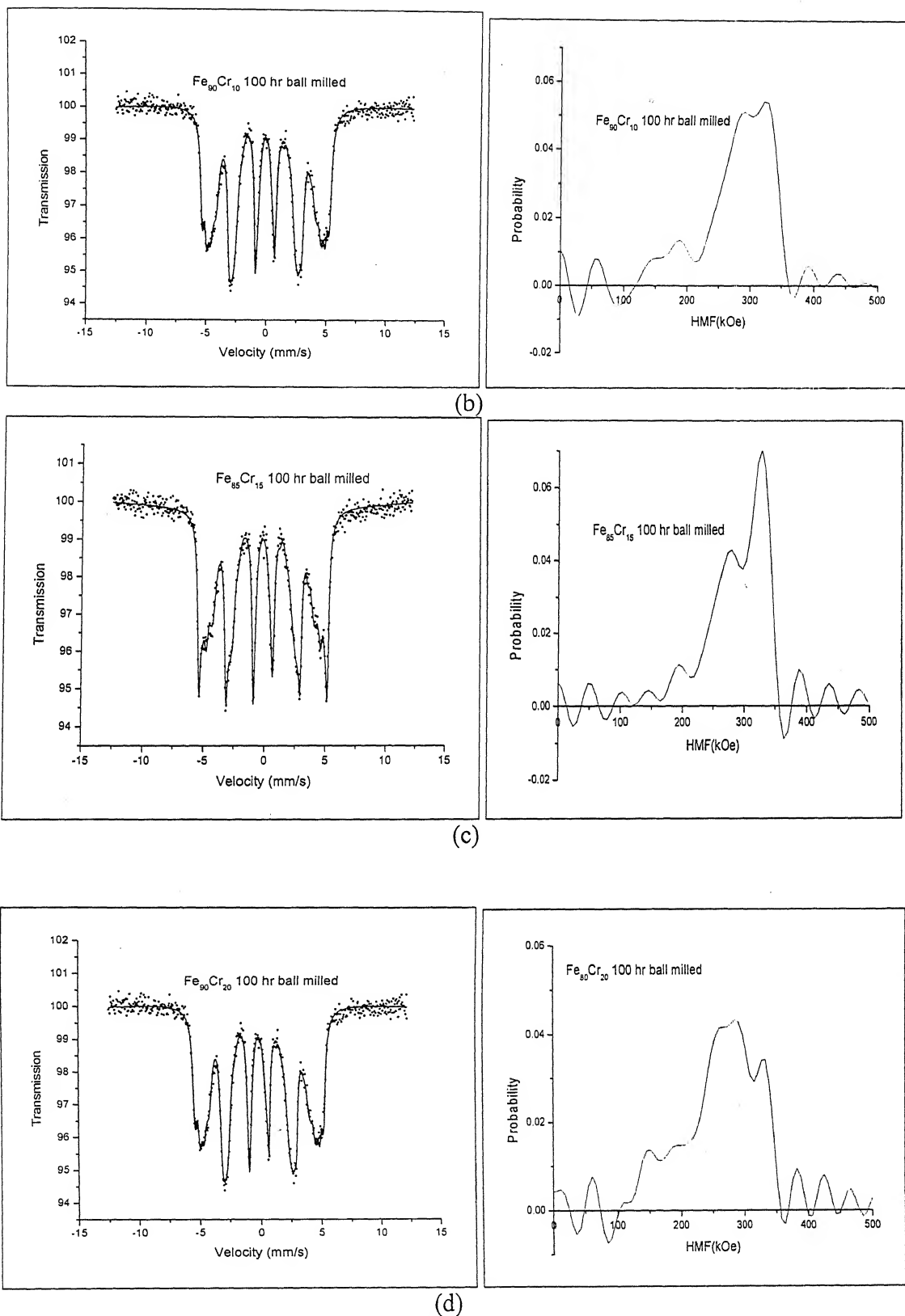
Figure4.5: Mossbauer spectra showing effect of composition on alloying of $Fe_{100-x}Cr_x$ powders ball milled for 100hrs.(a) 5Cr; (b) 10Cr; (c) 15Cr; (d) 20Cr.

4.1.4 Differential Thermal Analysis

The Fe-Cr equilibrium phase diagram, Figure2.11, shows a broad miscibility gap for a wide range of concentrations below the temperature of $\sim 830^{\circ}$C. At temperatures higher than 830°C, the Fe-Cr alloys form solid solutions. Thus during thermal treatment in the temperature range of 440–830°C, specially for the equiatomic compositions, an intermetallic phase σ can be formed. This phase is known to transform into bcc solid solution during ball milling.Fe-Cr alloys belonging to a wider compositional range can also be made to decompose into Fe-enriched and Cr-enriched solid solution either through nucleation and growth mechanism or through spinodal decomposition by heating between 400°C and 500°C. Below this temperature range the diffusion is too slow to allow the decomposition.

Nano crystalline materials, having metastable structures, can undergo a phase transformation and rapid grain growth. Differential thermal analysis for the milled Fe-Cr alloys was therefore used to investigate phase changes, if occurring, in their structure during heating.

Figure 4.6 shows the DTA output for Fe-10 wt% Cr alloy in terms of ΔH Vs T. It can be seen that the plot does not contain either endothermic peak or an exothermic peak. This implies that no phase transformation occurs in nanocrystalline mechanically milled Fe-10 wt% Cr alloy during its heating from room temperature to 1150°C at the heating rate of 5°C/min. Such a behavior is not surprising because the spinodal decomposition which is expected to occur in this alloy is known to be a sluggish phase transformation and could not be triggered during heating because of the high heating rate 5°C/min. Further, it can be seen that the rate of change in ΔH with respect to temperature is low up to 400°C (Regime 1) and increases substantially from 600°C onwards (Regime 2). It appears therefore that little microstructural changes, such as grain growth, occur in the alloy up to 400°C and become rapid after the heating beyond 600°C.

alloy, Since this alloy comes out of the spinodal decomposition range as shown in the phase diagram Figure 2.14 and expected to be no phase transformation occur during the temperature range. For mechanically milled nanocrystalline Fe-15 wt %Cr and Fe-20 wt% Cr alloys expected to be similar behavior as in the nanocrystalline Fe-10 wt %Cr alloy.
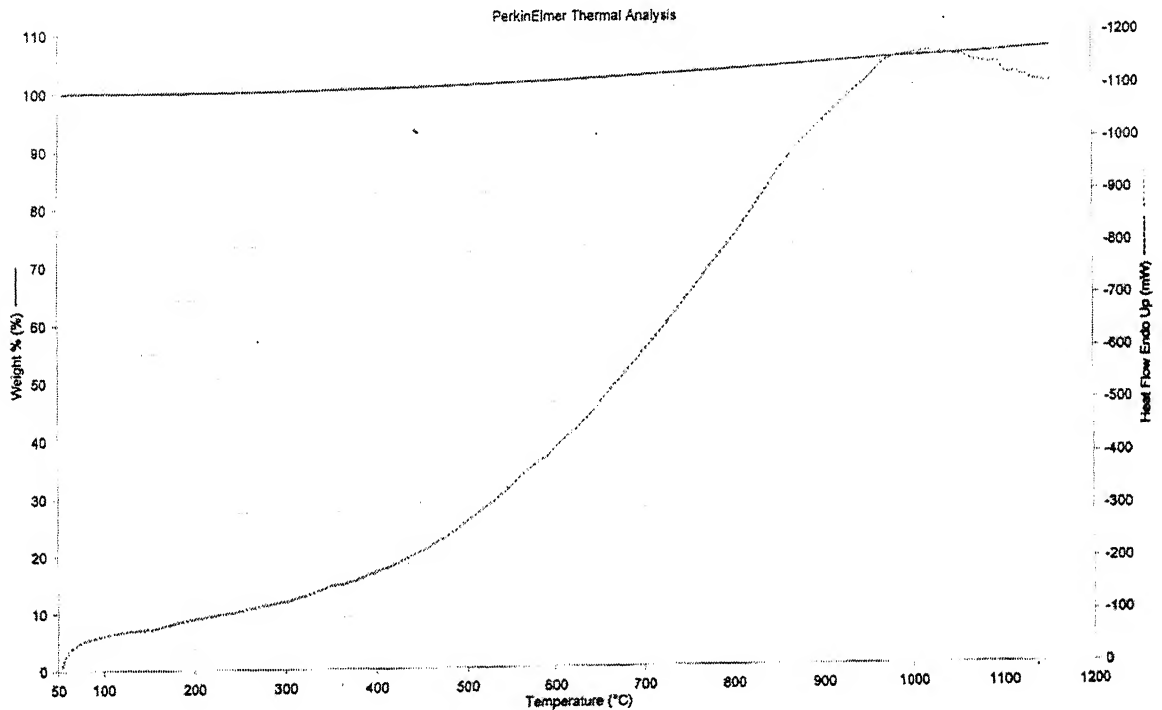

Figure 4.6 Figure showing the Diffrential Thermal Analysis of Milled Fe-Cr powder

4.1.5 Scanning Electron Microscopy

Effect of Milling Time on the Morphology of Fe-Cr alloy

Mechanism of mechanical alloying, schematically shown in Figure 4.7, it can be seen that the particle morphology develops through the repeated and intermittent cycles of flattening-impact welding-fracture of individual particles of Fe or Cr or Fe-Cr. Internal structure of particles thus comprises of impact welded flattened particles of Fe or Cr or Fe-Cr. Since the fracture within individual particles is expected to occur only after occurrence of sufficient work hardening of individual flattened particles, the particle size is expected to initially increase with increasing milling time. Subsequently due to the intermittent impacting, particles with increasing milling time get sufficiently work hardened and begin to undergo fracture[suryanarayana 1999]. The average particle size of the mechanically alloyed powder then starts decreasing.

Figure 4.8-4.13 showing the SEM images corresponding to the mechanically milled Fe-10 wt% of Cr alloy milled for 5hrs, 10hrs, 20hrs, 40hrs, 65hrs, 100hrs respectively. It can be seen that between 0-10hrs of milling time, the powder had an equiaxed morphology and with an aspect ratio of 1-1.5. And cold welding of the powder particles leads to average particle size getting increased to 50-100μm, is shown in the Figure 4.8 to 4.9. After milling time of 20 hrs and then to 40hrs, the powder morphology was changed from equiaxed to elongated with an aspect ratio of 2 - 3 and repeated cold welding and fracturing of the powders leads to average particle size getting reduced to 20-50μm is shown in Figure 4.10 to 4.11. Milling from this stage onwards implied further flattening and fracturing of powder particles. As shown in the Figure4.12 to 4.13, considerably flattened flaky particles of more or less same size were thus obtained after a milling time of 100hrs.

(a)

(b)

Fracture Paths

(c)

A   B   C

Fragment A, B or C

Fracture Paths

(d)
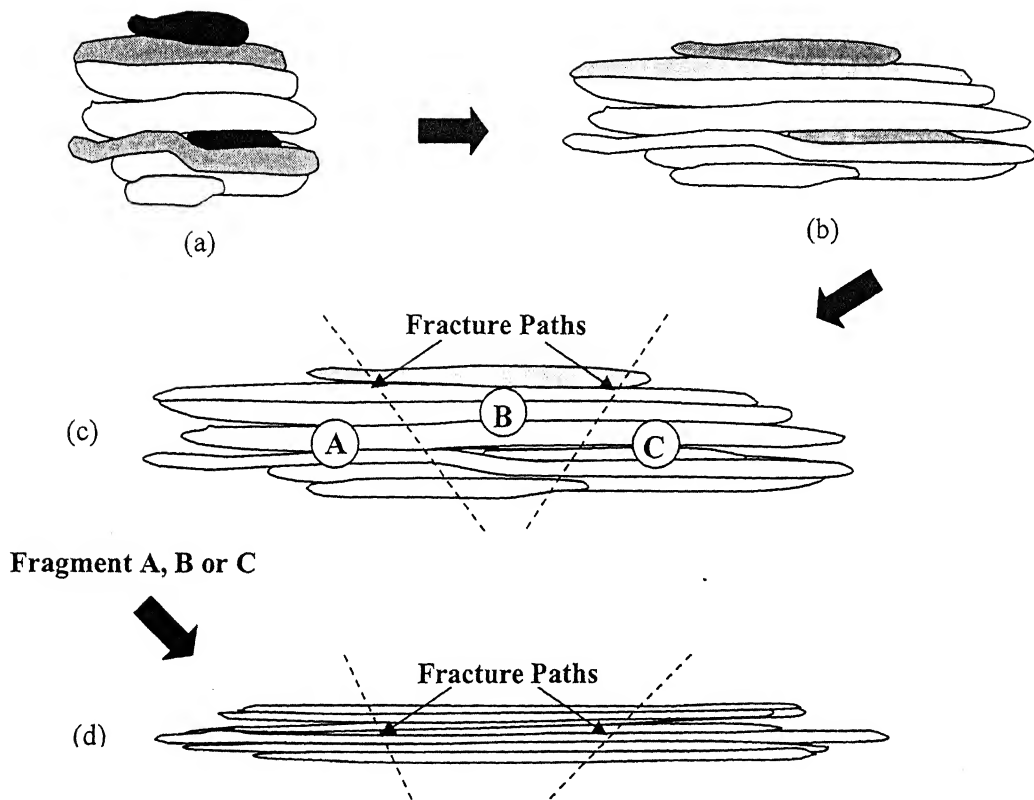
Figure 4.7 Different stages of development of lamellar structure during milling of $Fe_{90}Cr_{10}$ powders by mechanical alloying
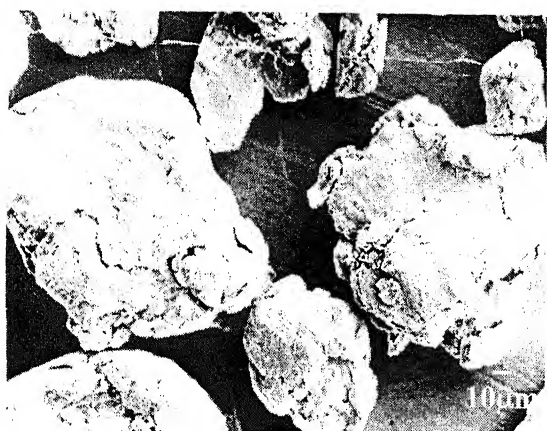
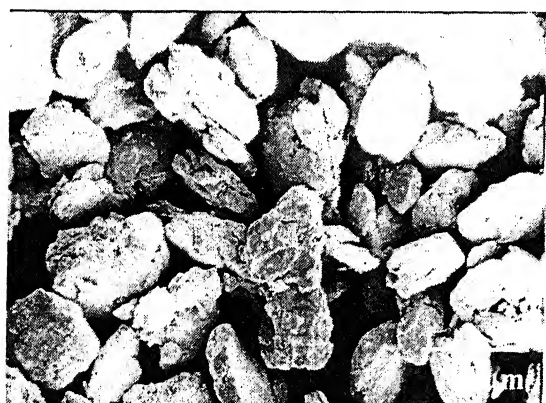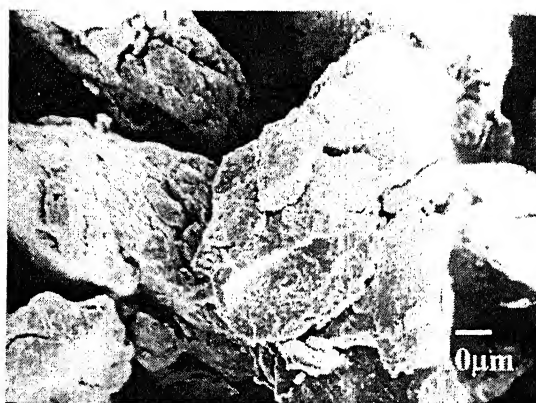(a)   (b)

Figure 4.8: Fe-Cr Powders Mechanically Milled for 5Hours

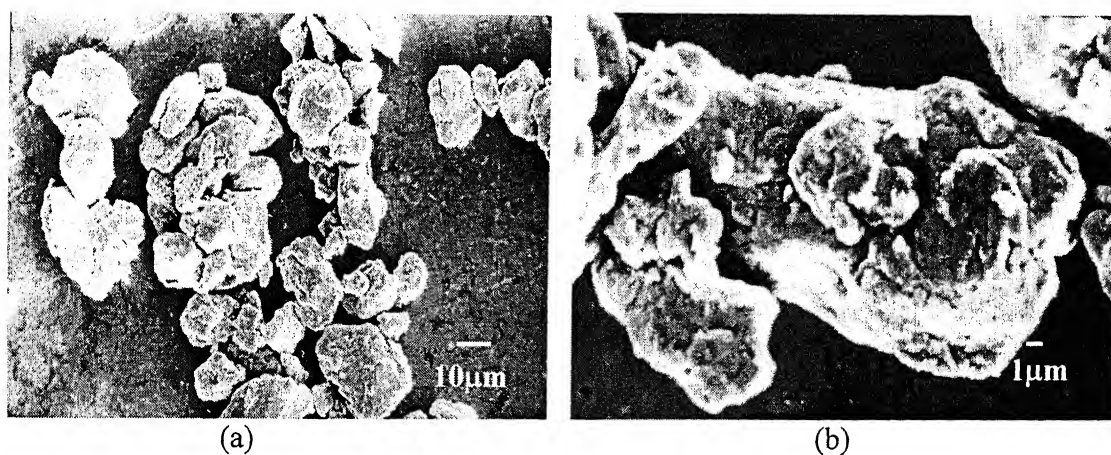(a)   (b)
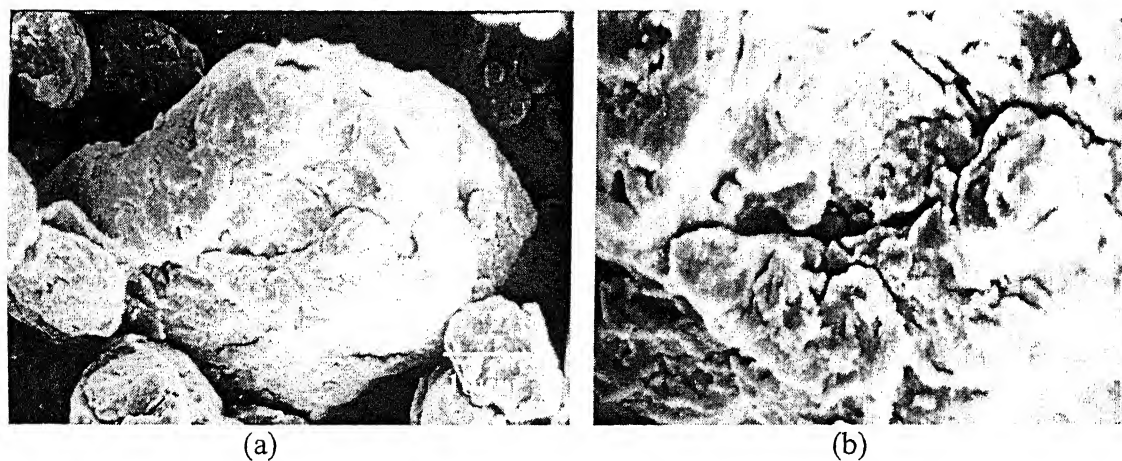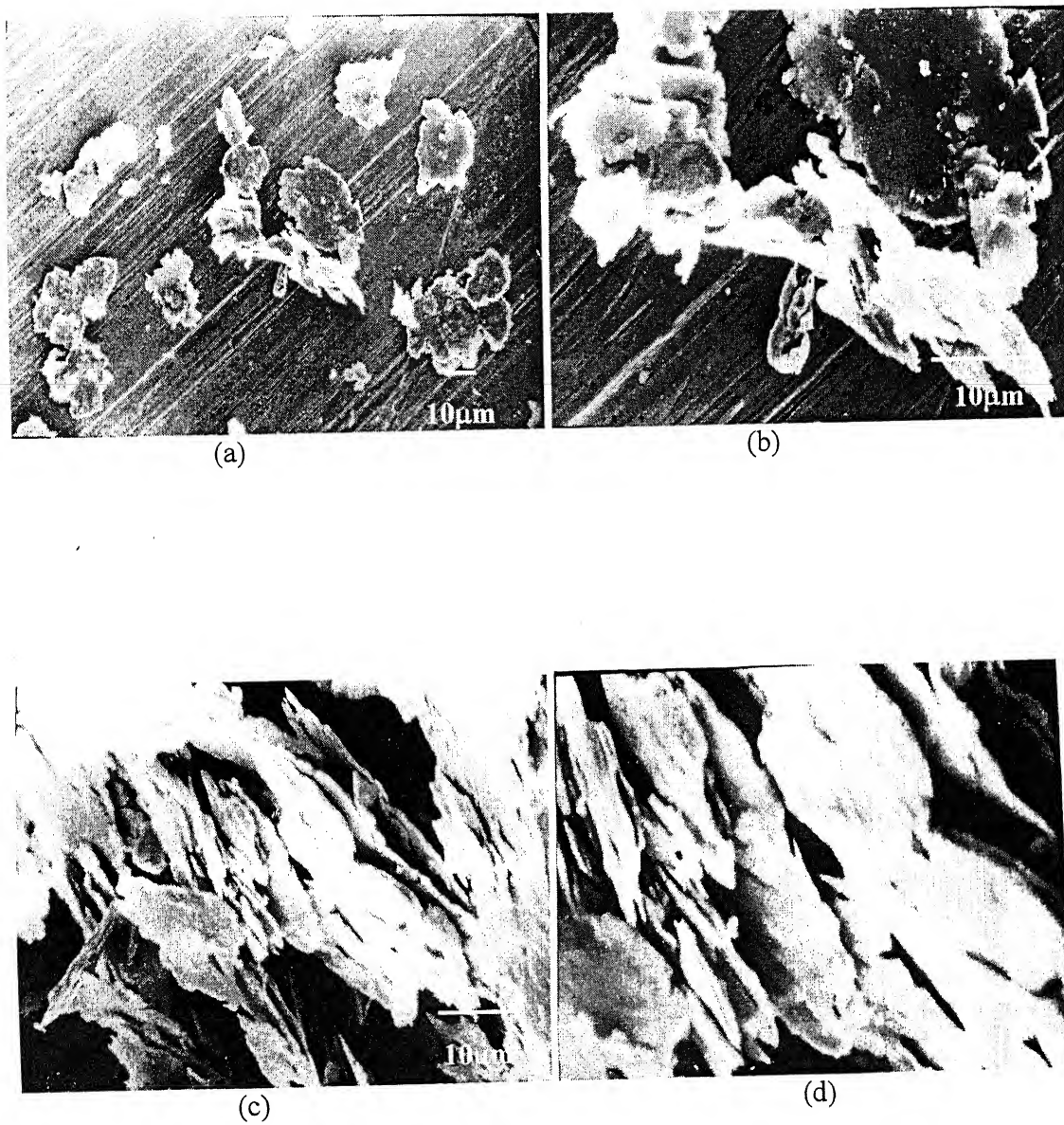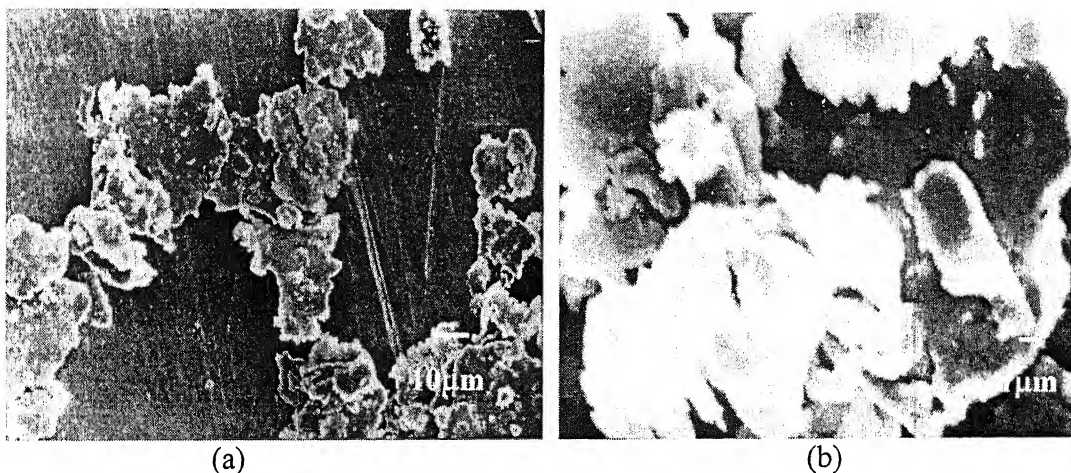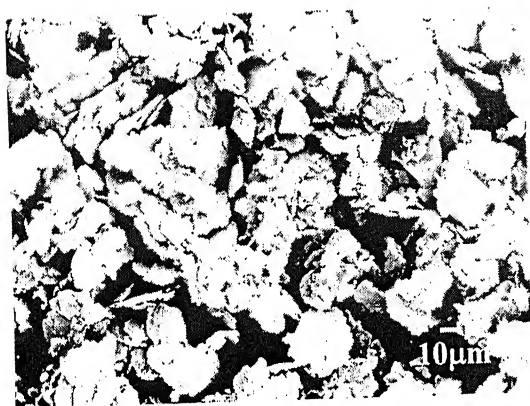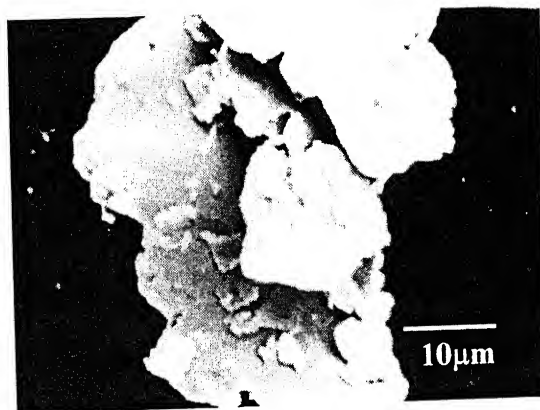
Figure 4.9: Fe-Cr Powders Mechanically Milled for 10Hours

(a)   (b)

Figure 4.10: Fe-Cr Powders Mechanically Milled for 20 Hours

(a)   (b)

Figure 4.11: Fe-Cr Powders Mechanically Milled for 40 Hours

(a)

(b)

(c)

(d)

Figure 4.12: Fe-Cr Powders mechanically milled for 65 Hours

<div align="center">(a)   (b)</div>

Figure 4.13: Fe-Cr Powders Mechanically Milled for 100 Hours

Effect of composition on the morphology of the Fe-Cr alloy milled for 65 Hours

Figure 4.14-4.15 showing the SEM images corresponding to the mechanically milled $Fe_{100-x}Cr_x$ x=10,20 alloys milled for 65hrs. It can be seen that the extent of flakiness appears to be increasing with increasing Cr content in the mechanically milled alloys. It was also observed that, the aspect ratio of the powder particles was increased with increase in % of Cr.

(a)

(b)

(c)

(d)

Figure 4.14: Fe-10Cr Powders Mechanically Milled for 65 Hours
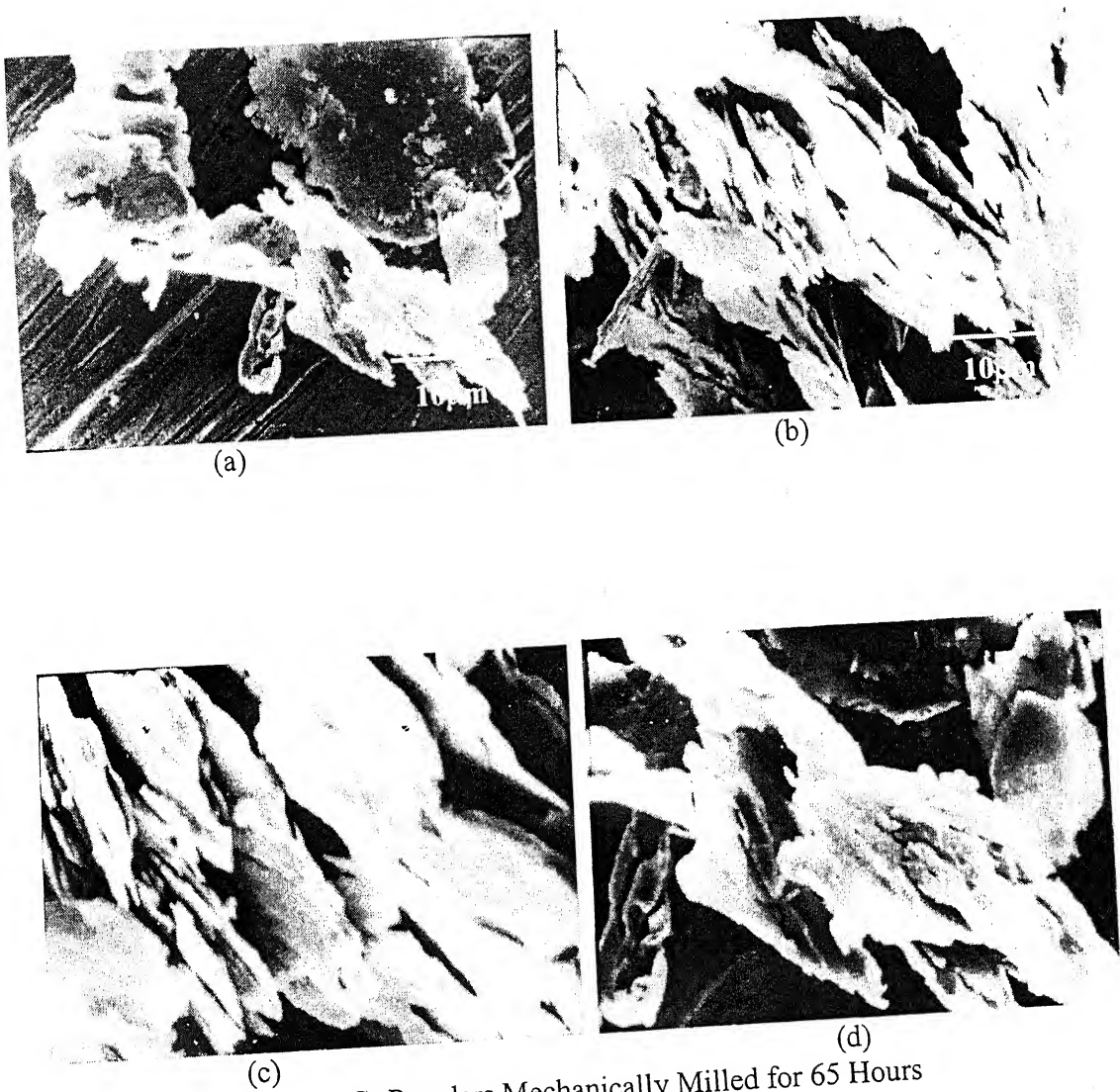
Figure 4.15: Fe-20Cr Powders Mechanically Milled for 65 Hours

4.1.6 Atomic Force Microscopy

Structural Features as Revealed by Atomic Force Microscopy

Characterization techniques such as X-ray diffraction, Mossbauer spectroscopy and scanning electron microscopy, though very useful in studying the progress of mechanical alloying, do fail to provide direct observations on parameters

such as inter-lamellar spacing, grain size and grain shape within individual lamallae, the scale of chemical inhomogeneity and surface topography of the milled particles. Such features of mechanical alloying were studied through AFM.

Surface Topography of Milled Powder as a Function of Milling Time

Nano-structured mechanically alloyed powders are known to sinter at an enhanced rate even at relatively lower temperatures. This is likely to occur due to (1) an enhanced diffusivity arising from a high order of the defect structure created in the material, (2) extremely refined grains which considerably increase the available grain boundary diffusion paths and (3) the sharp curvature effect arising from nano-scale deep valleys and ridges formed on very uneven surfaces of mechanically alloyed powders. The third factor, i.e. the sharp curvatures arising from the formation of nano-scale ridges and valleys on the surfaces has, in general, not been given due attention in discussing the enhanced sintering kinetics of nano-structured mechanically alloyed powders.

Figures 4.16(a) to 4.16(f) show the surface topography of mechanically alloyed powders produced by milling for 5 hrs, 20 hrs, 40 hrs, 65 hrs and 100 hrs respectively. As shown in these figures, the scanned surface area for obtaining these topographical features in all the cases ranged between 1000 nm x 1000 nm – 2500 nm x 2000 nm.

It must be noted that since, as revealed by SEM micrographs, the particle size during mechanical milling varied between 10 – 100 μm, the surface topography figures 4.8 to 4.13 shown here represent only a part of their respective particle surfaces. However, the features shown here are representative and similar features were observed on several other particles corresponding to the same milling time. It can be clearly see that the surface of milled particles comprised of a typical valley and ridge structure. However, the heights of the ridges decreased with an increase in the milling time.

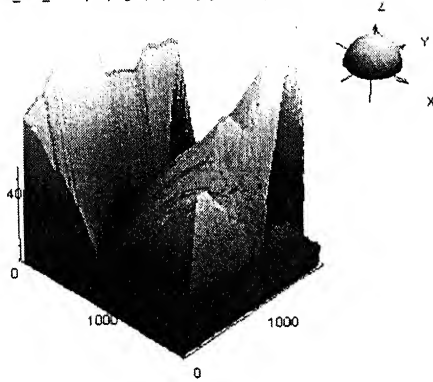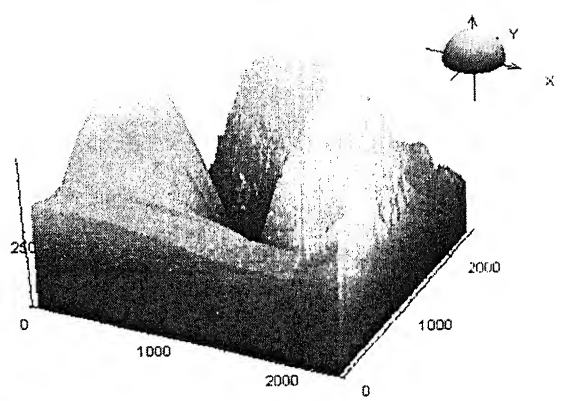Image: 'Fe10Cr_5Hr_film_2000', Topograph, 4.20[V] Bias, right-left

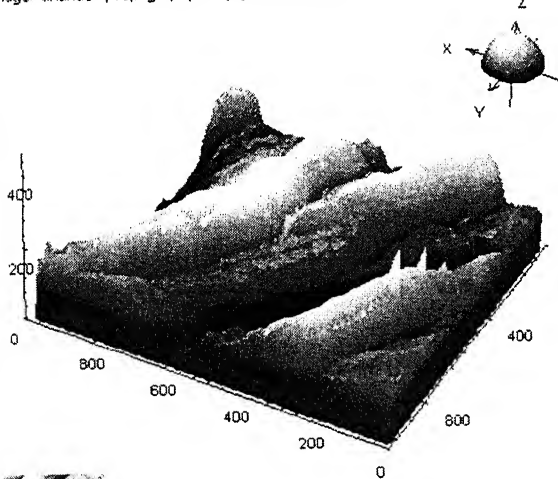Image: 'Fe10Cr_20Hr_film_2500', Topograph, 3.50[V] Bias, left-right

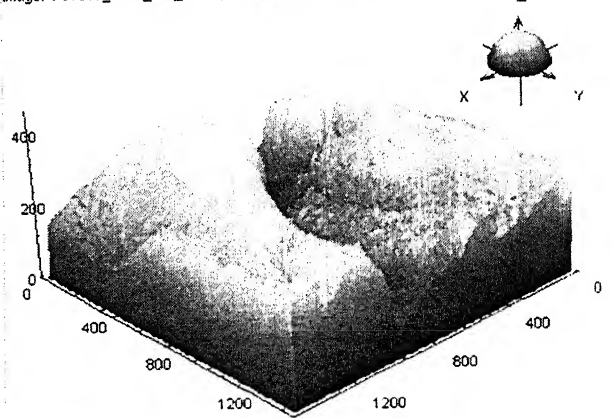Image: 'anand01', Topograph, 3.80[V] Bias, right-left

Image: 'Fe10Cr_65Hr_film_1500', Topograph, 3.60[V] Bias, right-left
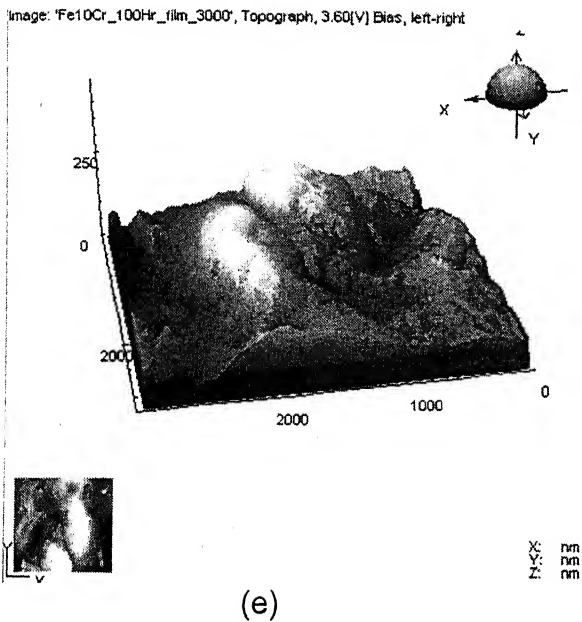
89

(e)

Figure4.16 Three dimensional AFM topographical images showing effect of milling time on the surface roughness for Fe-Cr alloy corresponding milling times of (a) 5 hrs; (b) 20 hrs; (c) 40 hrs; (d) 65 hrs; (e) 100 hrs.
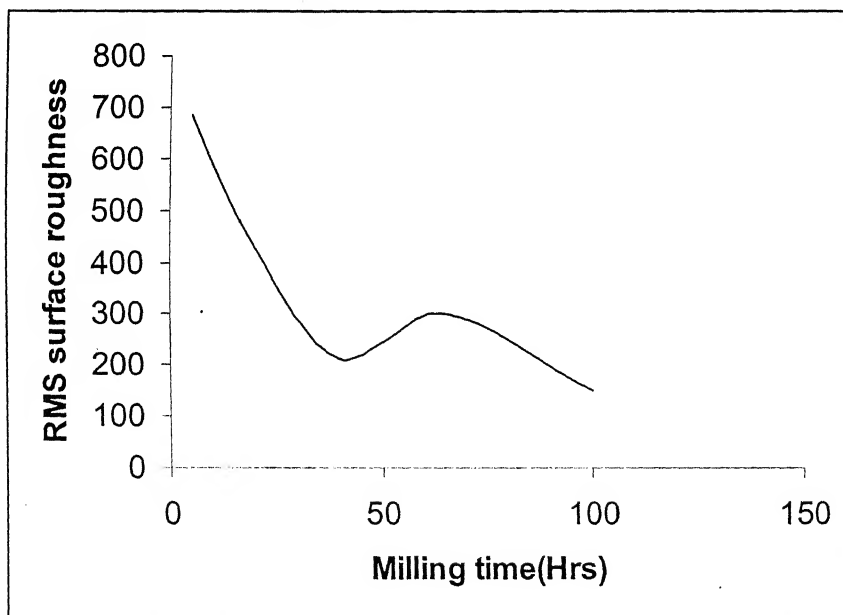
Figure4.17.Effect of milling time on the surface roughness

Figure 4.17 shows the RMS surface roughness as function of the milling time. The data for obtaining this curve was obtained by measuring surface roughness on sufficient number of particles belonging to a milling time lot. Thus, while the mean ridge height was found to be ~ 700 nm after a milling time of 5 hrs, it decreased to ~ 180 nm after a milling time of 100 hrs.

Inter-lamellar width in Milled Powder as a Function of Milling Time

Mechanically alloyed powders are known to have a lamellar structure, which results from the repeated cold welding and fracture of flattened particles. As the impact energy from the grinding balls causes elongation and flattening of particles prior to their cold welding on new particle(s), the lamellae width in mechanically alloyed particles is expected to decrease with the milling time. Figures 4.19 (a) to 4.19 (e) shows the surface topography figures obtained by the tapping mode AFM. The decreasing inter-lamellar width with increasing milling time can be easily seen from these figures. Details of the inter-lamellar width at different milling times are shown in Table4.5/Figure4.18

Table4.5. Effect of milling time on the interlamellar spacing

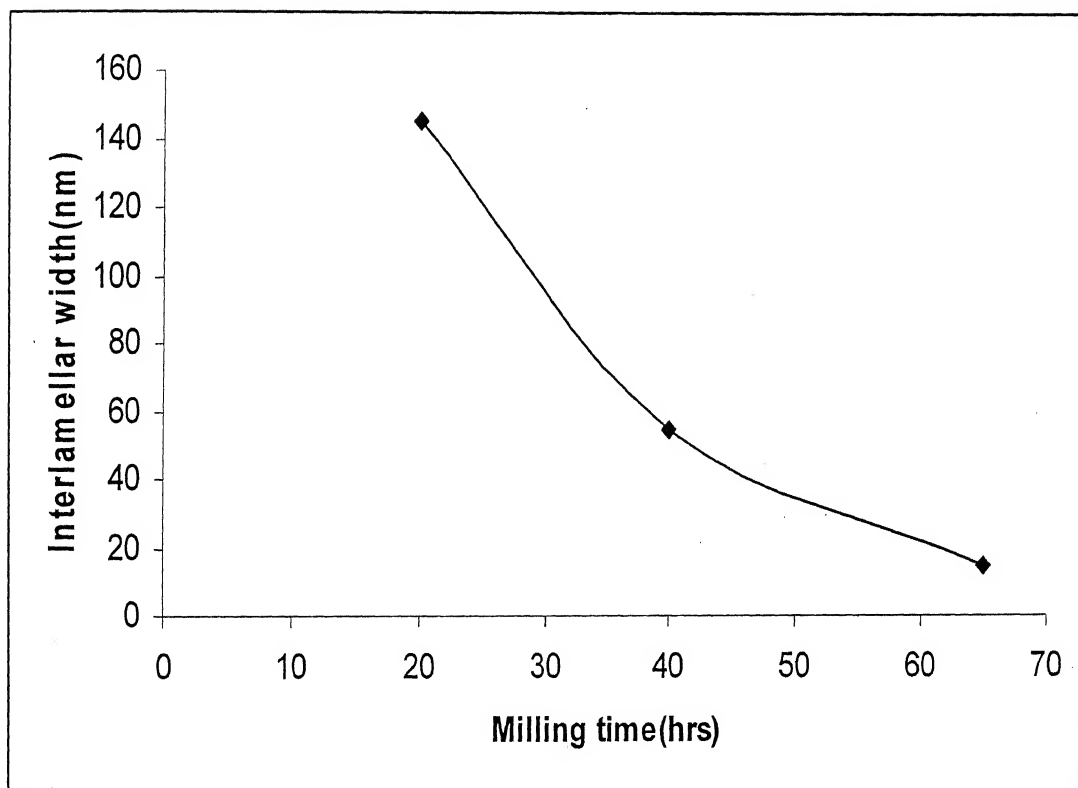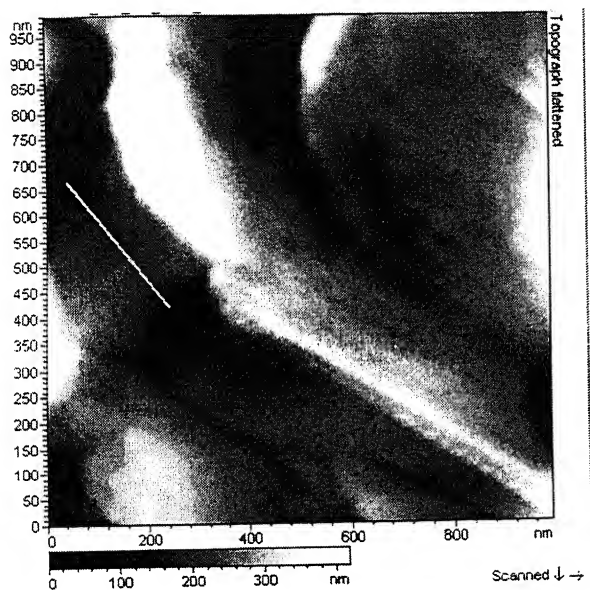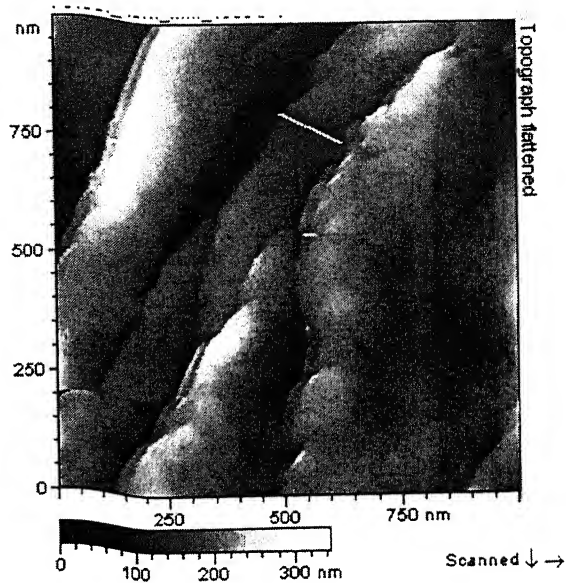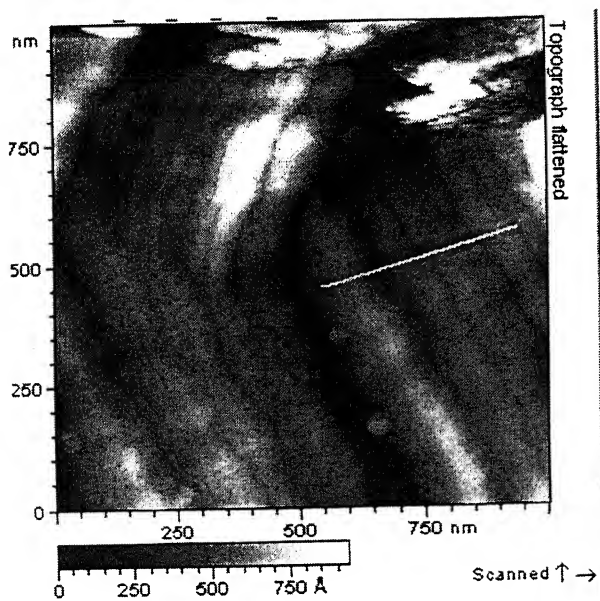| S.No	Sample	Inter lamellar width (nm)
1.	Fe-Cr Alloy Milled for 20 hrs	145
2.	Fe-Cr Alloy Milled for 40 hrs	55
3.	Fe-Cr Alloy Milled for 65 hrs	15

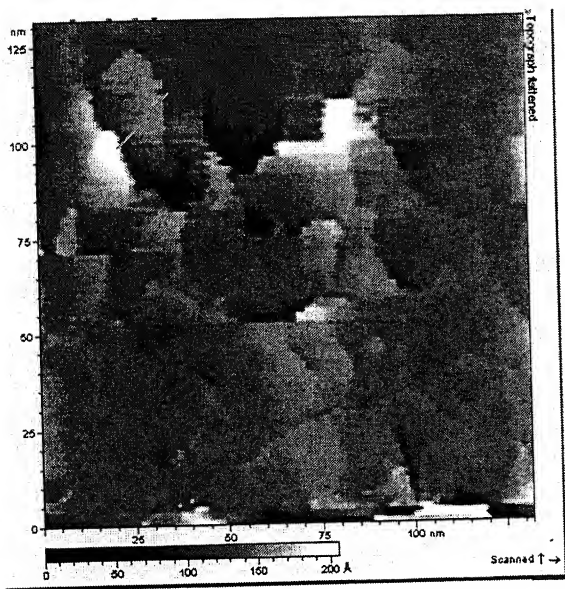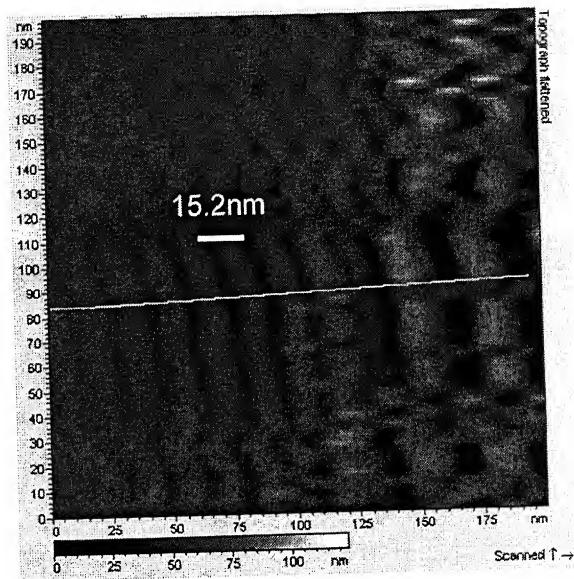Figure4.18. Effect of milling time on Interlamellar width
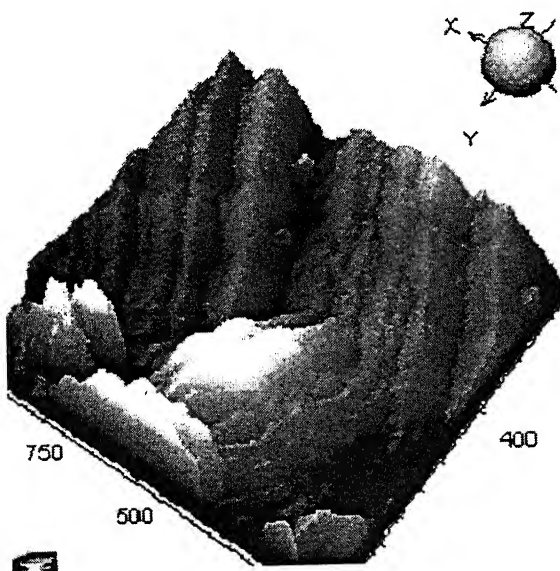
(a)

(b)

(c)

(d)

93

(e)

15.2nm
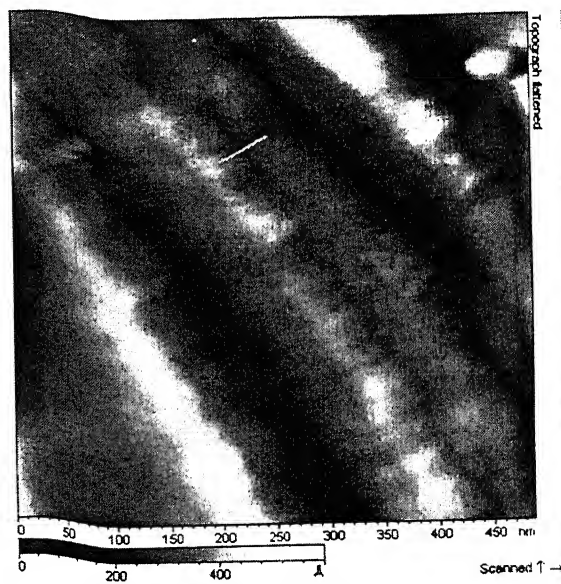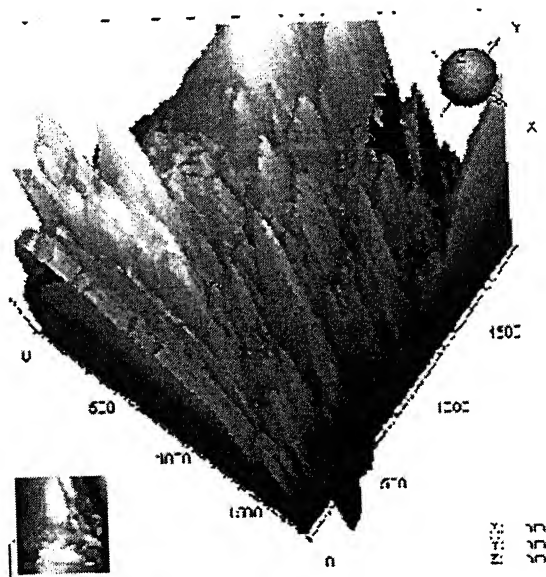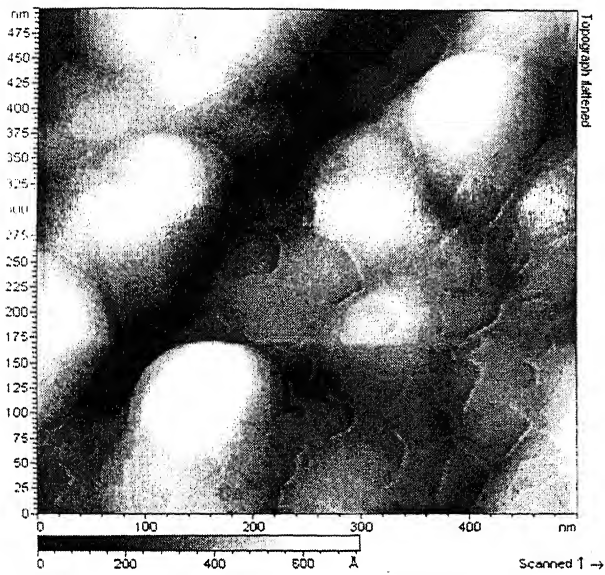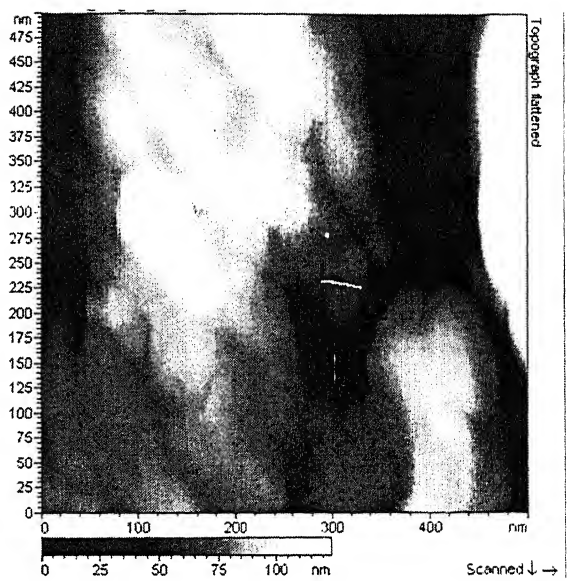
(f)

(g)

(h)

Figure 4.19 AFM photo graphs showing effect of milling time on the layer width of the particle corresponding milling times of (a) 5hr ; (b) 20hr ; (c, d, e) 40hr ; (f) 65hr ; and (g, h) 100hr.

94

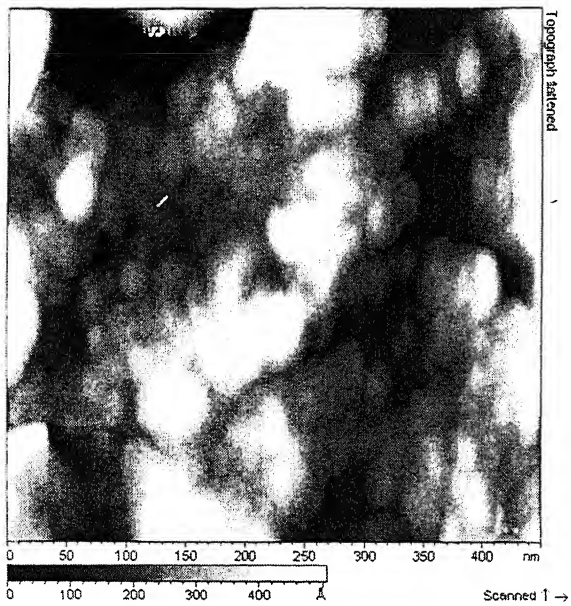## Nano Grain Shape and its Evolution during Mechanical Alloying

Individual particles undergo an extensive deformation by their flattening during mechanical alloying and get cold welded on each other. The lamellar structure within individual particles therefore forms. Due to (a) an extensive deformation of individual lamellae which must lead to a highly dislocated structure and (b) high diffusivity even at room temperature, individual lamellae are expected to develop sub-grains within. Atomic Force micrographs showing the sub-grain structure developed within individual lamellae of $Fe_{90}Cr_{10}$ particles milled for 5 hrs, 20 hrs, 40 hrs, 65 hrs and 100 hrs is shown in Figures 4.20(a) to 4.20(e). It can be seen from Figure 4.20(a) that the structure developed after a milling time of 5 hrs contained sub-grains, which had a size of about $10 - 30$ nm. The sub-grain size decreases with the milling time but stabilizes to ~ 10 nm. However, due to an extensive flattening of particles and thus of individual lamellae, these sub-grains tend to elongate and become somewhat oblate. Elongation of sub-grains was found to increase with increasing the milling time.

(a)

(b)

(c)

(d)

96

nm
250
200
150
100
50
0

Topograph flattened

0   50   100   150   200   250 nm

0   25   50   75 Å

Scanned ↓ →

(e)
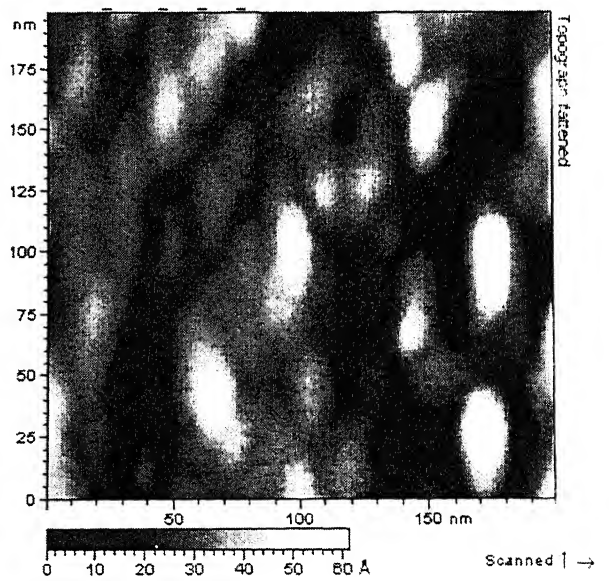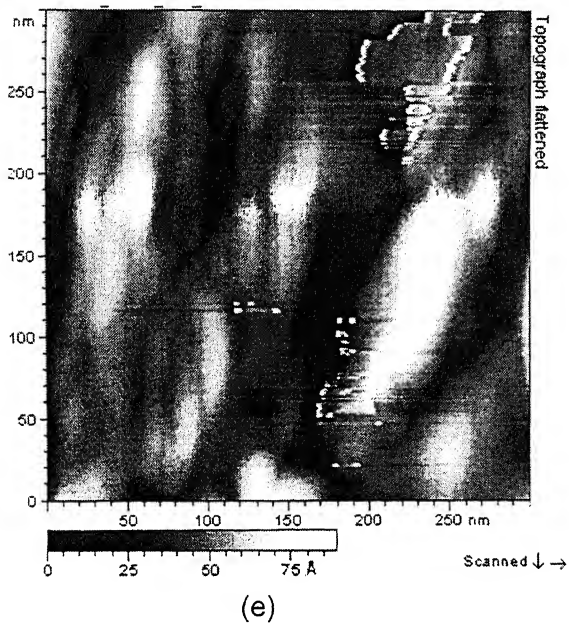
Figure 4.20 AFM photo graphs showing effect of milling time on shape of the grain corresponding milling time of (a) 5hr ; (b) 20hr ; (c) 40hr ; (d) 65hr ; (e) 100hr

Phase Contrast Study

Figure4.21 (a)-(f) showing the AFM images corresponding to the mechanically milled Fe-10 wt% of Cr alloy milled for 5hrs, 20hrs, 40hrs, 65hrs, and 100hrs. It can be seen that the powder distribution is not uniform and there should be possible to form some of the Iron rich areas or chromium rich areas, and uneven distribution of bright and dark areas corresponding to different phases in the milled powders. Dark and bright phase contrast found in these images may be due to the difference in stiffness of the powder particles[D.Raghavan et al 2000] is shown in Figure 4.21 (a)-(c). The powder particles were forming ladder of two metal powder constituents due to the repeated cold welding of the powder constituents is shown in Figure 4.21 (a). As the milling time was increased to 100hr, structure of the powder particles was refined with repeated cold welding and fracturing leads to uniform distribution of the two powder constituents was achieved is shown in Figures.4.21 (d)-(f).

(a)

(b)

(c)

(d)

99

<div align="center">(e)   (f)</div>
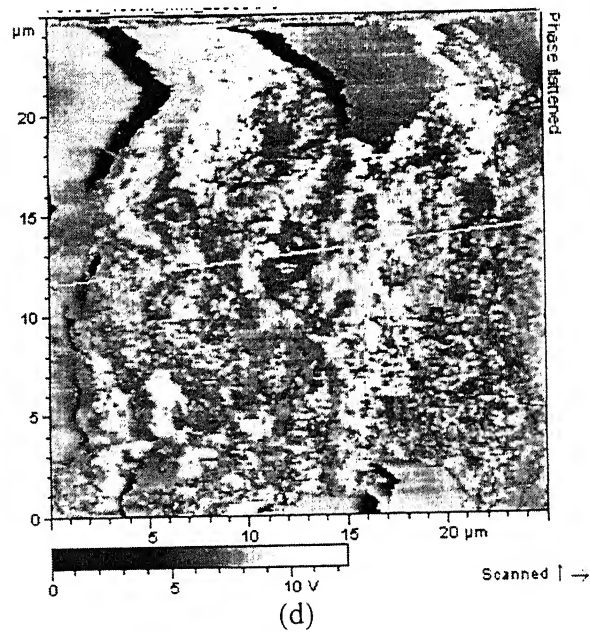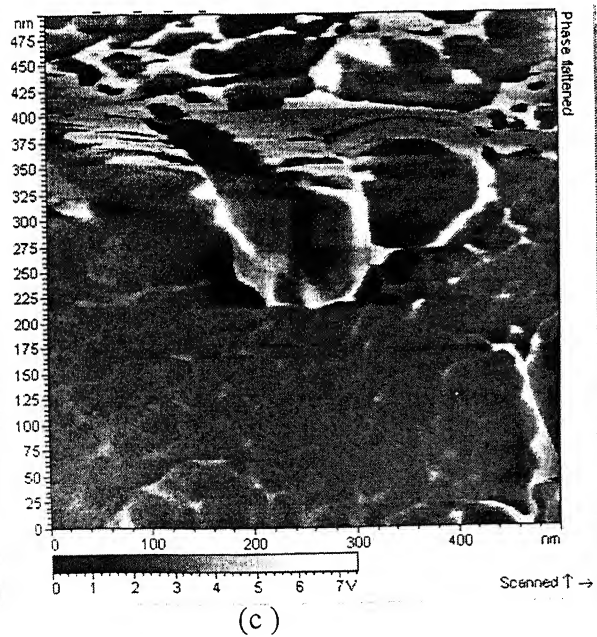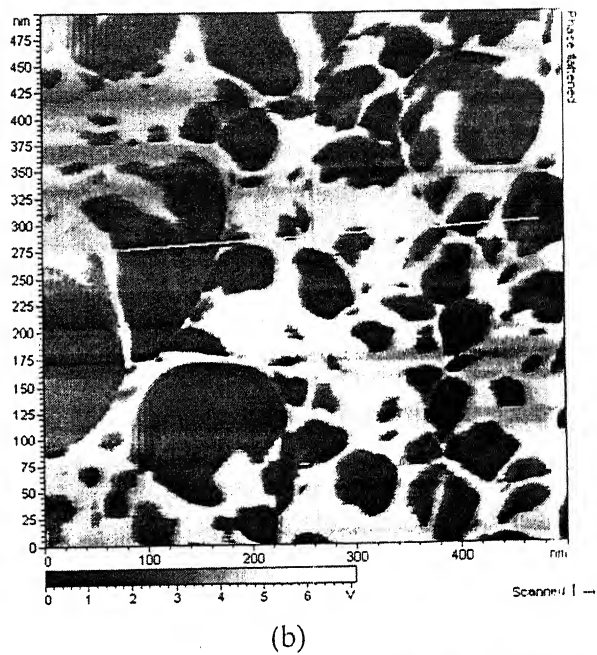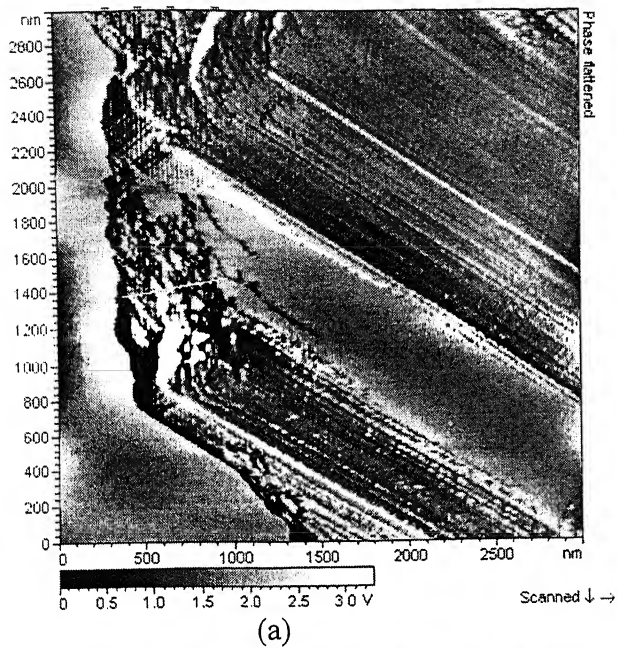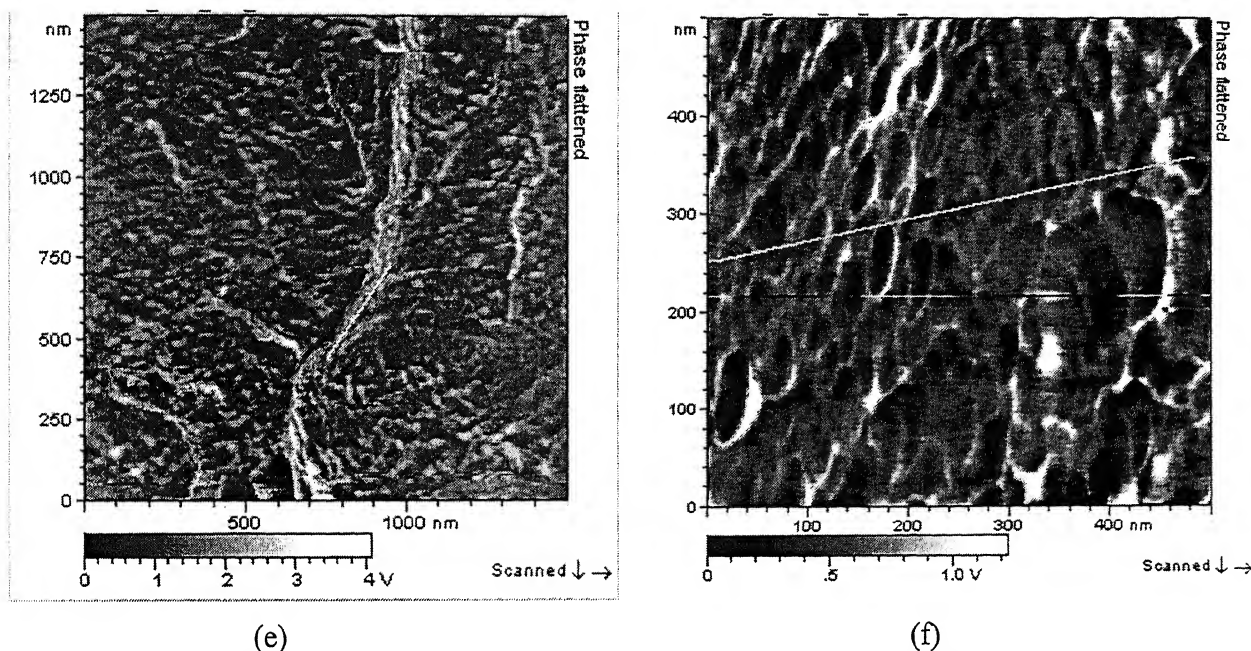
Figure4.21. AFM photographs showing effect of milling time on alloying corresponding milling time of (a, b) 5hr ; (c) 20hr ; (d) 40hr ; (e) 65hr ; (f) 100hr

4.2 HARDNESS OF MECHANICALLY ALLOYED $Fe_{100-X}Cr_X$ ALLOY POWDERS

The progress of mechanical alloying can also be estimated by the calculating the mechanical properties. Microhardness testing is the versatile technique to estimate the hardness of milled powder. The progress of solid solution formation with milling time can also been estimated for the milled powder.

Effect of Milling Time on the hardness

Figure 4.20 showing the microhardness of mechanically alloyed $Fe_{100-x}Cr_x$ X=10,20 function of milling time, it can be seen that as milling time was increased, hardness was increasing for the both the compositions of $Fe_{90}Cr_{10}$ and $Fe_{80}Cr_{20}$. This was because of as the milling time was increasing the material will transformed to highly dislocated structure, vacancies, stacking faults as a result of which strain

hardening of the powder so that the hardness was increased. As wt% of Cr was increased in the alloy micro hardness getting increased, this was because of there was formation of strong solid solution as concluded from the Mossbauer spectroscopy results, which contributes the more solid solution strengthening so that the hardness was increased

Table4.6 and Figure4.22 showing the microhardness of mechanically alloyed $Fe_{100-x}Cr_x$ X=5,10,15,20 function of milling time. It can be observed that at initial stages of milling time the scatter in the hardness value was more as compared to the higher milling time where the scatter in the hardness value was less. This is because of at initial stages of milling there is a possibility of formation of chromium rich areas and iron rich areas as explained in Phase contrast study by AFM, and Mossbauer spectroscopy results, So strain hardening of Fe, Cr powders will give different values of hardness, leads to the scatter in the hardness value at the initial milling time. As the milling was increased further alloying was progressed which contributes the solid solution strengthening to the Fe-Cr alloy so that the hardness will increased to higher values.

Table 4.6 Effect of milling time on the hardness of mechanically milled Fe-Cr alloy

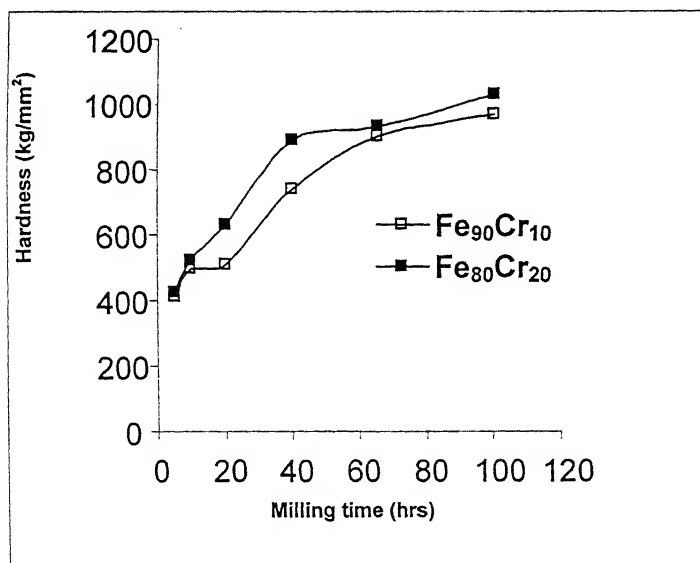| Sample	Hardness (g/mm^2)					
	Milling time 5Hrs	Milling time 10Hrs	Milling time 20Hrs	Milling time 40Hrs	Milling time 65Hrs	Milling time 100Hrs
Fe$_{95}$Cr$_5$						➢ 851 ➢ 905
Fe$_{90}$Cr$_{10}$	➢ 370 ➢ 438 ➢ 386	➢ 457 ➢ 501 ➢ 525	➢ 478 ➢ 501 ➢ 551	➢ 715 ➢ 756 ➢ 756	➢ 905 ➢ 905	➢ 905 ➢ 1030
Fe$_{85}$Cr$_{15}$						➢ 1030
Fe$_{80}$Cr$_{20}$	➢ 438 ➢ 457 ➢ 356 ➢ 457	➢ 457 ➢ 579 ➢ 525	➢ 609 ➢ 642 ➢ 642	➢ 964 ➢ 851 ➢ 851	➢ 964 ➢ 905	➢ 1030

Figure4.22 Effect of milling time on the hardness of Fe$_{100-x}$Cr$_x$ x=10, 20

4.3 CONSOLIDATION OF MECHANICALLY ALLOYED $Fe_{100-x}Cr_X$ MILLED FOR 100HOURS.

The consolidation of milled powders were done in cylindrical die and the applied pressure of 4 tons for the powders $Fe_{100-x}Cr_x$ x=5, 10, 15, 20. milled for 100hours. The size of the compacts was 5mm diameter and 5mm height. Fixing the sintering temperature for nano crystalline material is so sensitive, it should be such that there should not be grain coarsening in the material. The sintering temperature was estimated from Differential Thermal Analysis (DTA) data was discussed in the section 4.3. Sintering die compacted samples were did at 650ºC (0.41 T_m) for 45 min. under the hydrogen atmosphere, it was less than that of the conventional sintering normally did at $0.9T_m$..

Densification of the powder compact was depends on the applied pressure. The empirical relation that exist between P_x (pressure at a distance from x from the top) and X (distance from the top) is given by

$$P_x = P \exp (-4UZX/D)$$

Where P is the applied pressure, U is the coefficient of friction between powder and die wall, A is the area of cross-section, and Z is the proportionality constant. This indicates that pressure drops exponentially as the distance increases from the top surface. This is the reason why the top portion of the getting more densification compared to the bottom portion. Figure 4.23 showing that porosity getting increasing with decrease in height from the top. Mechanically alloyed structure is highly dislocated. The yield strength was maximum because of highly dislocated structure. Contact area between the powder particles was getting deceased as the material contains higher yield strength. Pressure is maximum at the top so that the powder particles having some chance to deform plastically and getting compact densified more at the top as shown in the Figure4.23 (a)(less porosity). When the height from the top was decreased the contact area between the particles getting decreased with decrease of effective pressure so that the densification getting decreasing (Porosity increasing) was shown in the Figures 4.23 (b) and (c)
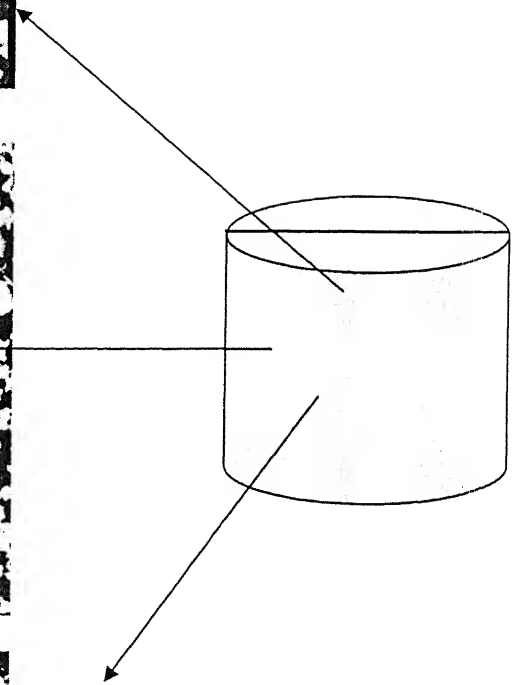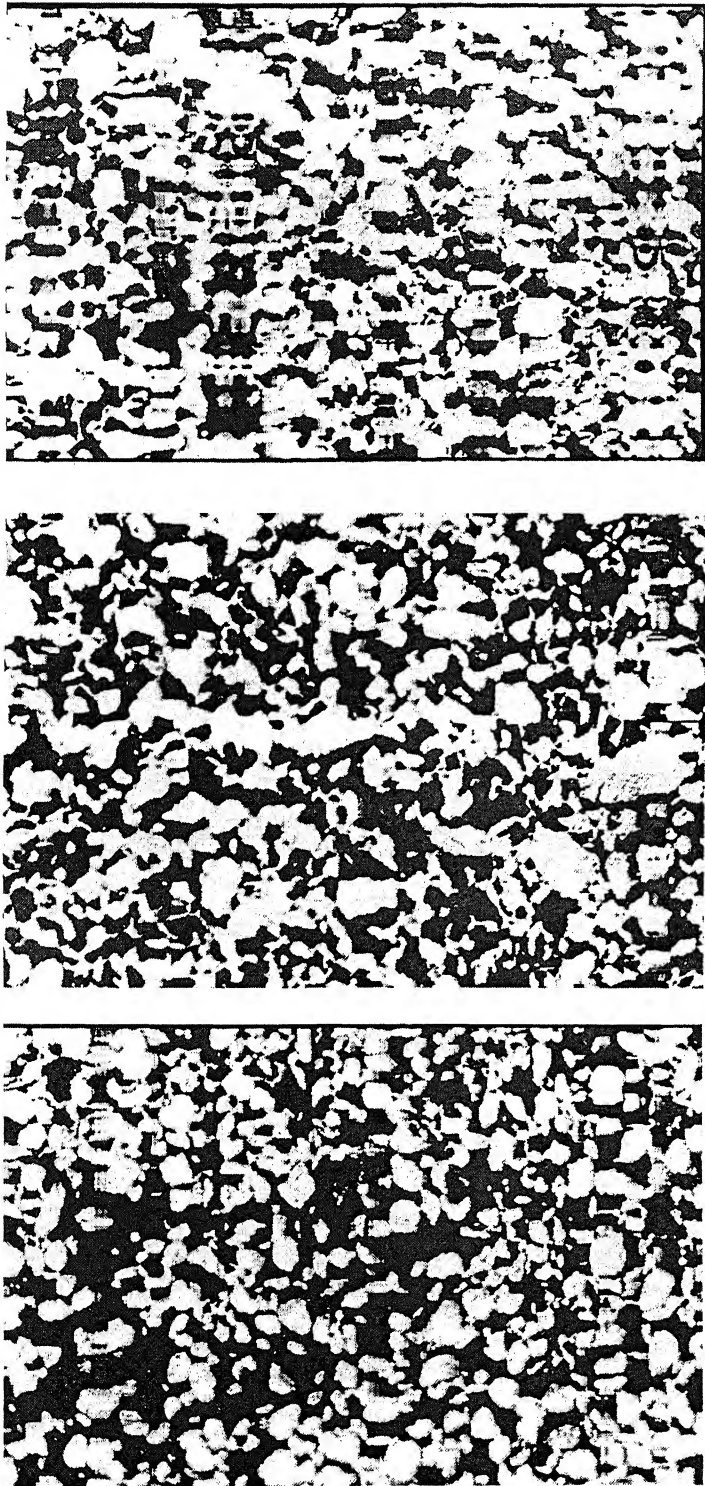
Figure 4.23 Optical Micrographs showing Effect of pressure on the densification of $Fe_{100-x}Cr_x$ alloy (a) at top (b) at middle (c) at bottom   (magnification of 200X)

CONCLUSIONS

The following conclusions can be drawn from the results of the present study:

1. The crystalline size of Fe −10 wt% Cr and Fe − 20 wt% Cr alloys, as determined by X − ray diffraction method, decreases with milling time. The rate of decrease in crystalline size is very rapid between 0 - 40 hrs milling time. The crystallite size between milling time of 40 hrs and 100 hrs remains nearly stable. At 100 hrs of milling time, the crystalline size in both the alloys was found to be 6 - 7 nm which is of the same order of magnitude as determined by AFM studies.

2. In view of both iron and Cr having the BCC crystal structure and both having very close parameters, X-ray diffraction studies are not very effective to monitor the progress of solid solution formation during mechanical alloying. In contrast, the progress of solid solution can be successfully studied using Mossbauer spectroscopy. As revealed by Mossbauer spectroscopy, it is found that regions of almost pure Fe still exist in the mechanically milled powder even after 65hrs of milling time. But Fe-Cr solid solution forms from 20hrs of milling time. Solid solution of an improved homogeneity is found to have occurred with increase in milling time

3. Particle morphology of mechanically milled Fe −10 wt% Cr and Fe − 20 wt% Cr alloy powders, as reveled by the scanning electron microscopy, changes with increase in milling time. The particle morphology changes from equiaxed to elongated and then to flaky as the milling time increases. The extent of flakiness appears to be increasing with increasing Cr content in the mechanically milled alloys.

4. As studied by AFM, the surface roughness of milled particles of Fe −10 wt% Cr decreases with increase in milling time. While the mean ridge height is found to be ~ 700 nm after a milling time of 5 hrs, the same decreases to ~ 180 nm after a milling time of 100 hrs.

5. As studied by AFM Interlamellar width in Fe –10 wt% Cr decreases with increase in milling time. While after a milling time of 20 hr the interlamellar width in Fe – 10 wt% Cr is found to be 145 nm, it decreases to15 nm as the milling time was increases to 65 hrs.

6. As studied by AFM, grain morphology of the milled Fe –10 wt% Cr alloy powder is changing from equiaxed to elongated as the milling time is increasing.

7. From the phase contrast study of the milled Fe –10 wt% Cr alloy, milling of the powder constituents is uniform as the milling time is increasing.

8. As studied by Microhardness Tester, Microhardness is getting increasing with increase in milling time for the both the Fe –10 wt% Cr and Fe – 20 wt% Cr alloys. From 40hrs of milling time onwards hardness is increasing sharply and it is also found that scatter in the hardness value is more at the initial stages of milling, as the milling time was increasing scatter is found to be getting decreasing..

REFERENCES AND NOTES

Yang H, Di L M and Bakker H Intermetallics 1 29

Bar, G.; Thomann, Y.; Brandsch, R.; Cantow, H. J.; Whangho,M. H. *Langmuir* **1997**, *13*, 3807.

Bhaduri and Bhaduri 1998: Bhaduri, S. and Bhaduri, S.B., JOM, 50(1) (1998), 44

Beck and Siegel 1992: Beck, D.D. and Siegel, RW., J.Mater.Res., vol.7(1992), p.2840.

Bradndsh, R.; bar,G.: Whangbo,M.H. Langmuir 1997,13,6349

Birringer 1989: Birringer, R., Mater. Sci. and Engg. , AI17(1989), 33-43.Eifert 2000:

Eifert, H., Kupp, D.and Gunther, B., Powder Metall., vol. 43, No.4, (2000),

310-313. Erb 1995: Erb, D., NanoStructured Mater. ,6(1995),533.

Gleiter 1989: Gleiter, H. (1989) Progress in Materials Science, vol.33, pp.223-315.

Gleiter 1991: Gleiter, H., J.Appl.Cryst., 24(1991), 79-90.

Gleiter 1995: Gleiter, H., Z.Metalkd. 86(1995)2, 78-83.

Gleiter 1998: Gleiter, H., Prog.Mater.Sci., 33(1998), 223.

Gleiter 2000: Gleiter, H., Acta Mater., 48(2000), 1-29.

Gleiter 1993: Gleiter, H., in "Mechanical Properties and Deformation Behavior of Materials having Ultrafine Microstructure", ed. M.Nastasi and M.Parkin-*, NATO Adv. Study Inst. Series E, Applied Science, Vol. 233, Kluwer, Dordrecht, 1993, p.3.

Grossard 1969: Grossard, AC., Thin Solid films, 57(1979), 3. ,Groza 1999: Groza, J.R, Chapter 13, Non-Equilibrium Processing of Materials

Herr et al. 1990: Herr, D., Jing, J., Gonser, D., & Gleiter, H., Solid State Commun. , 76(1990), 192.

Hofler et al. 1993: Hofler, H.J. et al, Mater Sci.Eng. AI16(1993), p.169-177.

Inoue, A. Nakazato, N., Kawamura, Y. and Masumoto, T., Mater.Sci. & Eng. A, (1994) AI79/180,654.

Krill et al. 1995: Krill et al., Materials Science Forum, 179-181(1995),443.

Krstic 1993: Krstic, V., Erb, D., and Palumbo, G., Scripta Metall. Mater., 29(1993), 1501

M.Murugesan and H.Kuwano IEEETransactions on Magnetics,Vol 35, No 5 (1999)

Ma and He 1996: Ma, E. and He, L., J.Mater.Res, vol.11(1996), no.l, p.72-79.

Ma and He 2000: Ma, E. and He, L. J.Mater.Res, v01.15(2000), noA, p.904-911. Manual: Manual for Vibrating Sample Magnetometer, Model 155.

McCandlish et al. 1994: McCandlish, L.E., Kevorkian, V., Jia, K. and Fischer, T.E. in "Advances in Powder metallurgy and Particulate Materials-1994", vol.5, compiled by Lall, C. and Neupaver, A.J. (Metal Powder Industries federation, Princeton NJ), (1994), p.329.

McHenry et al. 2000: McHenry, M.E. and Laughlin, D.E., Acta Mater. , 48(2000), 223 238.

Nieh et al. 1991: Nieh, T.G. and Wadsworth, J., Scr. Metall. Mater., 25(1991),955-958

Palumbo et al. 1990: Palumbo, G., Erb, D. and Aust, K.T., Scripta Metall. Mater., 24(1990),2347-2350.

Rangnathan et al. 2001: Ranganathan, S., Divakar, R. and Raghunathan, V.S., Scripta Mater., 44(2001), 1169-1174

Roco 2001: Roco, M.C., J. Nanoparticle Research, 3 (5-6) (2001), pp. 353-360.

Roco 2002: Roco, M.C., JOM, September 2002,22-23.

Roco et al. 2003: Roco, M.C.,Williams, R.S and Alivisatos, P., (2003) (on website www.nano.gov).

Schumacher et al. 1989: Schumacher, S., Birringer, R., Strauss, R. and Gleiter, H., Acta Metall.,37(1989), 2485-2488.

Siegel 1990: Siegel, R.W., MRS Bulletin, 15(10), (1990), 60.

Siegel 1993: Siegel, R.W., Mater.Sc.and Engg. , AI68(1993),189-197

Siegel 1994: Siegel, R.W., Nanostruct. Mater., 4(1994), 121.

Suryanarayana 1995: Suryanarayana, c., International Mater. Review, 40, 2, (1995), 41-64.

Suryanarayana 1999: Suryanarayana, c., 'Mechanical Alloying' in "Non-Equilibrium Processing of Materials", Pergamon, 1999, Editor C.Suryanarayana, p.49-88.

Suryanar.ayana 2001: Suryanarayana, c., Progress in Materials Science, 46(2001), 1-184.

Suryanarayana and Froes 1989: Suryanarayana, C. and Froes, F.H. (1989) "Nanocrystalline Metals: A Review", in "Physical Chemistry of Powder Metals Production and Processing", (ed. W.Murray Small), TMS, p.282-285.

Suryanarayana and Koch 1999: Suryanarayana, C. and Koch, C.C. 'Nanostructured Materials' in "Non-Equilibrium Processing of Materials", Chapter 12, Pergamon, 1999, editor C.Suryanarayana.

Suryanarayana 1997: Suryanarayana, c., Korth, G.E. and Froes, F.H., Metall. Mater. Trans., 28A(1997), 293.

Yulin and Liaw 2001: Yulin Lu and Peter K. Liaw, JaM, March (2001),31-35

Zhou et at. 2002: Zhou, B., Zhang, Y.W., Liao, C.S. and Yan, C.H., J. Magn. Magn. Mater., 247(2002), 70-76.

D. Raghavan, X. Gu, T. Nguyen, M. VanLandingham, A. Karim, Mapping polymer heterogeneity by phase imaging and nanoindentation AFM, *Macromolecules* 33(7) (2000) 2573-2583.